UNIVERSITÉ LIBRE DE BRUXELLES

Faculté des Sciences

Exploring copper(I) transmembrane transport with functionalized calixarenes

Nathan Renier
Supervisors : Pr. Ivan Jabin
Dr. Hennie Valkenier
Master thesis submitted in order to be awarded a
Master degree in Chemistry
2017-2018

I. Acknowledgements

Firstly I would like to thank Kristin Bartik and Fabrice Homblé for taking the time to read this master thesis.

I would like to thank my promoter, Ivan Jabin for allowing me to do my master thesis in his laboratory, for all the help, advise and corrections that he provided.
I would also like to thank Hennie Valkenier for introducing me to her fascinating field of work, transport measurement. For sharing her passion for research and for helping me with all the cumbersome tasks.

I would like to thank all the LCO team particularly Alice, Daniela and Pascal for taking the time to accompany me to the NMR, for the support and for advising me on calixarenes.
I would also like to thank all the EMNS team for the warm welcome. Especially Glenn, Lionel and Jerome for their interest and support during this project.
Many thanks to my friends and co-workers: Adrien, David, Felix, Tom, Thomas and Mounsef for their company and their humour.

Let's not forget to thank the CIREM for making all the NMR spectrometers available and keep them up and running. Mark, Mohammed , and Simon for maintaining the equipment's and the laboratories in working order. Jonathan Goole for the access to the DLS.

II. Summary

Copper is a metal involved in fundamental metabolic processes in living organisms, such as cellular respiration that requires constant intake of copper. In order to travel through a body, copper needs to cross cellular and organellar membranes, which are not permeable to copper. Various proteins are responsible for copper transport. Multiple mutations of genes encoding for such proteins can result in the inability to transport Cu^+, which leads to disruptions of copper homeostasis and causes human diseases.

In my Masters project, transport of Cu^+ through a bilayer membrane with synthetic molecules has been studied. Lipophilic molecules can be integrated (solubilized) in membranes in order to function as mobile carriers by extracting these ions on one side of the membrane, then diffuse to the other side and release the ions.

Calix[*n*]arenes are cyclic molecules composed of *n* p-^{t}Bu-phenol groups bridged with methylenes. In my Masters project, a calix[4]arene (**$X_4Me_2Im_2$**) was functionalized with two imidazole groups and two methyl groups through two consecutive alkylations of the phenol groups. **$X_4Me_2Im_2$** is known to linearly coordinate Cu^+ with the two imidazole groups.

A related calixarene (**$X_4Pr_2Im_2$**), also functionalized with imidazole groups, has been synthesized as well. Propyl groups were added instead of methyl groups, resulting in a higher conformational rigidity. Both calixarenes were characterized by ^{1}H NMR spectroscopy and the signals of **$X_4Pr_2Im_2$** were much better resolved than those of **$X_4Me_2Im_2$** due to the higher conformational rigidity of **$X_4Pr_2Im_2$**. **$X_4Pr_2Im_2$** had not been reported previously and was therefore fully characterized by HRMS, IR and NMR spectroscopy.

Binding properties of **$X_4Me_2Im_2$** and **$X_4Pr_2Im_2$** with cations (H^+, Na^+, K^+ and Cu^+) relevant to the transport process were studied by titrations in ^{1}H NMR spectroscopy in [$CD_3CN/CDCl_3$]. Both calixarenes showed high affinities for cations. Overall **$X_4Pr_2Im_2$** showed a higher selectivity than **$X_4Me_2Im_2$** for Cu^+.

A transport assay was developed in order to investigate Cu^+ transmembrane transport. Liposomes, which are spherical lipid bilayers, were used as model systems for cell membranes. **$X_4Me_2Im_2$** and **$X_4Pr_2Im_2$** were integrated in the membranes constituting the liposomes during their preparation.

The optical properties of the fluorescent probe bathocuproinedisulfonic acid (BCS) were studied by absorption and fluorescence spectroscopy upon addition of Cu^+. A clear decrease of the fluorescence intensity was observed when increasing the Cu^+ concentration. BCS was encapsulated inside liposomes in order to detect the presence of Cu^+. While monitoring the fluorescence, a solution of Cu^+ was added to the exterior of the liposomes in order to create a Cu^+ gradient.

A decrease of the fluorescence over time was observed when either **$X_4Me_2Im_2$** or **$X_4Pr_2Im_2$** was present in the membranes of the liposomes. From this we can conclude that **$X_4Me_2Im_2$** and **$X_4Pr_2Im_2$** both showed the ability to transport Cu^+ across a bilayer membrane. **$X_4Pr_2Im_2$** showed consistently higher rates of transport than **$X_4Me_2Im_2$**, in agreement with the superior selectivity of Cu^+ found for this compound. Various concentrations of **$X_4Pr_2Im_2$** were tested, a trend between rate of transport and calixarene concertation was observed. Experiments were set up in ways that transport of Cu^+ is compensated by transport of Na^+ or K^+ in the opposite way. Cu^+ transport rates were higher when exchanged with K^+, which is attributed to the lower affinity of both calixarenes for K^+ compared to Na^+.

III. Abbreviations

δ:	chemical shift
⊃:	included
Δδ:	difference of chemicals shift
Ar:	Aromatic groups
ArH:	Aromatic ^{1}H NMR signals
ATOX1:	copper chaperones protein
ATP:	Adenosine triphosphate
ATP7A/B:	ATP pump 7A/B
Barf:	tetrakis[3,5-bis(trifluoromethyl)phenyl]
BCS:	Bathocuproinedisulfonic acid
CD_3CN:	Deuterated Acetonitrile
$CDCl_3$:	Deuterated Chloroform
CH_2:	Methylene
CH_3:	Methyl
CH_3CN:	Acetonitrile
$CHCl_3$:	Chloroform
Cp:	Ceruloplasmin
CTR1:	Copper transporter 1
Cu^+:	Copper(I)
DCM:	Dichloromethane
DMF:	Dimethylformamide
DPPC:	Dipalmitoylphosphatidylcholine
EMNS:	Engineering of Molecular Nanosystems
eq.:	equivalent
EtOH:	Ethanol
Im:	imidazole group
ImH:	Imidazole ^{1}H NMR signals
K_a :	Complexation constant
LCO:	Laboratoire de Chimie Organique
LUVs:	Large Unilamellar Vesicles
Me:	Methyl group
MeOH:	Methanol
NMR:	Nuclear Magnetic Resonance
Phos.:	Phosphate
POPC:	1-Palmitoyl-2-oleoylphosphatidylcholine
Pr:	Propyl group
S:	Solvent
^{t}Bu:	tert-Butyl
THF:	Tetrahydrofuran
X:	para-^{t}Bu-phenolate group
$X_4Me_2Im_2$:	calix[4]arene bis-methyl bis-imidazole
$X_4Pr_2Im_2$:	calix[4]arene bis-propyl bis-imidazole

IV. Table of Contents

1. Introduction

1.1. Transmembrane transport

1.1.1. Cellular membrane

Biological membranes are fluid and dynamic structures formed of lipids, proteins, and carbohydrates. The plasma membrane serves as a barrier between the interior and the exterior of cells and defines the boundary between the two. The lipids forming the membrane are amphiphilic and therefore, in an aqueous medium, they self-assemble to form bilayers in order to reach a more stable state. The bilayer structure is semipermeable, meaning that certain species are able to go through easily, while most others do not. The ability of a species to go through the membrane mainly depends on its permeability coefficient (expressed in cm/s) and varies with size and polarity. Some species, such as ions, cannot go through the membrane but are still necessary for the cellular machinery to operate. Therefore, membrane proteins are required to transport these species.[1]

1.1.2. Active/passive transport

Three main factors involved in transport through a membrane are the concentration gradient, the electric potential, and the permeability coefficient. The concentration gradient between the two sides of the membrane induces a movement of the species towards the less concentrated side. The electric potential drives charged species to diffuse towards the oppositely charged side of the solution. The permeability coefficient is specific to each species/membrane pair. A concentration gradient of charged species or an electric potential between the two sides separated by the membrane can induce transport of charged species. If the transport occurs in the same direction as the concentration gradient, it is referred to as passive. On the contrary, if the transport occurs in the opposite direction, it is referred as active and this process requires additional energy (see Figure 1).[1]

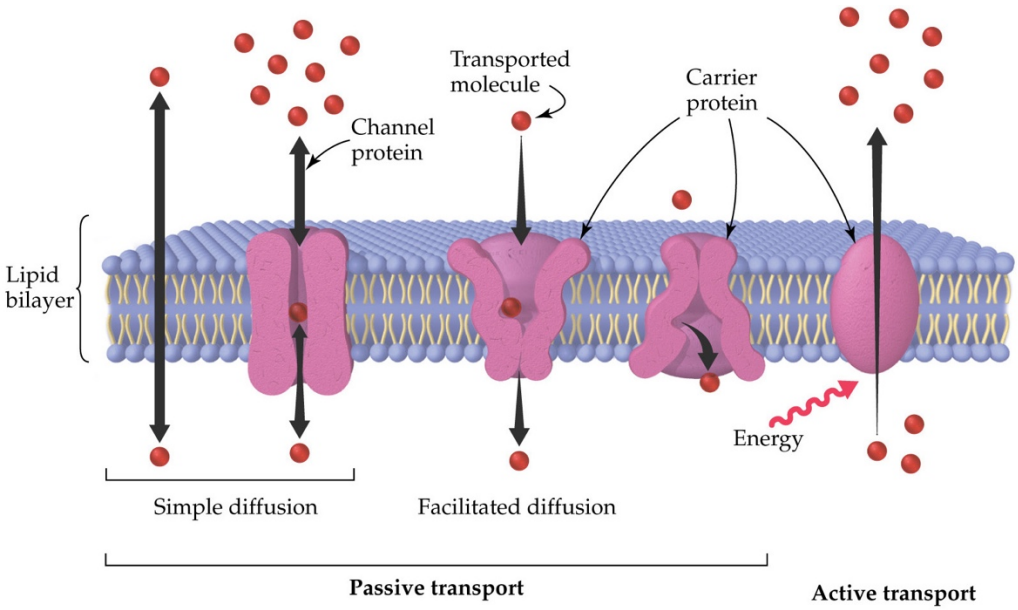

Figure 1 : Transmembrane transport through a lipid bilayer by different transporter proteins.[2]

1.1.3. Membrane transport proteins

There are two main types of transporter proteins, ionic channels and carriers (Figure 1).
Ionic channels are proteins that form hydrophilic channel across the membrane to allow the passage of ions and hydrophilic molecules. Carrier proteins also spread across the membrane but are not open to both sides simultaneously. They bind one or multiple species on one side and then change conformation to release it to the other side.
Carriers can move a species against its concentration gradient in two different ways. Primary active transporters are protein that utilize the energy released upon hydrolysis of ATP molecules to transport a species through the membrane in the opposite direction than the electrochemical gradient. Secondary active transporters use energy to form a electrochemical gradient to transport species across the membrane.[1]

1.2. Copper(I) in biology

1.2.1. Role of copper in the human body

Copper plays a critical role in the human body as it allows structures to form and reactions to occur that would not be possible otherwise. A key feature of copper in biology is its ability to alternate between its reduced (Cu^{+}) and its oxidised form (Cu^{2+}).
Copper is necessary for a lot of essential biological functions, for example as an intermediate in electron transfer in the respiration process that produces energy for the body. Copper also plays a role in oxidoreductase proteins that allow the reduction of L-ascorbate. Copper takes part in proteins responsible for the scavenging of free radicals that are detrimental to the cells. Copper is involved in the production of key components for the body such as melanine and it catalyses the formation of elastin precursors and collagen.
Some proteins interact with other metals in similar ways as with copper, and competition between metal ions can take place. Thus, copper is able to displace other metals (e.g. zinc) from their ligands. Copper can interact with metallothioneins which are responsible for cation detoxification and copper also takes part in processes that involve transport of cations, such as iron uptake into the circulatory system.[3]

1.2.2. Copper homeostasis and transport

The processes involving copper take place in different parts of the cells and in different part of the body. To get from nutrition to the organelles in the cells, the copper needs to be transported, distributed, stored, and excreted when an excess is present.
Copper transport occurs at the intracellular and intercellular levels and needs to be carefully regulated. Copper intake ranges from 2 to 5 mg per day but 0.8 mg can be enough to maintain homeostasis (Figure 2). Most of the copper is transported to the liver via the blood, from where it is redistributed to parts of the body that require it. Copper homeostasis is thus mainly regulated by the liver. Most of the copper ingested is sent back to the digestive system by the liver through the bile, after which it exits the body. The rest of the copper is distributed across the body and will be used or excreted through the kidneys. When transported in the blood, few of the copper ions are free in solution and most of it (90%) is bound to the protein ceruloplasmin.[4]

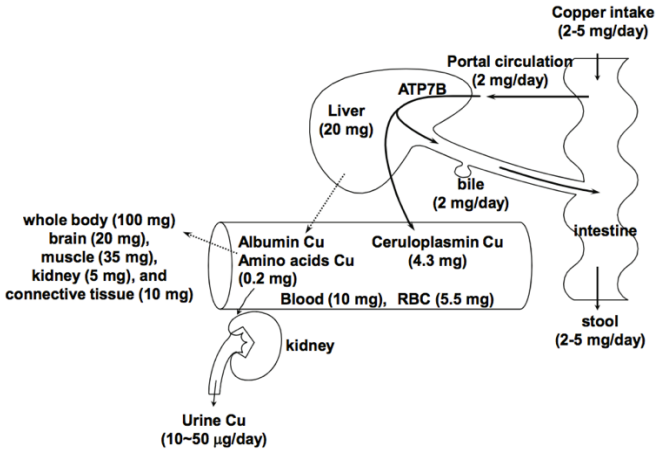

Figure 2 : Copper metabolism in humans.[5]

Copper is mainly transported into cells by CTR1, a transmembrane protein highly expressed in the liver and kidney. It is firstly reduced in Cu^{+} by another transmembrane protein and transferred to CTR1 in order to be more easily transported. CTR1 is a methionine rich protein and is believed to interact with copper with a Met-Cu-Met motif.[4] Although other studies have also proposed additional interactions with histidine motifs as seen in Figure 3.[6,7]

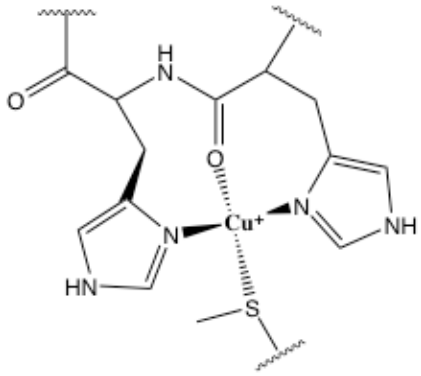

Figure 3 : Cu^{+} binding with histidine and methionine residues.[6]

Once copper has passed the bilayer membrane it is transferred to chaperones, such as Atox1, that will bind and deliver it to different organelles. Copper is mainly distributed to the Golgi apparatus where it is loaded on secretary proteins. In order to go through the membrane of the Golgi apparatus, other types of copper transporters are required (ATP7A/B). Atox1 chaperones have been shown to bind and transfer Cu(I) to ATP7A/B with cysteine residues (

Figure 4). [4]

Figure 4 : Mechanism of copper binding and trafficking in eukaryotes.[8]

Similarly to CTR1, ATP7A and ATP7B are transmembrane proteins able to transport copper across a membrane. They are pump type ATPase, which use the energy released by the hydrolysis of ATP to transport copper. ATP7A transports copper into the Golgi apparatus in order to be distributed to nascent proteins. This transporter is expressed in almost all cells excepted hepatocytes.
A similar protein (ATP7B) is responsible for the excretion of copper into the bile in order to avoid too high copper concentrations.[4] Copper is also distributed through other paths as it serves numerous other functions that will not be discussed herein.

1.2.3. Copper related disease

Defects in the genes coding for ATP7A and ATP7B proteins can occur and results in a disruption of copper homeostasis. This causes a lack or an accumulation of copper in certain organelles and cells, resulting in human diseases.[5]

- Menkes disease and occipital horn syndrome

Menkes disease is result of a variety of mutations in the ATP7A gene. These mutations prevent ATP7A to transport copper into the Golgi apparatus. As a results copper cannot be excreted and accumulates in the cytosol (Figure 5). The activity of the secreted copper enzymes is decreased, as copper is lacking inside the Golgi apparatus. The symptoms of the disease are: neurological degeneration, abnormal hair, hypothermia, and connective tissue disorder. The neurodegeneration of Menkes disease is due to the inability of copper to cross the blood brain barriers. This results in a decrease of the activity of the cytochrome c oxidase of the neuron cells in the brain. The usual treatment consists of Cu-histidine injections to provide copper to proteins. However, as copper cannot cross the blood brain barrier, these treatments do not prevent neurological abnormalities of Menkes disease. Cu-histidine injections do not improve enzyme activity either as copper cannot cross the membrane of the Golgi apparatus.
Occipital horn syndrome is the mildest form of Menkes diseases and also implies a reduced activity of copper dependant proteins. It results in connective tissue disorders, muscle hypotonia, and walking impairment.[5]

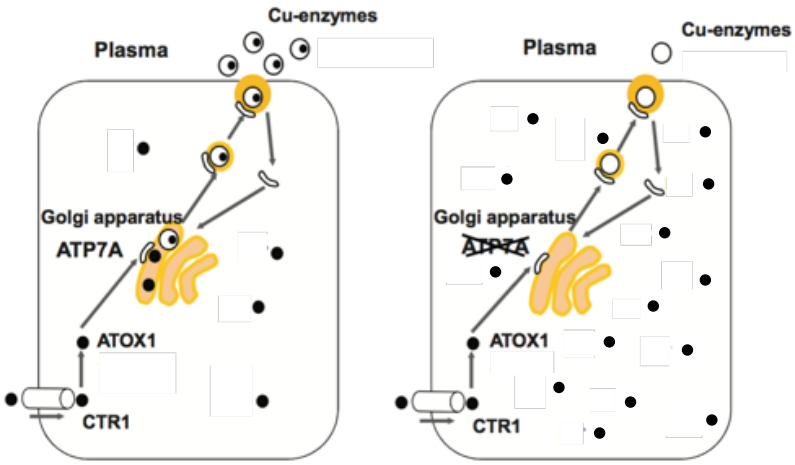

Figure 5 : Left, normal cell; Right, cell affected by Menkes disease.[5]

- Wilson disease

Wilson disease is an autosomal recessive disorder caused by mutations in the ATP7B gene, over 480 variations have been reported although only two mutations make up for most cases. Without functional ATP7B proteins, copper cannot be transported into the Golgi apparatus in hepatocytes cells (Figure 6). As a consequence, the secretion of copper bounded to ceruloplasmin in the blood and the excretion of copper into the bile are decreased. It results in a large accumulation of copper in the liver causing chronic hepatitis and leading to hepatocellular carcinoma. The excess of copper induces also free radical production, which causes cellular damage due to oxidative stress.
Copper bound to amino acids is released into the plasma, which results in high copper concentrations in urine and deposition in the brain, cornea, muscle, bone, and joints. The main symptoms of Wilsons diseases are hepatic and neurological. Current therapy aims to remove excess copper and treatments are based on copper-chelating agents.[5]

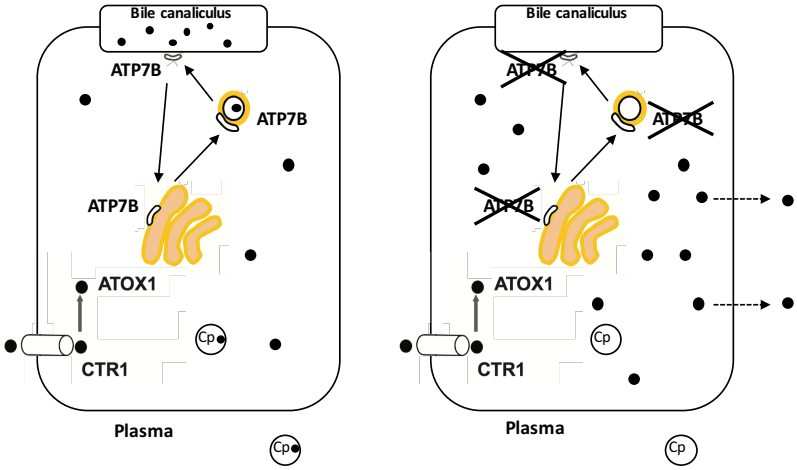

Figure 6 : Left, normal hepatocyte cell; Righ,; hepatocyte cell affected by Wilson diseases.[5]

1.3. Transmembrane transport of ions by small carriers

Multiple diseases have been linked with dysfunction or dysregulation of ion transport through membranes. A potential method to treat these diseases is to provide alternative ways to activate and regulate the transport phenomenon's in the human body. For this, small molecules functioning as carriers could be used. They function by forming a supramolecular complex with ions, that is able to cross the membrane, and then deliver the ions to the other side of the membrane (Figure 7).[9] They are not to be confused with carrier proteins, which are larger and span the membrane.

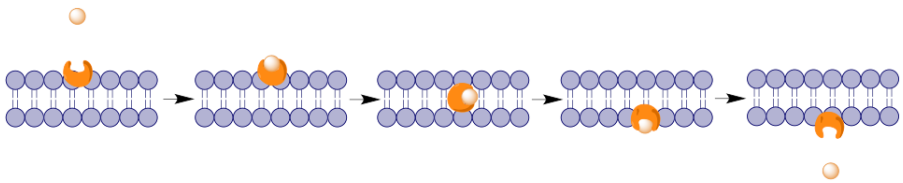

Figure 7 : Transport of ions through a bilayer membrane by a carrier.

Two examples of naturally occurring carriers, also referred to as ionophores, are valinomycin and monensin, which are able to transport monovalent metallic cations. They play crucial role in the chemical process occurring in the environment and in the functioning living organisms.[10]

Monensin is an ionophore with a similar binding pattern as crown ethers (Figure 8a) which is able to complex and transport numerous cations such as Li^+, Na^+, K^+, Rb^+, Ag^+, and Ti^+. The ability to transport cations causes monensin to collapse Na^+ and H^+ gradients, leading to antibacterial effects and applications as an antibiotic.[11]

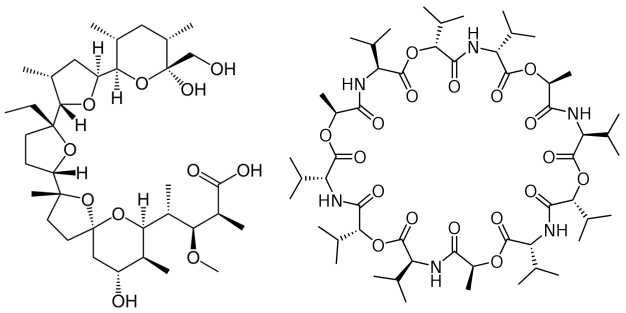

a) Monensin b) Valinomycin

Figure 8 : Chemical structures of natural cation carriers.

Valinomycin is a macrocyclic peptide analogue, containing both amide and ester linkages (Figure 8b), it is able to complex and transport K^+. Valinomycin also has antibacterial properties.
In transport studies both molecules can be used to break up the electrochemical gradient created or accumulated. In the same way, it has been shown that small synthetic molecules able to bind anions can facilitate the transport of anions when integrated in membranes.[12]

1.3.1. Transport studies by fluorescence spectroscopy

An easy means of assessing the transport capabilities of a molecule through a bilayer membrane is with liposomes. They are used to mimic the structure of a cell membrane. They can be easily prepared from lipids and can integrate a transporter molecule of choice. As the liposomes are made artificially, a lot of parameters can be easily modified and their impact on the transport phenomena can be evaluated. For example, the type of lipids used and thus the membrane properties can be modified. The type and the concentration of synthetic transporter can be controlled. The interior composition of the liposomes can be chosen and thus the ions present inside the liposomes can be chosen. Additionally, in order to detect the transport process, the liposomes can also contain a probe specific to the transported species.

The main goals in transport studies are to determine if transport occurs and at which rate. In order to detect the transport of a species, a specific fluorescent probe is often encapsulated inside liposomes. The fluorescent properties of the probe change upon transport and are followed in time by fluorescence spectroscopy. The changes observed can result from the

transport of a targeted species (direct monitoring), or from the transport of another species through an exchange or a co-transport process (indirect monitoring).

1.4. Calixarenes

Calix[n]arenes are macrocycles formed by n phenol units ($4 \leq n \leq 20$) linked by methylene bridge. Their syntheses take place in a basic medium and consists of the condensation of a p-^{t}Bu-phenol with formaldehyde (Figure 9).[13] The size of the macrocycle depends on the nature of the base.[14]

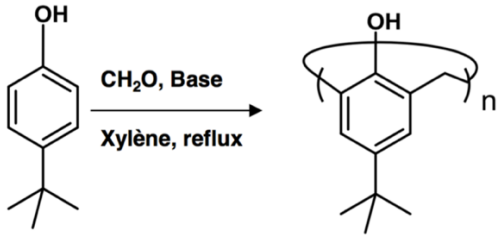

Figure 9 : p-^{t}Bu-calix[n]arenes syntheses.[14]

1.4.1. Conformations of calixarenes

When all the hydroxy groups of a calixarene are oriented in the same direction, the conformation is referred to as cone. In this conformation two parts of the molecules can be distinguished: the narrow rim, where the hydroxy groups lie, and the wide rim where the ^{t}Bu groups are located (Figure 10). Calixarenes show great conformational flexibility due to the ability of the phenol units to rotate around the bridging methylene. Two rotations are possible: one where the hydroxyl group goes through the cavity (pathway 1), the other where all of the rest of the aromatic groups does this (pathway 2) (Figure 10). For a calix[4]arene bearing ^{t}Bu groups, only the first rotational pathway is possible due to the limited size of the cavity.[15]

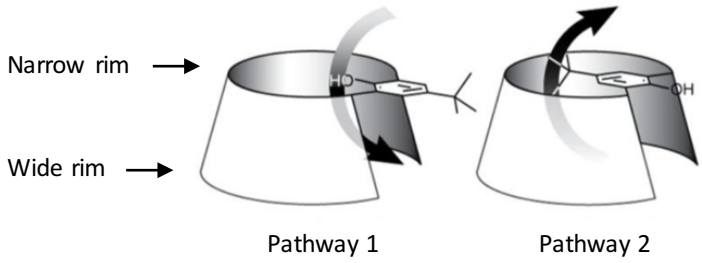

Figure 10 : Diagram of the two rotation pathways for a calix[n]arene.[15]

P-^{t}Bu-calix[4]arene can adopt four different conformations which are referred as to cone, partial cone, 1,2 alternate, and 1,3 alternate (Figure 11). Additionally, a variant of the cone conformation is the pinched cone conformation, in which two phenol units are parallel to each other and the other two are tilted.

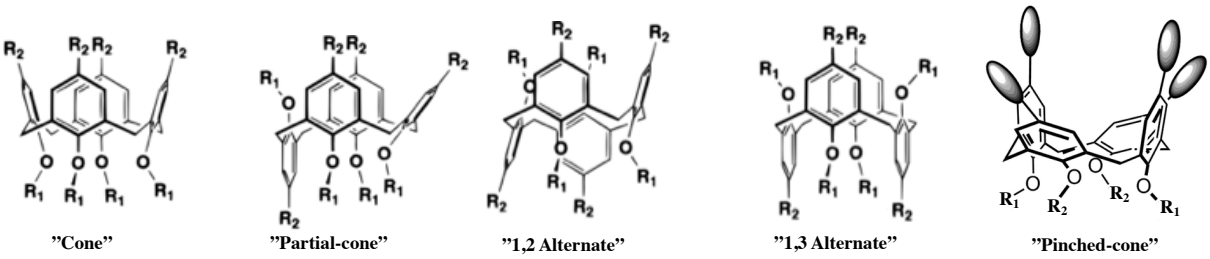

Figure 11 : Different conformations of p-^{t}Bu-calix[4]arenes.[15,16]

1.4.2. Functionalization of calix[4]arene for coordination

Through chemical reaction, calixarenes can be functionalized in various ways and in different positions (Figure 12).

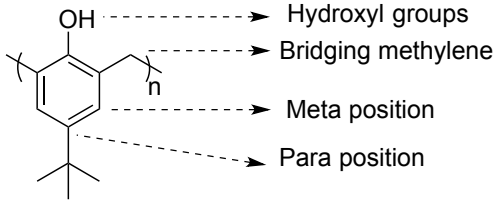

Figure 12 : Positions for the functionalization of calix[n]arenes.[17]

The motive for functionalization of calixarenes is to provide the calixarenes with selective coordination or other tailored properties. In order to achieve such properties, chemical groups are linked to the calixarene. Often the chemicals groups linked to a calixarene work together to allow coordination of a specific species such as Zn^{2+} or, in this case, Cu^{+}.[18]

1.4.3. $X_4Me_2Im_2$ and copper(I)

Reinaud and co-workers have developed a calix[4]arene to complex Cu^{+}, which was designed according to a binding model of Cu^{+} with Aβ fragment[I] and also other small peptides (Figure 13a and b).[19] This calix[4]arene is functionalised with two imidazole groups and two methyl groups on its narrow rim (Figure 13c) and is referred to as $X_4Me_2Im_2$.[II]

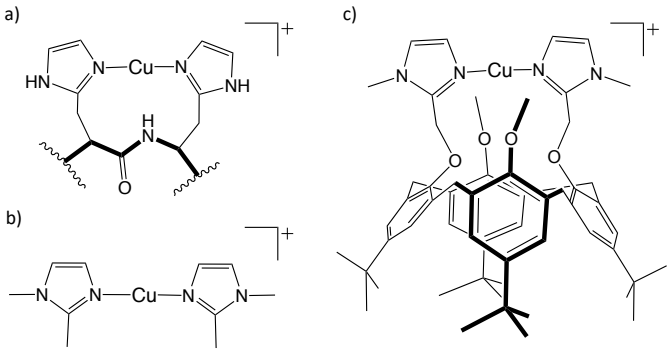

*Figure 13 : Schematic representation of the coordination mode of Cu^{+} as characterised in Aβ peptide fragments (a), complex obtained with 1,2-dimethylimidazole (b), and with **$X_4Me_2Im_2$** (c) as reported in reference [19].*

[I] Aβ fragments are small polypeptides that form the amyloid plaques found in Alzheimer diseases.
[II] Calixarenes are often referred as such: X is the p-^{t}Bu-phenolate group; Im is the imidazole group and Me the methyl group.

In these structures two histidine residues linearly coordinate to Cu^+ through interaction with the lone electron pair of the nitrogen atoms. The crystallographic structure of **$X_4Me_2Im_2$⊃Cu^+** showed a mononuclear complex where Cu^+ is coordinated by two imidazole groups (Figure 14), in a geometry that is almost linear (178.5°). When exposed to oxygen **$X_4Me_2Im_2$⊃Cu^+** was observed to be more stable and inert than two imidazole groups bonded with copper. The better stabilization of the Cu^+ coordinated to imidazole could be explained by the increased overlapping of the orbital of the imidazole nitrogen atoms and Cu^+ and the preorganization effect of the calixarene.[20]

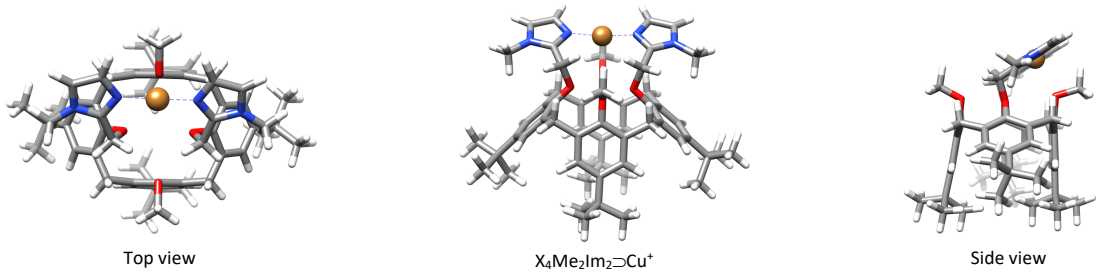

Figure 14 : Crystallographic structures of $X_4Me_2Im_2$⊃Cu^+ as reported in reference [20].

1.4.4. Calixarenes as ions transporters

Calixarenes and similar macrocyclic molecules have been previously studied as ion transporters through bilayer membranes. Two different types of transport have been reported: one where long units formed a channel through the membrane, the other as carriers where the transporter is free to rotate and move from one side to another in the membrane (Figure 15).

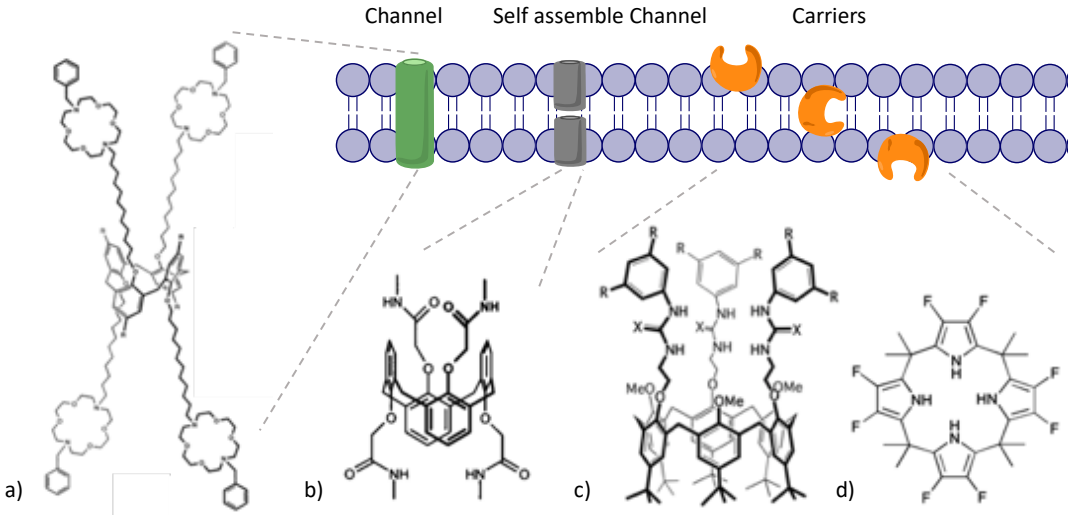

Figure 15 : Calixarenes as ions transporter; a) 1,3 alternate calix[4]arene as Na^+ and K^+ channel; b) calix[4]arene tetramethylamide which self-assembles to form a HCl channel; c) calix[6]arene (thio)ureas as Cl^- carrier; d) octafluorocalix[4]pyrrole as HCl and CsCl ion pair carrier and Cl^-/NO_3^- antiporter.[I]

Although anion transport is more frequently studied, cation transport with calixarenes has also been reported. For instance, calixarenes forming channels have been reported as

[I] Here antiporter is used to refer to the transport of chemical species in both ways to balance the charges and do not to function in the same way as antiporter proteins

transporter of Na^+ and K^+.[21] Some channels are formed by calix[4]arenes in an 1,3 alternate conformation functionalised with long alkyl groups equipped with aza-crown ethers which span across the membrane (Figure 15a).[21] Other calix[4]arene have been shown to self-assemble into multimers forming a channel across the membrane and transporting HCl ions pairs (Figure 15b).[22] Multiple calixarenes functionalised with H bond donor groups such as amide, urea, or thiourea have also been reported as Cl^- transporters (Figure 15b and c).[23,24] Transmembrane transport of Cl^- through a carrier transport mechanism has been reported with octafluorocalix[4]pyrrole and calix[6]arene (thio)ureas (Figure 15c and d) .[24,25] Transport of chloride with octafluorocalix[4]pyrrole was observed through co-transport of HCl, transport of cesium-chloride ion pair, and chloride-nitrate antiport process.[25]

1.5. Objectives

The objective of this project is to test if functionalized calixarenes, such as **$X_4Me_2Im_2$**, can transport copper(I) cations through lipid bilayer membranes (Figure 16).
Therefore, **$X_4Me_2Im_2$**, known to strongly bind copper(I) with two imidazole groups, will be synthesised and characterised. Another similar calixarene, **$X_4Pr_2Im_2$**, functionalized with propyl groups instead of methyl groups, will also be synthesised and characterized. As a result of the propyl groups, **$X_4Pr_2Im_2$** will have less conformational freedom and is thus expected to facilitate NMR studies. **$X_4Pr_2Im_2$** may also have a better affinity for copper as it will remain in a cone conformation, which is the conformation in which **$X_4Me_2Im_2$** binds copper. The presence of longer alkyl groups might also facilitate its solubilisation in the bilayer membrane and thus its ability to function as a carrier.

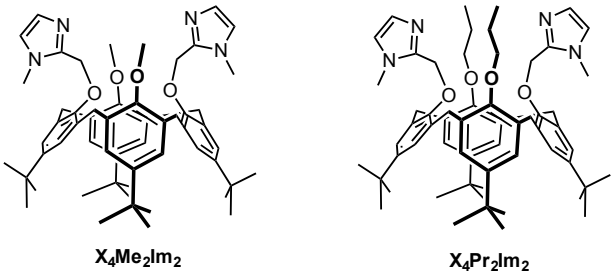

Figure 16 : Target compounds for the study of Cu^+ transmembrane transport.

The binding properties of the calixarenes will then be studied by ^1H NMR spectroscopy. Not only binding of copper(I) will be verified, but also their affinity for cations relevant in the transport process, such as Na^+ and K^+, will be studied.
Once the properties of the calixarenes are well characterised, an assay will be developed to study if the functionalized calixarenes can transport copper. The transport assay will use liposomes as a model for the bilayer membrane, which can be prepared to include a transporter of choice. Transport across the membrane can be followed by fluorescence spectroscopy with a dye encapsulated in liposomes. The dye will be used as a detector of transport.
Bathocuproinedisulfonic acid (BCS), a phenantroline derivative which has been reported to bind copper(I), can be used to directly monitor the copper(I) presence in the liposomes.[26] Optical properties of BCS will be studied through absorption and fluorescence spectroscopy. The encapsulation of this dye in liposomes will be tested.

Once the assay is implemented and a proof of concept is established, transport characteristics will be examined. The influence of different parameters of the assay can then be evaluated such as: buffer solution, transporter type and transporter concentration. Copper(I) transport could also be monitored with a pH sensitive dye, 8-hydroxypyrene-1,3,5-trisulfonic acid (HPTS), if copper(I) transport occurs through Cu^+/H^+ exchange.

The organic synthesis and NMR spectroscopic studies will be conducted at the Laboratoire de Chimie Organique (LCO). Transport measurements will be conducted at the Engineering of Molecular Nanosystems (EMNS) at ULB.

2. Results and discussion

2.1. Syntheses of target compounds $X_4Me_2Im_2$ and $X_4Pr_2Im_2$

2.1.1. Calix[4]arene bis-methyl bis-imidazole ($X_4Me_2Im_2$)

The synthesis of **$X_4Me_2Im_2$** is described in the literature in two steps from p-^{t}Bu-calix[4]arene **X_4H_4**.[20] The two-step synthesis is shown in Figure 17 with the yields obtained in this study. The first step consists of the selective alternate methylation of two of the phenol groups of the narrow rim, while the second step is the alkylation of the two residual phenol groups with 2-(chloromethyl)-1-methyl-1H-imidazole.

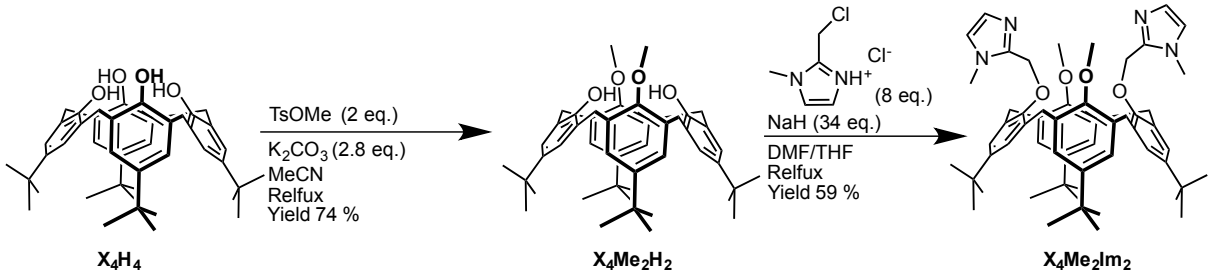

*Figure 17 : Synthesis of **$X_4Me_2Im_2$**.*

The introduction of the methyl groups requires a base (K_2CO_3) and an alkylation agent (TsOMe). The reaction is selective as it will only give the bis-methyl calix[4]arene (**$X_4Me_2H_2$**) with the two methyl groups opposite to each other. The regio-selectivity is due to the fact that compound *A* is better stabilized through H bonds than *B* (Figure 18). Furthermore, K_2CO_3 is a weak base and provides a control over the iteroselectivity, as it will not be able to deprotonate the phenol groups of the bi-alkylated compound, preventing the formation of compound *C* (Figure 18).[27]

The base and alkylation agent were both mixed with **X_4H_4** in CH_3CN. The mixture was stirred and heated under reflux overnight under inert atmosphere. **$X_4Me_2H_2$** was obtained in 74 % yield after flash chromatography purification.

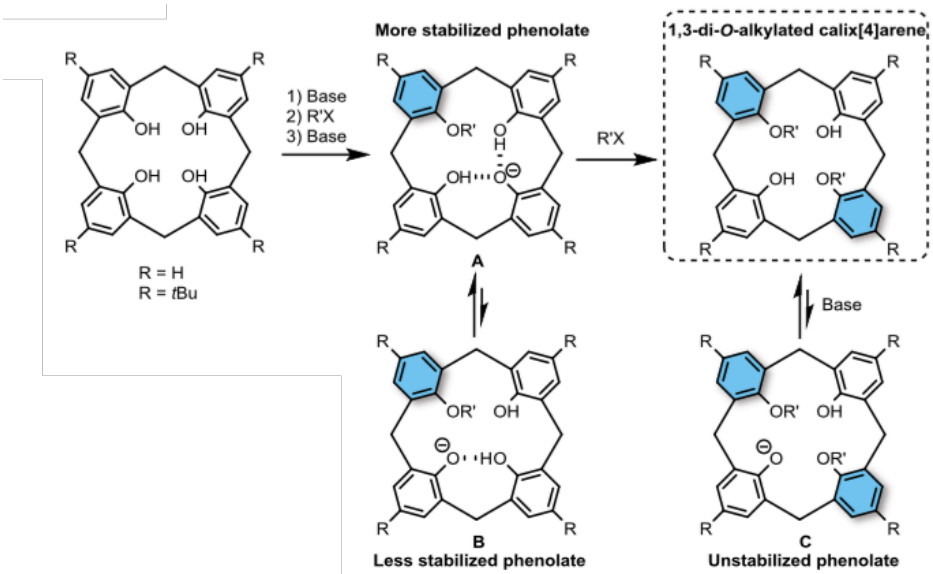

Figure 18: Rationalization of the alternate alkylation of the phenol groups of a calix[4]arene.[27]

The second reaction requires a strong base (NaH) because the residual phenolic groups are harder to deprotonate (see above). Even if the reaction was conducted in presence of an excess of chloromethylimidazole (7 equiv.), a small amount of mono-alkylated compound (X_4Me_2ImH) remained at the end of the reaction and was separated by flash chromatography purification. The desired compound **$X_4Me_2Im_2$** was isolated in 59 % yield.

A ^{1}H NMR spectrum of **$X_4Me_2Im_2$** was recorded in $CDCl_3$ at 298 K. It showed broad and poorly defined signals (Figure 19). The methylated aromatic parts of **$X_4Me_2Im_2$** are able to rotate through the annulus and thus the calixarene framework is not locked in the cone conformation (see Figure 11). Depending on the rate of exchange between conformations relative to the NMR time-scale, the signals in the ^{1}H NMR spectrum can be significantly broadened as observed in Figure 19. [19]

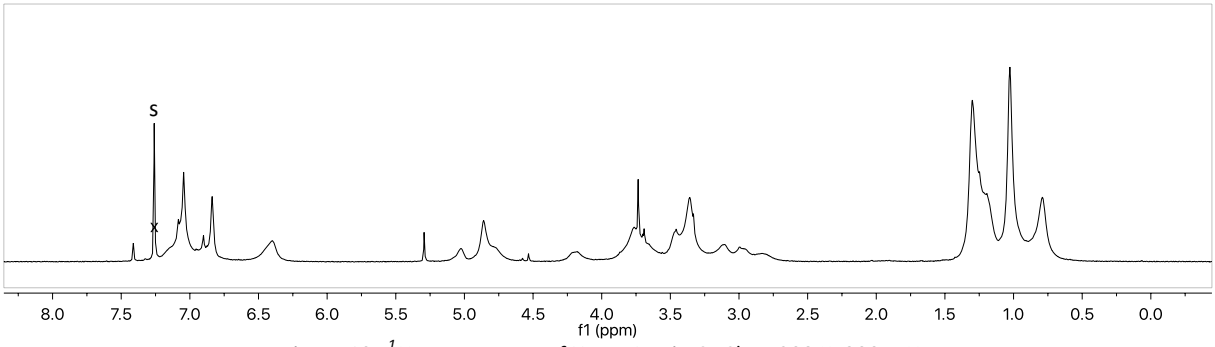

Figure 19 : ^{1}H NMR spectra of **$X_4Me_2Im_2$** in $CDCl_3$ at 298 K, 300 MHz.

2.1.2. Calix[4]arene bis-propyl bis-imidazole ($X_4Pr_2Im_2$)

The compound **$X_4Pr_2Im_2$** is very similar to **$X_4Me_2Im_2$** but it bears propyl groups instead of methyl groups on the narrow rim. In contrast to **$X_4Me_2Im_2$**, this compound has not been yet reported in the literature.

$X_4Pr_2Im_2$ was synthesized in one step from **$X_4Pr_2H_2$**, this latter being already available at the LCO. Similarly to compound **$X_4Me_2Im_2$**, **$X_4Pr_2Im_2$** was reacted with an excess of chloromethylimidazole in presence of NaH. The final compound **$X_4Pr_2Im_2$** was isolated in 51 % yield after flash chromatography purification.

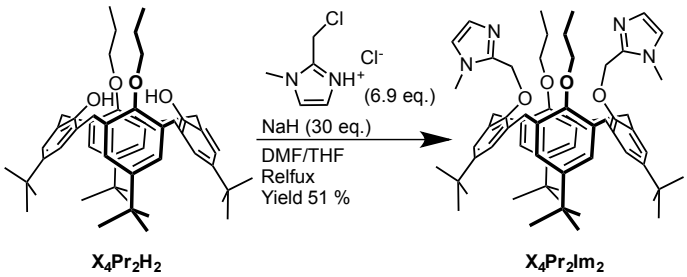

Figure 20 : Synthesis of $X_4Pr_2Im_2$.

Due to the presence of sodium in the reaction mixture, two species were detected by NMR analysis of the product: the free ligand **$X_4Pr_2Im_2$** and the corresponding sodium complex **$X_4Pr_2Im_2 \supset Na^+$**. The product was thus washed multiple times with water to remove the sodium salt. However, a small amount of the complexed species was still detected (<5 %), highlighting the high affinity of **$X_4Pr_2Im_2$** for Na^+.

A ^{1}H NMR spectrum of **$X_4Pr_2Im_2$** was recorded in $CDCl_3$ at 298 K and showed sharp signals which could be assigned unambiguously (Figure 21).

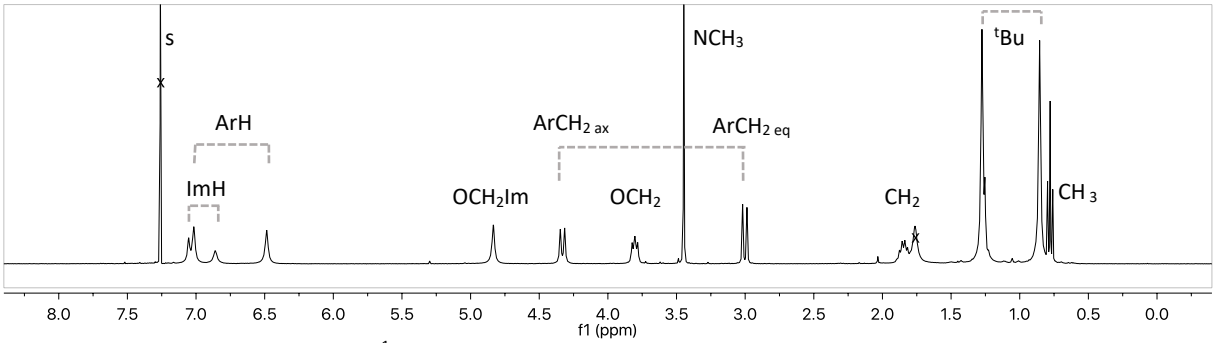

Figure 21 : ^{1}H NMR spectrum of **$X_4Pr_2Im_2$** in $CDCl_3$ at 298 K, 300 MHz.

The spectrum is characteristic of a C_{2v} symmetrical calix[4]arene in a pinched cone conformation with the large imidazole groups pointing outwards of the calixarene and with the propyl chain oriented inwards. The pinched cone conformation is characterized by a significant difference in chemical shifts ($\Delta\delta$) for the ^{t}Bu groups (0.42 ppm) as well as for the ArH (0.52 ppm).
$X_4Pr_2Im_2$ is not reported in the literature and was thus fully characterised. Its melting point, NMR spectra, and HRMS are described in the experimental section.

When comparing the ^{1}H NMR spectra of **$X_4Me_2Im_2$** and **$X_4Pr_2Im_2$** (Figure 19 and Figure 21) showed significant differences. The spectrum of **$X_4Pr_2Im_2$** is better defined than that of **$X_4Me_2Im_2$**. This difference is likely due to the higher conformational flexibility of **$X_4Me_2Im_2$**. Indeed, the anisole units of **$X_4Me_2Im_2$** can still rotate through the annulus.

2.2. Complexation studies

The ability of **$X_4Pr_2Im_2$** and **$X_4Me_2Im_2$** to interact with cations (H^+, Na^+, K^+, and Cu^+) was evaluated through ^1H NMR studies. In order to transport Cu^+, **$X_4Pr_2Im_2$** and **$X_4Me_2Im_2$** need to be able to bind this cation. The complexation of copper(I) by $X_4Me_2Im_2$ had already been observed but this is not the case for **$X_4Pr_2Im_2$**.[19] The study of the cations H^+, Na^+, and K^+ is also relevant as they may compete with Cu^+ in the transport experiments.

A ^1H NMR spectrum of **$X_4Pr_2Im_2$** and **$X_4Me_2Im_2$** was recorded, then a solution containing a cation was added by 0.2 equivalent increments until the ^1H NMR signals did not show any significant changes. For solubility reasons, the ^1H NMR spectra of **$X_4Pr_2Im_2$** were recorded in a mixture of $CD_3CN/CDCl_3$ (4/1). Note that the spectrum of **$X_4Pr_2Im_2$** in this mixture of solvents is highly similar to that recorded in pure $CDCl_3$.

2.2.1. Protonation of $X_4Pr_2Im_2$

The protonation of the imidazole groups of **$X_4Pr_2Im_2$** was evaluated by addition of a solution of trifluoroacetic acid (TFA). Note that the pKa of imidazole on histidine is around 6.[28] A comparison of the ^1H NMR spectrum of **$X_4Pr_2Im_2$** before and after addition of 1.1 equivalents of TFA is shown in Figure 23 (a and b).
Over the course of the titration, the intensities of the initial signals decreased and another set of signals appeared. This new set of signals was assigned to **$X_4Pr_2Im_2$**$\supset H^+$. Only a slight difference in chemicals shifts ($\Delta\delta$) between the different aromatic signals and the different ^{t}Bu signals was observed, indicating minor conformational changes observed (Table 1). Two imidazole aromatic signals (ImH) on the ^1H NMR spectrum of **$X_4Pr_2Im_2$**$\supset H^+$ were distinguishable and far apart, as one was down the low field from 6.93 ppm to 8.04 ppm. The shifted ImH signal integrate for two protons and are assigned to the hydrogens closest to the symmetry axis (Figure 22 in red).[l] The NMR signal of the two hydrogens in red are not distinguishable and thus the exchange rate of the added proton between the two imidazole is fast on the NMR time-scale.

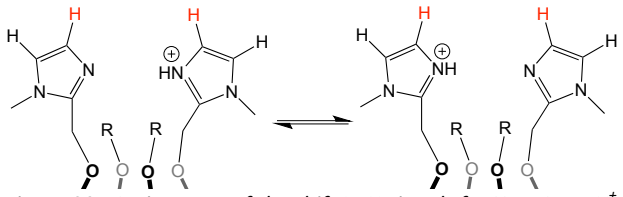

*Figure 22 : Assignment of the shift ImH signals for **$X_4Pr_2Im_2$**$\supset H^+$.*

[l] The spectra of the titration are shown in the appendices (Figure X 16).

2.2.2. Na^+, K^+, and Cu^+ complexation by $X_4Pr_2Im_2$

In order to determine if **$X_4Pr_2Im_2$** is able to complex Na^+, K^+, and Cu^+, solutions of NaBarf (tetrakis[3,5-bis(trifluoromethyl)phenyl] borate), KPF_6, and $(Cu(I)(CH_3CN)_4BF_4$ in CD_3CN were separately added to different solutions of **$X_4Pr_2Im_2$**. The ^1H NMR spectra of the free ligand **$X_4Pr_2Im_2$** and the complexes are shown in Figure 23 [I].

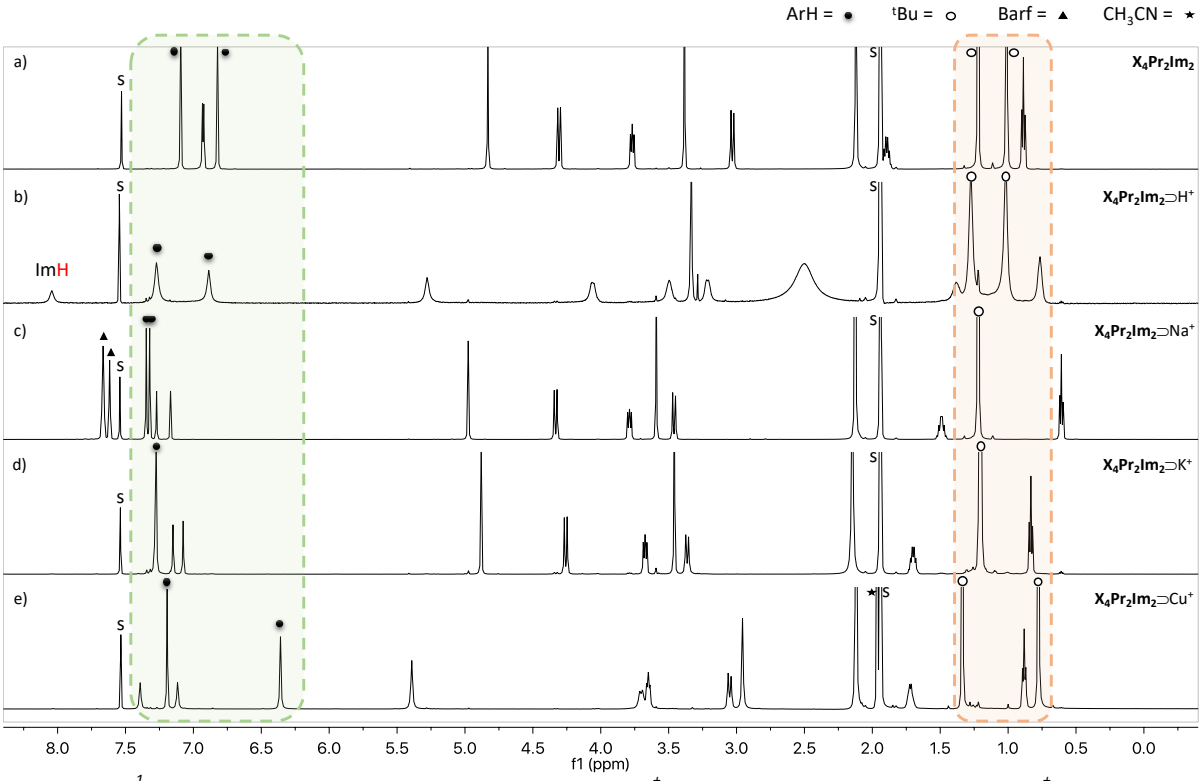

*Figure 23 : a) ^1H NMR spectra of **$X_4Pr_2Im_2$** (4.9 mM) b) $X_4Pr_2Im_2 \supset H^+$ (1.1 eq. of TFA added) c) **$X_4Pr_2Im_2 \supset Na^+$** (1 eq. of NaBarf added) d) **$X_4Pr_2Im_2 \supset K^+$** (1.8 eq. of $K^+PF_6^-$ added) e) **$X_4Pr_2Im_2 \supset Cu^+$** (1.1 eq. of $Cu(I)(CH_3CN)_4BF_4$ added) all spectra in $CD_3CN/CDCl_3$ at 298 K, 600 MHz.*

Firstly, this NMR study showed that **$X_4Pr_2Im_2$** is able to interact and form a metal complex with all the cations tested. Over the course of the titration of **$X_4Pr_2Im_2$** with Na^+ and Cu^+, the intensities of the initial signals decreased, and another set of signals appeared (Figure 23c and d). Two distinguishable sets of signals were thus clearly observed, which implies that the rate of exchange between the free ligand **$X_4Pr_2Im_2$** and the metal complex is slow on the NMR time scale.[II]

Only one set of signals was observed in the case of K^+, indicating that the exchange rate is fast on the NMR time scale and that the signal observed is thus a weighted average of the signals of the two species.

[I] All the spectra are given in the experimental section (in Figure X 16 to Figure X 18).

[II] The amount of Cu^+ added was verified by comparing the intensity of the signals of the CH_3CN with a signal of the host. The amount of Na^+ was also verified by measuring the integrals of the aromatic signals of the Barf counter ion and was similar to the predicted amount. The number of equivalents measured were similar to the predicted amount

The complexation of a cation may cause changes in the conformation of the host **$X_4Pr_2Im_2$**. For example, two ^{t}Bu signals were observed on the ^{1}H NMR spectra of **$X_4Pr_2Im_2$** but only one for the potassium complex. A way to observe the conformational changes upon complexation is by measuring the difference in chemicals shift ($\Delta\delta$). $\Delta\delta$ is calculated between ^{1}H NMR signals of a certain chemical group. δ depends on the distance of a chemical group from the C_2 axis of the calixarene (Figure 24). This is due to the shielding effect of the aromatic rings and implies that the further a group is from the main symmetry axis the higher its δ will be. Thus, a high $\Delta\delta$ indicates a large difference between the distance of a chemical group from the C_2 axis on different aromatic units.

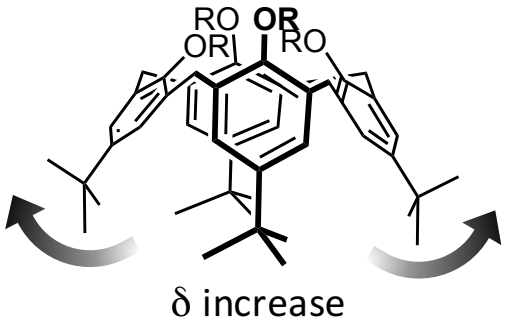

Figure 24 : Correlation between the calixarene conformation and the chemical shifts observed for the ArH and ^{t}Bu protons.

Thus, by measuring the $\Delta\delta$ of a chemical groups situated on the wide rim of **$X_4Pr_2Im_2$**, such as ArH and ^{t}Bu, and then comparing the measured values for the free ligand and the complexes, information on their conformation can be obtained (Table 1).

*Table 1 : $\Delta\delta$ of the ArH and ^{t}Bu of **$X_4Pr_2Im_2$**, **$X_4Pr_2Im_2\supset H^+$**, **$X_4Pr_2Im_2\supset Na^+$**, **$X_4Pr_2Im_2\supset K^+$**, and **$X_4Pr_2Im_2\supset Cu^+$** in ppm.*

	$\Delta\delta$ ArH (ppm)	$\Delta\delta$ ^{t}Bu (ppm)
$X_4Pr_2Im_2$	0.27	0.20
$X_4Pr_2Im_2\supset H^+$	0.39	0.25
$X_4Pr_2Im_2\supset Na^+$	0.03	0
$X_4Pr_2Im_2\supset K^+$	0	0
$X_4Pr_2Im_2\supset Cu^+$	0.83	0.56

When compared to the free ligand **$X_4Pr_2Im_2$**, the ArH $\Delta\delta$ of **$X_4Pr_2Im_2\supset Na^+$** decreased and the ^{t}Bu signals were overlapping each other, which indicates that all the aromatic units are oriented similarly and the calixarene scaffold is in a cone conformation (Figure 11).

Upon complexation of K^+, **$X_4Pr_2Im_2$** showed similar conformational changes as those of Na^+. Furthermore, only one ArH signal and one ^{t}Bu signal were observed on the ^{1}H NMR spectrum of **$X_4Pr_2Im_2\supset K^+$**, which also indicates a cone conformation. Even though K^+ (1.33 Å) has a larger ionic radius than Na^+ (0.97 Å), similar conformations between the two corresponding complexes are observed.

In contrast, on the ^{1}H NMR spectrum of **$X_4Pr_2Im_2\supset Cu^+$**, the $\Delta\delta$ of the ArH and ^{t}Bu increased from those of the free ligand. This implies that **$X_4Pr_2Im_2\supset Cu^+$** is in an even more pinched conformation than the free ligand. The aromatic units linked to the propyl groups are believed

to be upright and parallel to each other and the aromatic units linked to the imidazole groups are tilted towards the centre. This was hinted by the crystallographic structures of **$X_4Me_2Im_2$** presented above (Figure 14). As the interaction with the Cu^+ occurs specifically with the imidazole groups, their movements are likely to be responsible for the conformational changes observed.

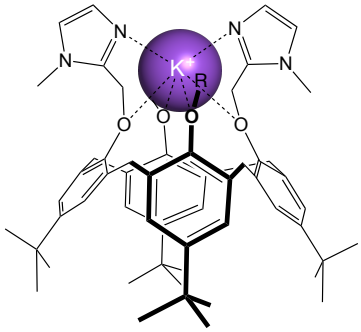

*Figure 25 : Cone conformations of **$X_4Pr_2Im_2$**⊃K^+ and potential interactions between **$X_4Pr_2Im_2$** and K^+.*

These observations suggest that Cu^+ interacts with **$X_4Pr_2Im_2$** in a different way than Na^+ does, despite the similar size of Na^+ and Cu^+ (0.96 Å). Na^+ and K^+ might not only or not at all interact with the lone electron pair of the nitrogen of the imidazole groups, but might interact with the lone pairs of oxygen of **$X_4Pr_2Im_2$** as previous studies highlighted.[20] Thus, in contrast to the interactions between **$X_4Pr_2Im_2$** and Cu^+, the interactions with Na^+ and K^+ are not specific to the imidazole groups.

2.2.3. Estimation of the affinity constants of $X_4Pr_2Im_2$ for K^+ and other cations

The complexation process involves a host (H), a guest (G) and a host-guest complex (HG), and is defined by a complexation constant K_a (Equation 1).

$$K_a = \frac{[HG]}{[H][G]} \qquad \textit{Equation 1}$$

Considering that when adding 1.0- 1.5 equivalent of H^+, Na^+, or Cu^+ to the free ligand **$X_4Pr_2Im_2$** (separately), the initial set of ^{1}H NMR signals was not observable anymore. The complexation constant K_a (Equation 1) of **$X_4Pr_2Im_2$** for H^+, Na^+, and Cu^+ could not be determined directly as the amount of free host is too low to be detectable by ^{1}H NMR spectroscopy. Considering that the detection limit of ^{1}H NMR spectroscopy is in the order of 10^{-4} M and that the free guest was not observable after adding only one equivalent of guest, it is estimated that the concentration of free host is lower than 10^{-4} mol. Thus, the K_a of **$X_4Pr_2Im_2$** for H^+, Na^+, and Cu^+ is at least 10^4 mol^{-1}. The number of equivalents of H^+, Na^+, K^+ and Cu^+ added in order for the initial set of signals to be undetectable were compared and a ranking of the K_a was established.

$$K_a\,(Na^+) > K_a\,(Cu^+) \cong K_a\,(H^+) >> K_a\,(K^+)$$

As the affinity of **$X_4Pr_2Im_2$** for K^+ was lower, the K_a could be determined directly from the titration. The complexation constant for the binding of **$X_4Pr_2Im_2$** with K^+ was evaluated by following the chemical shift ($\Delta\delta$) of the two CH_2 signals of the propyl chain and an aromatic signal during the titration.

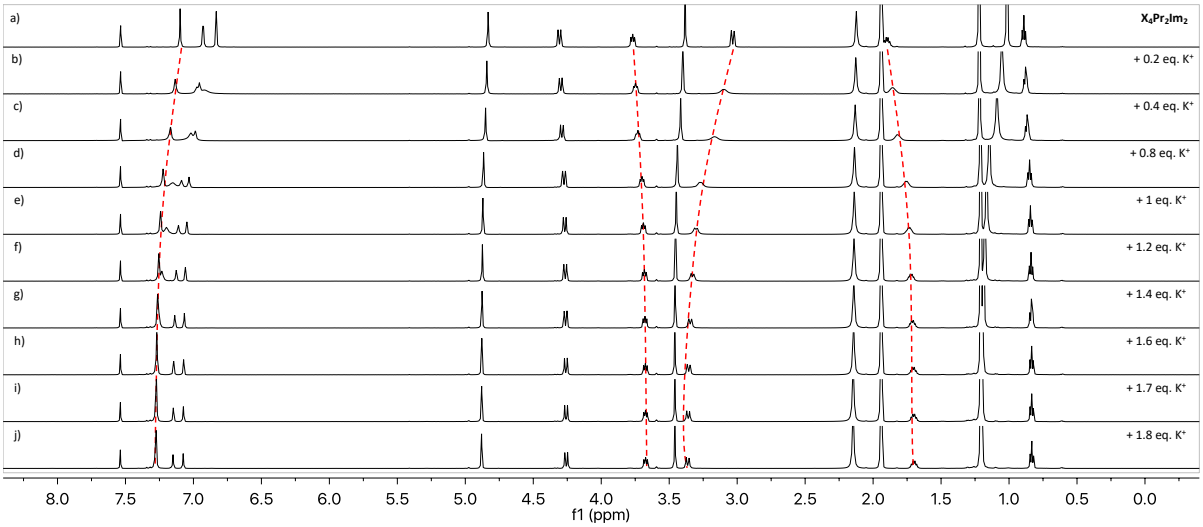

Figure 26 : ^1H NMR titration of $X_4Pr_2Im_2$ (4.9 mM in CD_3CN/$CDCl_3$ 4:1) with $K^+PF_6^-$ (245 mM in CH_3CN) at 298 K, 600 MHz.

By combining the formula of the complexation constant, the mass balance equations (Equation 2 and Equation 3), and the measurement of a physical value (observed chemical shifts $\Delta\delta_{obs}$) proportional to the concentration of the free species and host guest complex in the systems (Equation 4) a value for K_a was determined. [I]

$$[H]_0 = [H] + [HG] \qquad \textit{Equation 2}$$

$$[G]_0 = [G] + [HG] \qquad \textit{Equation 3}$$

$$\Delta\delta_{obs} = \Delta\delta_H[H] + \Delta\delta_{HG}[HG] \qquad \textit{Equation 4}$$

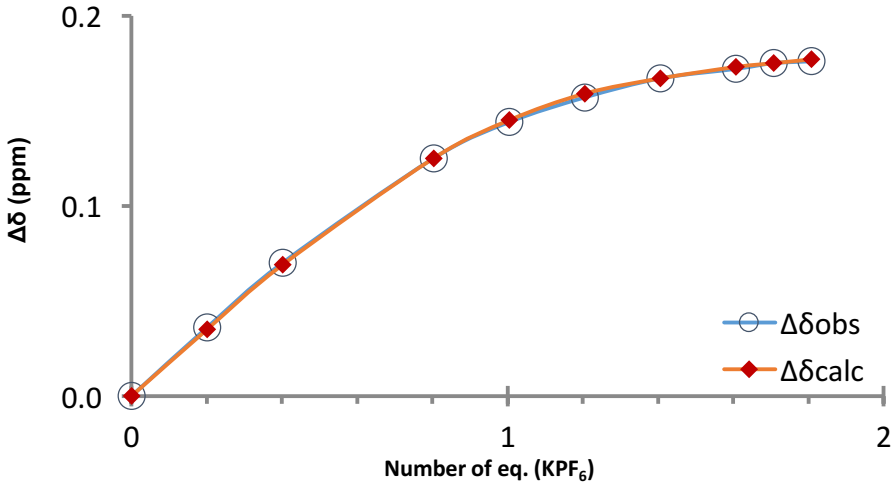

*Figure 27 : Fitting curve for the complexation of **$X_4Pr_2Im_2$** by K^+ ($K^+PF_6^-$).*

[I] The titration could have been extended until the signal did not change anymore and a plateau was reached.

The experimental data were fitted using a non-linear least square regression, which gave a value for K_a of $2400 \pm 70\ M^{-1}$ (error from the fit) which is at least one order of magnitude lower than for H^+, Na^+, and Cu^+. The lower affinity of **$X_4Pr_2Im_2$** for K^+ might be due to the bigger size of K^+ cations resulting in a poorer fit between the host and the guest.

2.2.4. Competitive binding studies

Competitive binding studies were conducted in order to determine the K_a of H^+, Na^+ and Cu^+ with **$X_4Pr_2Im_2$**. The objective was to obtained a value for K_{rel} (Equation 5) between K^+ and Cu^+ with $X_4Pr_2Im_2$ in order to calculate $K_a(Cu^+)$. Similar additions of Cu^+ were used to also obtain $K_a(H^+)$ and $K_a(Na^+)$.
The NMR tubes used for the protonation of **$X_4Pr_2Im_2$** and its complexation with Na^+ and K^+ were then used to evaluate the relative affinity of **$X_4Pr_2Im_2$**, between Cu^+ and these cations. The tubes were titrated with a copper solution by 0.5 equivalent increments until the same number of equivalent as the other cation already present was reached. The integral of the signals corresponding to the different species were compared on the ^1H NMR spectra in order to calculate the relative affinity (Equation 5) of **$X_4Pr_2Im_2$** (H) for copper relative to other cations (X^+). The integrals of the OCH_2Im signals of both species were measured and compared (Figure 28d).

$$K_{rel} = \frac{K_a(Cu^+)}{K_a(X^+)} = \frac{[H{\supset}Cu^+]}{[H{\supset}X^+]} \frac{[X^+]}{[Cu^+]} \qquad \textit{Equation 5}$$

As the affinity of **$X_4Pr_2Im_2$** for Cu^+ is significantly higher than for K^+, when added in the same amount, **$X_4Pr_2Im_2$**$\supset K^+$ concentration was too low to be observable, thus K_{rel} and $K_a(Cu^+)$ could not be calculated. The K_{rel} calculated with H^+ and Na^+ were highly variable between different spectra and the results are thus not presented.
However, by measuring a ratio between the integrals of the complexes signals (in blue on Figure 28) with the same amount of both guest, qualitative information on the competitive binding of **$X_4Pr_2Im_2$** with cations were obtained. The results are summarised in Table 2 (see page 22).

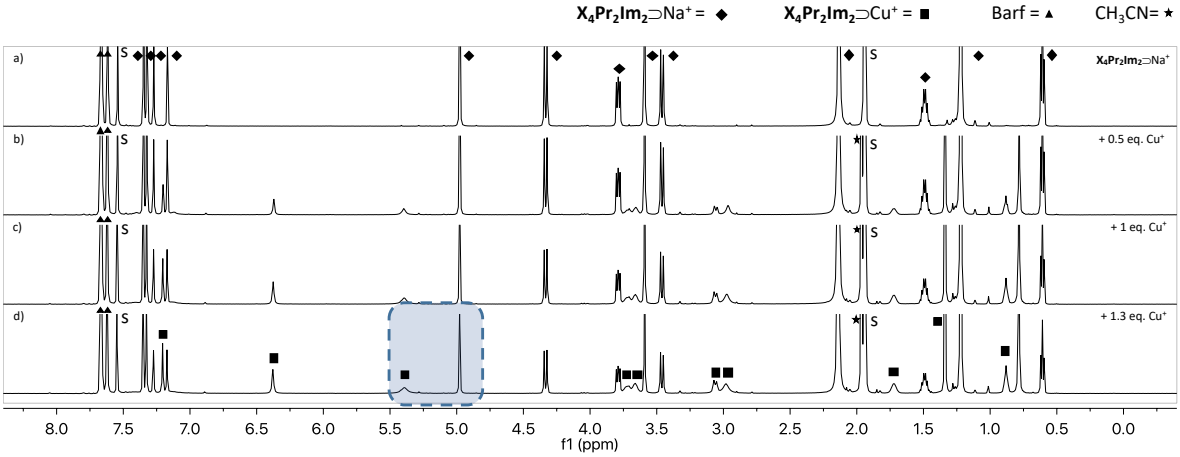

*Figure 28 : ^1H NMR titration of **$X_4Pr_2Im_2$**$\supset Na^+$ (1.3 eq. of NaBarf added) with Cu(I)$(CH_3CN)_4BF_4$ (37.8 mM in CH_3CN) at 298 K, 600 MHz.*

Two sets of signals were visible on the ^{1}H NMR titration of **$X_4Pr_2Im_2$⊃Na^+** by Cu^+ (Figure 28d), the initial complex and the Cu^+ complex. This means that the exchange rate between **$X_4Pr_2Im_2$⊃Na^+** and **$X_4Pr_2Im_2$⊃Cu^+** was slow on the NMR time scale. The same observations were made when titrating **$X_4Pr_2Im_2$⊃H^+** and $X_4Pr_2Im_2$⊃K^+ with Cu^+.
$X_4Pr_2Im_2$ showed a similar affinity for Cu^+ than for H^+, a higher one than for K^+ and a lower one than for Na^+. When adding only one equivalent of Cu^+, **$X_4Pr_2Im_2$⊃K^+** was not observable anymore in the ^{1}H NMR spectra. In contrast, with the same number of H^+ and Cu^+ equivalents, the intensities of the respective **$X_4Pr_2Im_2$** complexes were on par. The relative intensities observed on the ^{1}H NMR spectra where the same amount of Na^+ and Cu^+ is present were calculated at 1.5 (Table 2 p22). These observations are in agreement with the ranking of the affinity of **$X_4Pr_2Im_2$** for H^+, Na^+, K^+, and Cu^+.

2.2.5. ^{1}H NMR complexation studies of $X_4Me_2Im_2$

The same NMR studies as done with **$X_4Pr_2Im_2$** were performed with $X_4Me_2Im_2$. As mentioned previously, the ^{1}H NMR signals of the free ligand are broad and poorly defined. In contrast, all the complexed species of **$X_4Me_2Im_2$** were sharp, and the complexes formed with Cu^+ and Na^+ are well defined (Figure 29). This is likely to be caused by the conformational rigidification of the complexed species, as the presence of the guest prevents the rotation of the aromatic units. This was already proposed by previous complexation studies of calix[4]arenes able to adopt 1,3 alternate conformation.[19] The complexation of **$X_4Me_2Im_2$** with K^+ showed a third species which could not be assigned.[I]

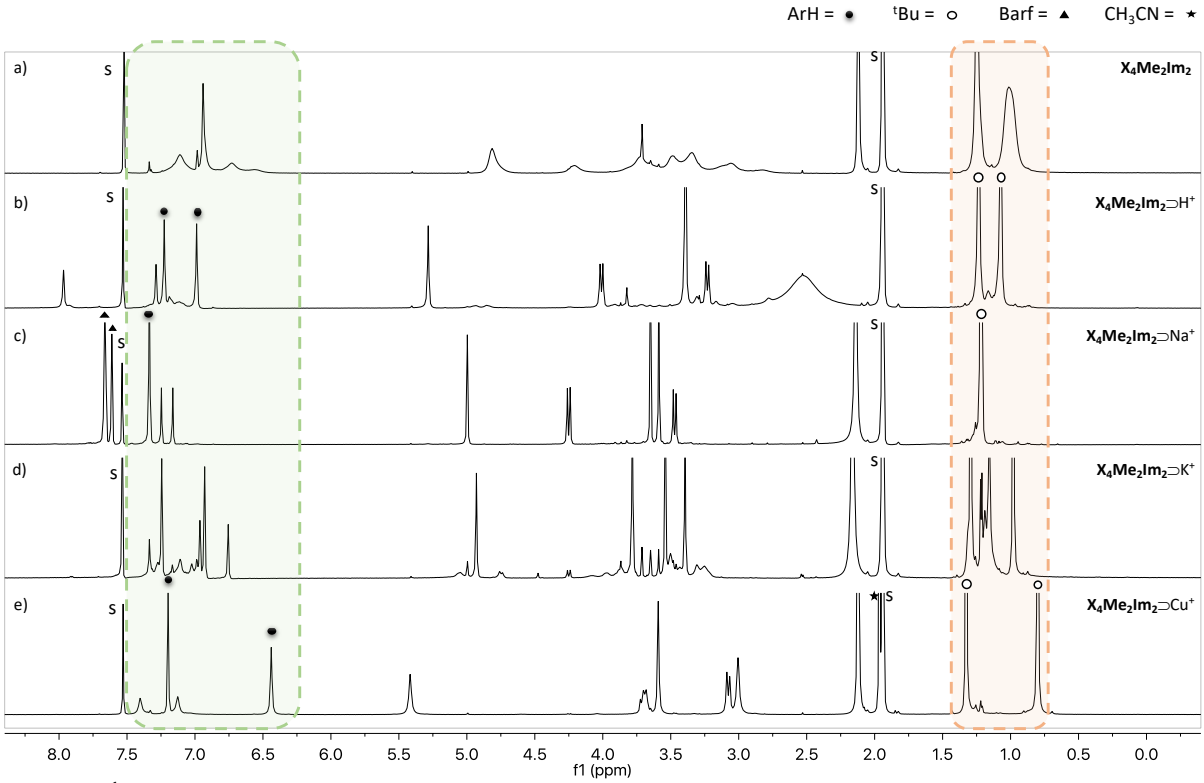

*Figure 29 : ^{1}H NMR spectra of **$X_4Me_2Im_2$** (4.5 mM), **$X_4Me_2Im_2$⊃Cu^+** (1 eq. of $Cu(I)(CH_3CN)_4BF_4$ added), **$X_4Me_2Im_2$⊃H^+** (1.3 eq. of TFA added), **$X_4Me_2Im_2$⊃Na^+** (1.1 eq. of NaBarf added), and **$X_4Me_2Im_2$⊃K^+** (1.4 eq. of $K^+PF_6^-$ added) in $CD_3CN/CDCl_3$ at 298 K, 600 MHz.*

[I] The full set of ^{1}H NMR spectra of the titrations can be found in the experimental section (Figure X 12 to Figure X 15).

Similarly, to **$X_4Pr_2Im_2$** the exchange between H^+, Na^+ and Cu^+ was slow on the NMR time scale because two sets of signals were observed. The changes in conformation due to the protonation and the complexation of Na^+ and Cu^+ by **$X_4Me_2Im_2$** were similar as with **$X_4Pr_2Im_2$**. However, the complexation of K^+ with **$X_4Me_2Im_2$** was not in slow exchange. Instead, the ^1H NMR spectra were difficult to assign as a third species was observed as well.
The ratios of the integral of the OCH_2Im signals between complexes were also measured and compared (Table 2) giving an idea of the selectivity of **$X_4Me_2Im_2$** and **$X_4Pr_2Im_2$** for Cu^+.
The relative affinity for H^+ and Na^+ compared to Cu^+ is higher with **$X_4Me_2Im_2$** than with **$X_4Pr_2Im_2$**. However, the ranking of the affinities for **$X_4Me_2Im_2$** with cations remained the same as **$X_4Pr_2Im_2$**.[I]

*Table 2 : Ratios of the OCH_2Im signals integrals on the ^1H NMR spectra of **$X_4Me_2Im_2$** and **$X_4Pr_2Im_2$** with an equal amount of Cu^+ and of H^+, Na^+, and K^+ added.*

Ratio	**$X_4Me_2Im_2$**	**$X_4Pr_2Im_2$**
H^+/Cu^+	1.5	1
Na^+/Cu^+	4	1.5
K^+/Cu^+	/	<0.05

$X_4Pr_2Im_2$ showed a greater selectivity for Cu^+ than **$X_4Me_2Im_2$**. Both calixarenes **$X_4Me_2Im_2$** and **$X_4Pr_2Im_2$** were able complex Cu^+ in presence of H^+, Na^+, and K^+. A previous study has highlighted the affinity of alkali metal cations for calix[4]arene in 1,3 alternate conformations.[13] The difference in Cu^+ selectivity between **$X_4Me_2Im_2$** and $X_4Pr_2Im_2$ could depend on their ability to adopt 1,3 alternate conformations. As **$X_4Me_2Im_2$** is able to adopt 1,3 alternate conformations and **$X_4Pr_2Im_2$** is not, it has higher affinities for alkali metal cations than **$X_4Pr_2Im_2$**.

Still both **$X_4Pr_2Im_2$** and **$X_4Me_2Im_2$** were tested as potential Cu^+ transmembrane transporters. The link between affinity for cations in organic solvents and transport capabilities in water has been observed already but has never been proven to be valid in all conditions, the relations between the two phenomena will be discussed later on. [29]

[I] All other ^1H NMR spectra can be found in the experimental section (in Figure X 19 to Figure X 21).

2.3. Transmembrane transport studies of copper(I)

In order to test the capacities of **$X_4Pr_2Im_2$** and **$X_4Me_2Im_2$** to transport copper(I) cations through a bilayer membrane, an assay was developed. As copper transport by synthetic transporters has never been tested or reported in the literature, developing an assay to evaluate the transport came with a set of challenges.

The water-insoluble transporter **$X_4Pr_2Im_2$** and **$X_4Me_2Im_2$** had to be incorporated in a bilayer membrane. To allow transport studies, large unilamellar vesicles (LUVs) were used as model systems for the bilayer membrane to monitor transport of copper(I) from the outside to the inside of LUVs (Figure 30).

A mean of detection and quantification of the copper(I) transport through the membrane had to be found. A probe sensitive to copper(I) (BCS, see 2.3.2) was encapsulated inside the liposomes, allowing to monitor the transport of copper(I) through a bilayer membrane by fluorescence spectroscopy.

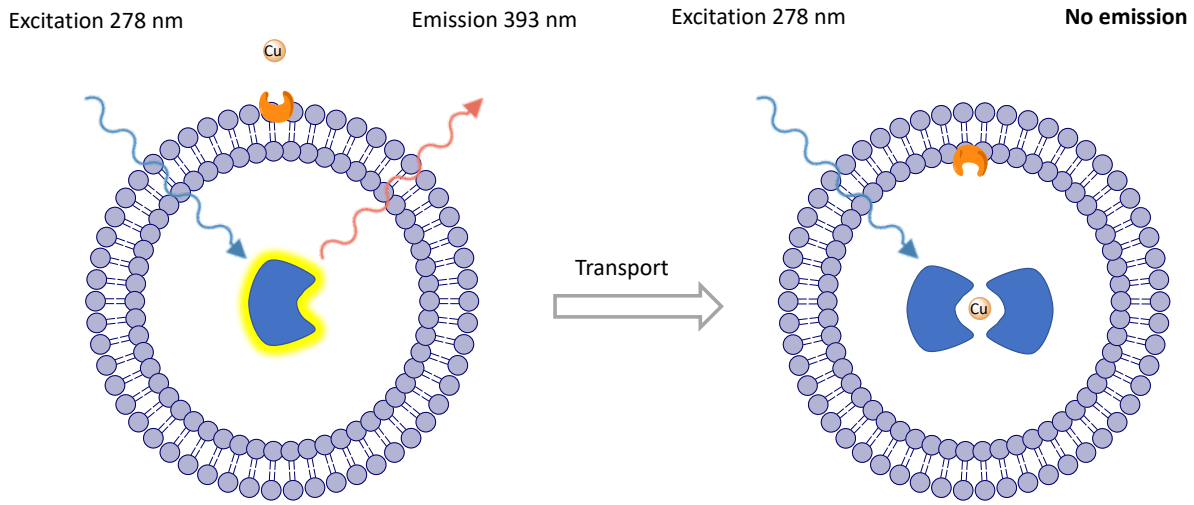

Figure 30 : Transport of Cu^+ (orange) into a liposome by a carrier: diagram of the transport process as monitored by fluorescence spectroscopy.

The transport of a charged species by a transporter into the liposomes creates a charge imbalance which must be compensated (Figure 31). It is likely that the charge imbalance is compensated by the transport of another cation out of the liposome. As these experiments are set up artificially, the transporter counter ions (X^+) can be chosen. The main cations made available to the transporter in the system were Na^+ or K^+ from the phosphate buffer solutions.

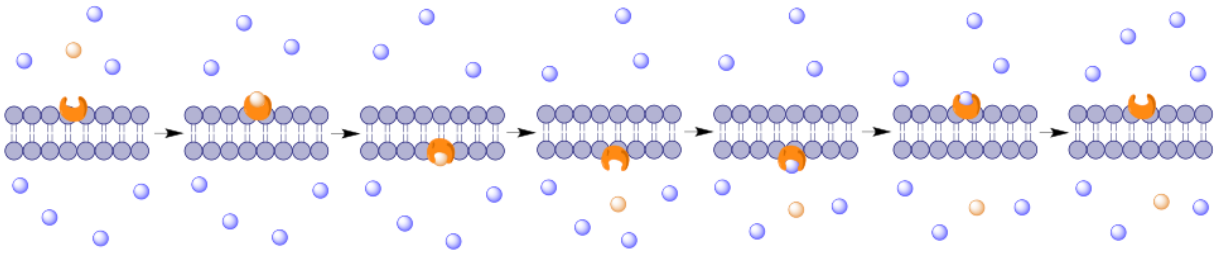

Figure 31 : Diagram of Cu^+ transport: exchange of cations X^+ (blue) with Cu^+ (orange) by a carrier through a lipid bilayer of LUVs.

Another challenge was to obtain an aqueous solutions of copper(I) at high enough concentrations for transport experiments as the solubility of copper(I) in water is low and reported to be around 50 mg/L at room temperature.[30] In order to obtain a higher amount of copper(I) in solution, an aqueous solution of copper(II) was mixed with sodium ascorbate (or ascorbic acid). It has been reported that ascorbate reduces copper(II) into copper(I). [31]

2.3.1. Preparation of liposomes

In order to make a lipid bilayer membrane containing the transporter, lipids (POPC and cholesterol) and calixarene were gathered in $CHCl_3$. Upon evaporation of the solvent, lipid films containing the transporter were formed. To obtain stable (and flexible) liposomes, the ratio of POPC/cholesterol was kept constant (7/3) and the ratio of transporter to lipid was varied from 1/200 to 1/5000.
A solution containing the fluorescent probe is added to the lipid films in order to encapsulate the probe inside the liposomes. The mixture was briefly sonicated to break up the lipid films and stirred to allow the formation of the liposomes. In order destroy multilamellar vesicles, the solution was frozen with liquid nitrogen and heated back to room temperature multiple times. The mixture was then passed through a membrane with 200 nm pores, to get liposomes around that size. The size distribution was verified by dynamic light scattering and showed a size distribution close to 200 nm (Figure X 32).
In order to remove most of the dye molecules that were not encapsulated in the liposomes, the solution was passed through a size exclusion column. Since the liposomes are significantly larger than the dye molecules, they elute before the dye. Although the separation was never complete and some of the dye molecule remained outside of the liposomes.

Liposomes were then diluted with a buffer solution to obtain the desired concentration (0.4 mM in lipids). Apart from the dye, the inside and the outside of the liposomes had the same salt concentration and the system is at equilibrium. To avoid the potential risk that the dye molecules could leak out of the liposomes. The transport measurements were made in hours following the preparation of the liposomes.

2.3.2. Detection of copper(I) with the dye BCS

Bathocuproinedisulfonic acid (BCS), a derivative of phenantroline, is reported in the literature as a copper(I) chelator and forms a 1:2 copper complex. [26] When exposed to light at specific wavelengths BCS is fluorescent, but upon interaction with copper(I) the fluorescence is quenched.[32]

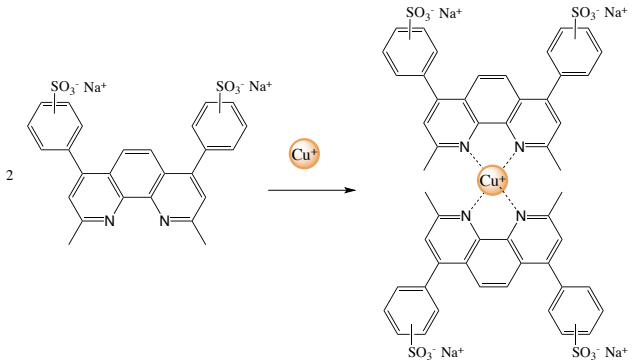

Figure 32 : Reaction of BCS with copper(I) : formation of a 2:1 BCS:Cu^+ complex.

The absorption and emission spectra of the dye solution were measured and titrations with copper(I) were performed in order to verify the reported properties and to potentially obtain a relation between the amount of quenched fluorescence and the amount of copper(I). This could allow to measure the speed at which the copper(I) transport occurs.

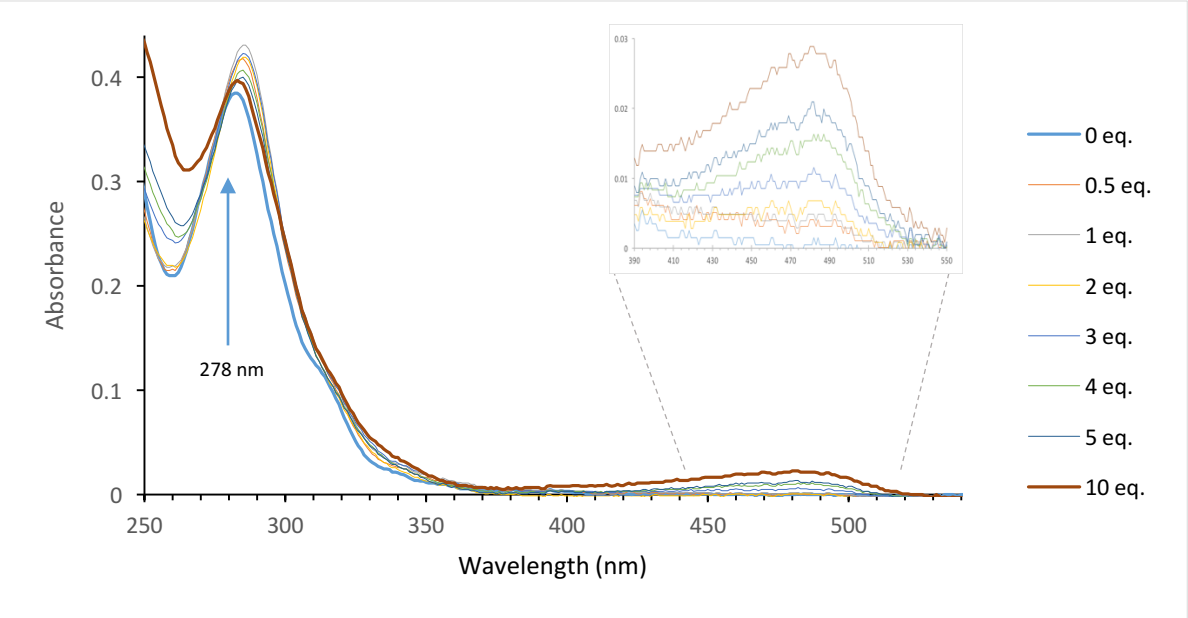

Figure 33: Absorption spectra of a 10 μM BCS solution (in a 100 mM potassium phosphate buffer at pH 7) titrated by a solution of $CuCl_2$ 0.5 mM and 0.5 mM sodium ascorbate The added amount of copper (I) expressed in number of equivalent relative to BCS.

The absorption spectrum of BCS showed an absorption band at 280 nm. The addition of copper(I) induced a slight bathochromic shift and a new absorption band was observed at 479 nm, which gave an orange colour to the solution. At 278 nm, an isobestic point was observed. These results matched with what was reported in the literature although the isobestic was never mentioned.

The titration of the BCS solution was also followed by fluorescence spectroscopy. The excitation was set at the isobestic point (278 nm) in order to maintain the same amount of absorption throughout the measurements, as it allows to guarantee that the changes observed in the emission spectrum were only due to a change in fluorescence.

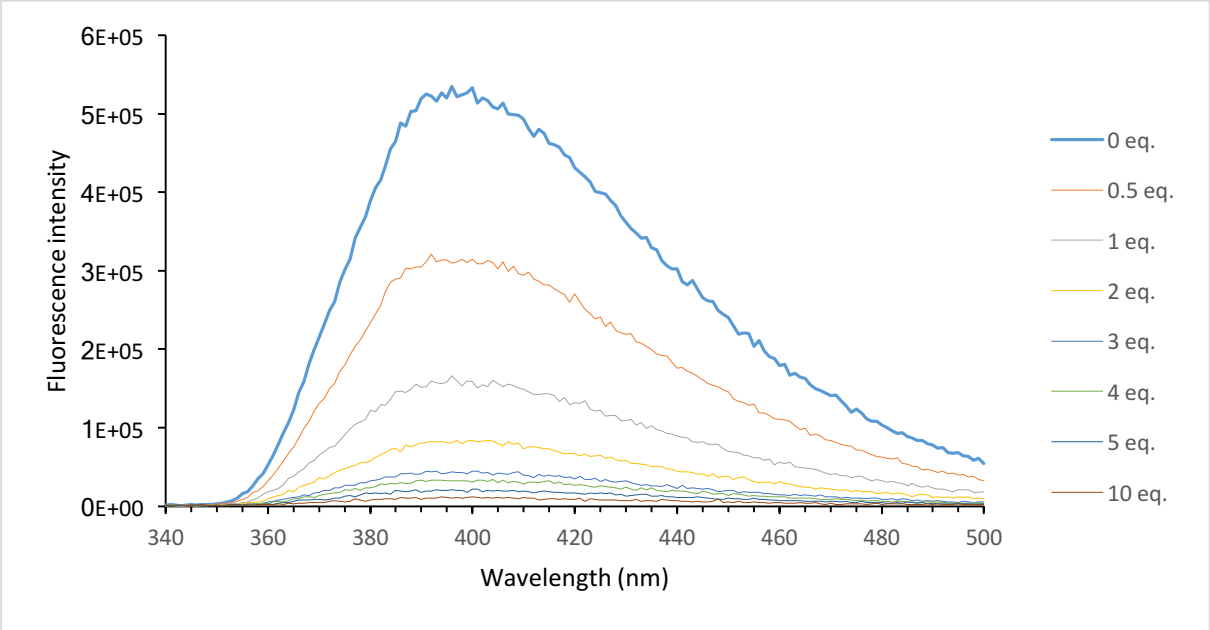

Figure 34: Emission spectra of a 10 μM BCS solution (in a 100 mM potassium phosphate buffer at pH 7) titrated by a solution of $CuCl_2$ 0.5 mM and 0.5 mM sodium ascorbate The added amount of copper (I) expressed in number of equivalent relative to BCS.

The emission spectra of the BCS solution showed a spectral band at 395 nm. The emission band shows a significant decrease in intensity with the addition of the copper solution. The decrease of the fluorescence intensity and its inverse were plotted in Figure 35, the second according to the Stern-Volmer equation (Equation 6), which describes a photophysical intermolecular deactivation process).[33]

$$\frac{F_0}{F} = 1 + K_{sv}[Cu^+] \qquad \textit{Equation 6}$$

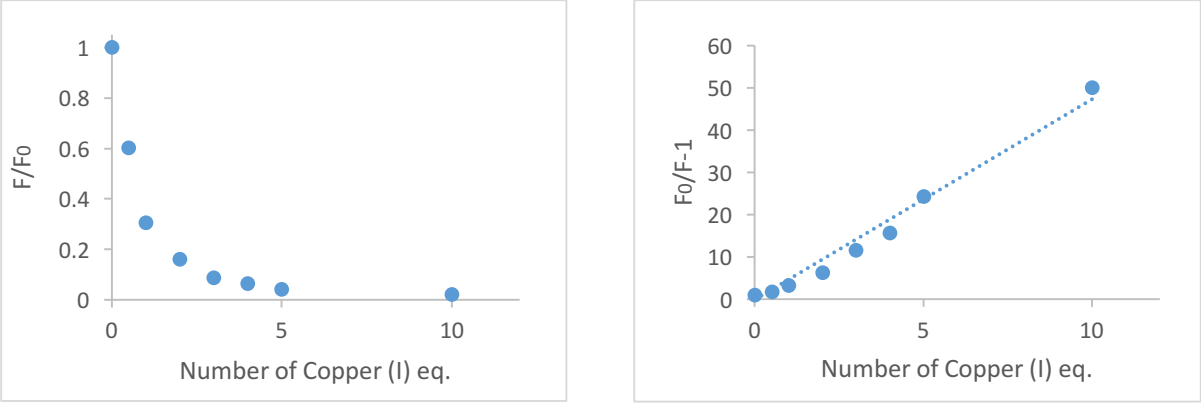

Figure 35 : Normalized fluorescence intensity decrease and Stern-Volmer plot of a 10 μM BCS solution (in a 100mM potassium phosphate buffer at pH 7) titrated by a solution of $CuCl_2$ 0.5 mM and 0.5 mM sodium ascorbate The added amount of copper (I) expressed in number of equivalent relative to BCS. Reduction of intensity expressed as the maximum fluorescence value (F_0) divided by the fluorescence (F), the fraction is subtracted by one.

The Stern-Volmer plot did not show a convincing linear trend and thus another fitting was performed according to a 1:2 binding process. This gave out a good fit but large errors on the high K_a values. A value for the product of the Ka's for the formation of the 1:1 complex and the 1:2 was reported in the literature and was in agreement with the results given here. BCS is also able to complex copper(II) but has a significantly higher affinity for copper(I).[26] Still

upon addition of copper(I) the fluorescence intensity decreased significantly enabling the detection of copper(I) transport.

It was also verified whether the complex showed a fluorescence signal when excited at 479 nm. Such fluorescence would allow to follow the formation of the complex instead of its disappearance. However, no significant fluorescence was observed when the solution of the complex was excited at 479 nm.
When compared to the literature on BCS, results obtained in this optical study showed interesting differences. Some of the literature on the optical properties of BCS described an emission band at 770 nm when excited at 580 nm and a linear decrease of the fluorescence with the Cu^+ concentration.[26] Similar observations were made but the intensity of the spectral band at 770 nm was very low, and it turned out that the fluorescence observed was only second order diffracted light, so that the reported phenomenon was the result of a common artefact. This was verified in another report by adding an optical filter (which to cut out light at wavelength under 460 nm) and no emission at 770 nm was found.[34]

2.3.3. Test of the transport assay

When designing an assay for copper(I) transport some parameters had to be determined such as the concentration of species in the system. The fluorescence intensity of BCS at different concentrations was evaluated and optimised. The objective was to determine the lowest concentration were the signal was still significant in order to observe large signal variation. A solution of 10 μM BCS had the desired characteristics and as a rule of thumb the dilution factor between the solution used to hydrate the lipid film and the final concentration in LUVs is around a thousand. Thus the liposomes were prepared with 10 mM BCS concentration inside. For copper a concentration of copper(II) and sodium ascorbate (or ascorbic acid) low enough to be soluble in all the tested salt solution was found and was 0.5 mM. Ascorbate was added in excess in order to reduce all copper(II), the ascorbate concentration was set at 0.5 mM.
For each molecules of ascorbate, two copper(II) will be reduce.[31]

Having established all key components for an assay to test transport of Cu^+ a first experiment was performed with a high ratio of transporter (**$X_4Pr_2Im_2$**, 1:200) as a proof of concept. The liposome solution was transferred into a cuvette and placed in the spectrometer. For each measurement, the amount of fluorescence at 393 nm was measured over time when exciting at 278 nm. After 30 seconds of measurement, a copper solution prepared in the same buffer solution as the liposomes was added with a pipette through an opening situated above the cuvette. This creates a gradient of copper(I) of approximately 0.1 mM. The changes in signal were then recorded for at least 10 minutes or until the signal did not change significantly anymore. If the signal reaches a plateau, it means that the equilibrium is reached and thus that the concentrations of free copper(I) inside and outside of the liposomes are equal. In order to verify if the measurements were reproducible, the experiments were repeated two to four times. The signal was expected to drop abruptly at the start of the measurement due to the complexation of remaining external dye, thus the signal was plotted only after this initial drop. The results obtained were normalised and averaged.
For each experimental condition, a blank experiment was also prepared as a mean of control. For these blank experiments, liposomes were prepared without any transporter and tested in the same conditions as the other experiments. The fluorescence signal of the blank is not

expected to decrease significantly, apart from an initial drop due to the quenching of the remaining external dye.

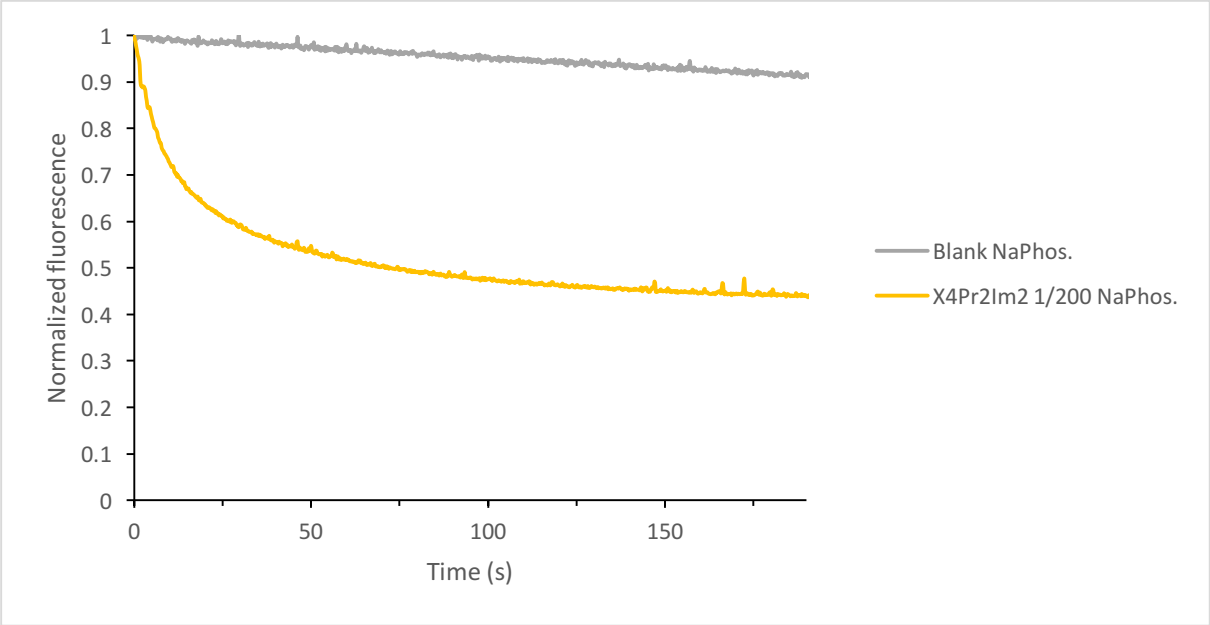

Figure 36 : Transport measurements of Cu(I) by following the decrease of fluorescence of BCS (excitation at 278 nm, emission at 393 nm) encapsulated inside LUVs with ***$X_4Pr_2Im_2$*** *(1/200 transporter to lipids ratio) in 100 mM sodium phosphate buffer (pH 7). Addition of 200 µL of a 1.8 mM $CuCl_2$ and 0.9 mM sodium ascorbate in 100 mM sodium phosphate buffer (pH 7) to 2.8 mL LUVs (0.4 mM lipids) created a Cu^+ gradient. Results were normalized and averaged and a blank measurement is shown for comparison.*

The curve observed in Figure 36, showing a progressive decrease of the fluorescence with time, was a first potential sign of copper(I) transport. Further control experiments were conducted to confirm that the decrease of signal intensity was due to copper(I) transport. Additions of either $CuCl_2$, Cu_2SO_4, or sodium ascorbate were made and also showed a decrease in signal but less than with $CuCl_2$ and sodium ascorbate added together. The decrease of the signal upon addition of copper(II) was assigned to the partial spontaneous reduction of copper(II) into copper(I) in solution and thus its interaction firstly with the external dye and then potential transport into the LUVs. The decrease of the signal upon addition of sodium ascorbate was assigned to the degradation of the external dye molecules. When no addition was made still the signal upon excitation slightly decreased with time due to photobleaching or decomposition of the dye.

2.3.4. Transport results

The impact of different parameters on transport such as the buffer solution, transporter structure, and transporter concentration were evaluated. The results were compared by looking at the rate at which the fluorescence intensity decreased. The faster the decrease in fluorescence intensity, the faster the transport of copper(I) occurred. But in order to compare the results quantitatively, the recorded curves were fitted to a single exponential (Equation 7) and half-life values (Equation 8) were obtained.

$$\frac{F}{F_0} = y - ae^{-bt} \qquad \text{Equation 7}$$

$$t_{1/2} = \frac{ln\,(2)}{b} \qquad \text{Equation 8}$$

- Concentration dependence

The capacities of the two synthesized calixarenes to transport copper(I) were tested using the developed assay. Different transporter to lipid ratios of **$X_4Pr_2Im_2$** were tested, and the transport rates were expected to be proportional to the concentration of transporter in the membrane. The time needed for the system to reach equilibrium should follow the same trend.

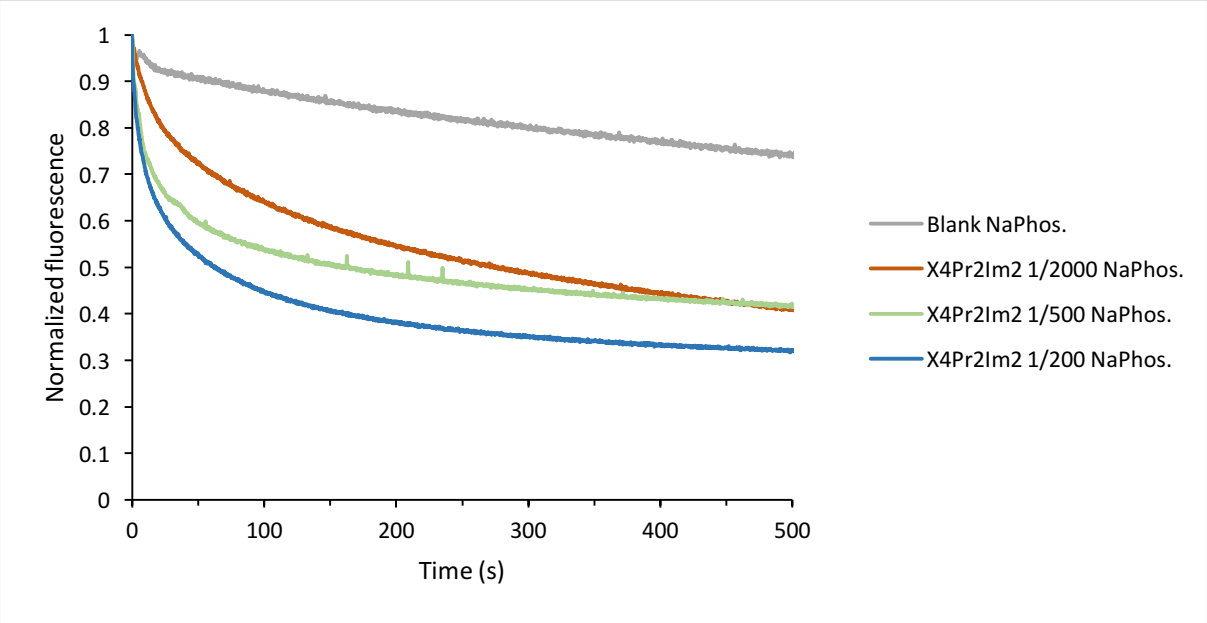

*Figure 37: Comparison between different transporter (**$X_4Pr_2Im_2$**) concentrations. Transport measurements of Cu(I) by following the decrease of fluorescence of BCS (excitation at 278 nm, emission at 393 nm) encapsulated inside LUVs with $X_4Pr_2Im_2$ (1/200, 1/500, 1/2000 transporter to lipid ratios) in 100 mM sodium phosphate buffer (pH 7). Addition of 200 µL of a 0.5 mM $CuCl_2$ and 0.5 mM sodium ascorbate in 100 mM sodium phosphate buffer (pH 7) to 2.8 mL LUVs (0.4 mM lipids) created a Cu^+ gradient. Results were normalized and averaged and a blank measurement is shown for comparison.*

The half-life values obtained indeed showed a trend, with higher transporter concentrations showing shorter half-life. The measurements recorded with a 1/200 transporter to lipid ratio showed a half-life of 140 seconds, the 1/500, 170 s and the 1/2000, 430 s.

- Influence of the alkyl chain on the calixarene

The only structural difference between the two molecules are the size of the alkyl chain on the narrow rim. **$X_4Pr_2Im_2$** has a higher relative affinity for copper(I) relative to sodium, potassium and protons than **$X_4Me_2Im_2$** so it was expected to display better transport abilities.

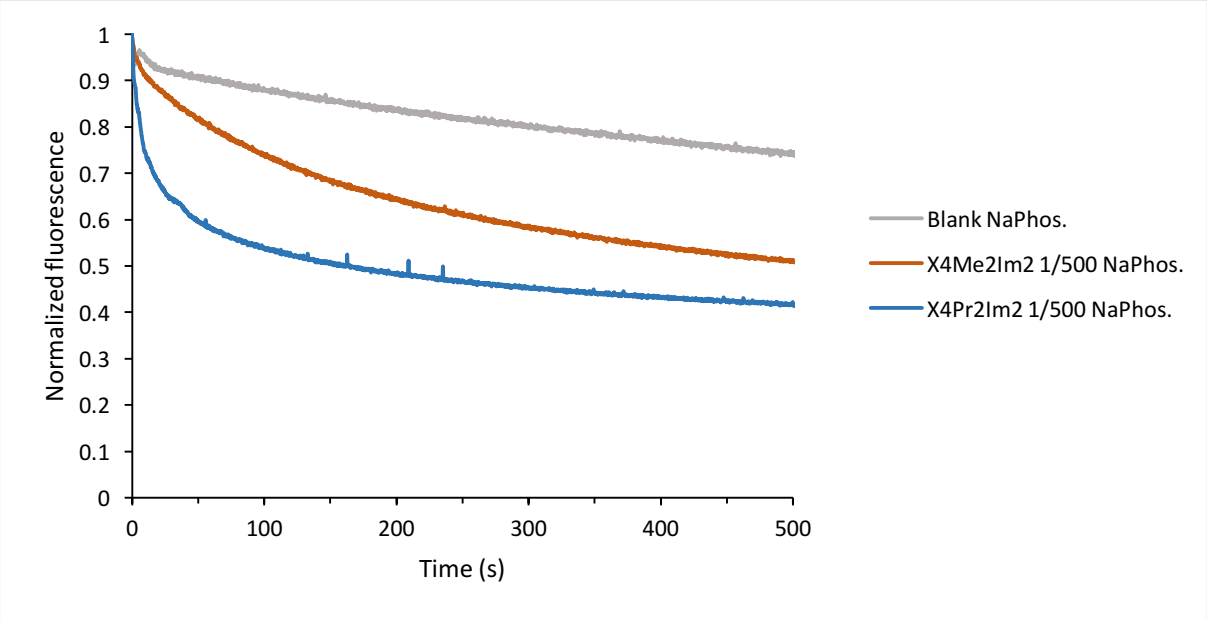

*Figure 38: Comparison between **$X_4Pr_2Im_2$** and **$X_4Me_2Im_2$**. Transport measurements of Cu(I) by following the decrease of fluorescence of BCS (excitation at 278 nm, emission at 393 nm) encapsulated inside LUVs with $X_4Pr_2Im_2$ and $X_4Me_2Im_2$ (1/500 transporter to lipids ratio) in 100 mM sodium phosphate buffer (pH 7). Addition of 200 μL of a 0.5 mM $CuCl_2$ and 0.5 mM sodium ascorbate in 100 mM sodium phosphate buffer (pH 7) to 2.8 mL LUVs (0.4 mM lipids) created a Cu^+ gradient. Results were normalized and averaged and a blank measurement is shown for comparison.*

$X_4Me_2Im_2$ showed significantly slower transport than **$X_4Pr_2Im_2$** at the same transporter concentration (Figure 38). The half-life value obtained for **$X_4Me_2Im_2$** was 400 seconds which is more than double that for $X_4Pr_2Im_2$ at the same concentration (1/500, 170 s). These observations are consistent with the ^{1}H NMR cations complexation results, the selectivity for copper(I) of **$X_4Pr_2Im_2$** was higher than **$X_4Me_2Im_2$** and could explain the difference in transport rates between the two transporters.

- Salt solution implications: cation exchange

By changing the buffer solution, the cation transported to compensate the charge is changed and this could impact copper(I) transport. Two conditions were tested: sodium and potassium phosphate, with of **$X_4Pr_2Im_2$** and **$X_4Me_2Im_2$** at the same concentration and the rates of transport were compared. As the affinity of $X_4Pr_2Im_2$ and **$X_4Me_2Im_2$** for Na^+ is higher than for K^+ different transport rates were expected between the two conditions.

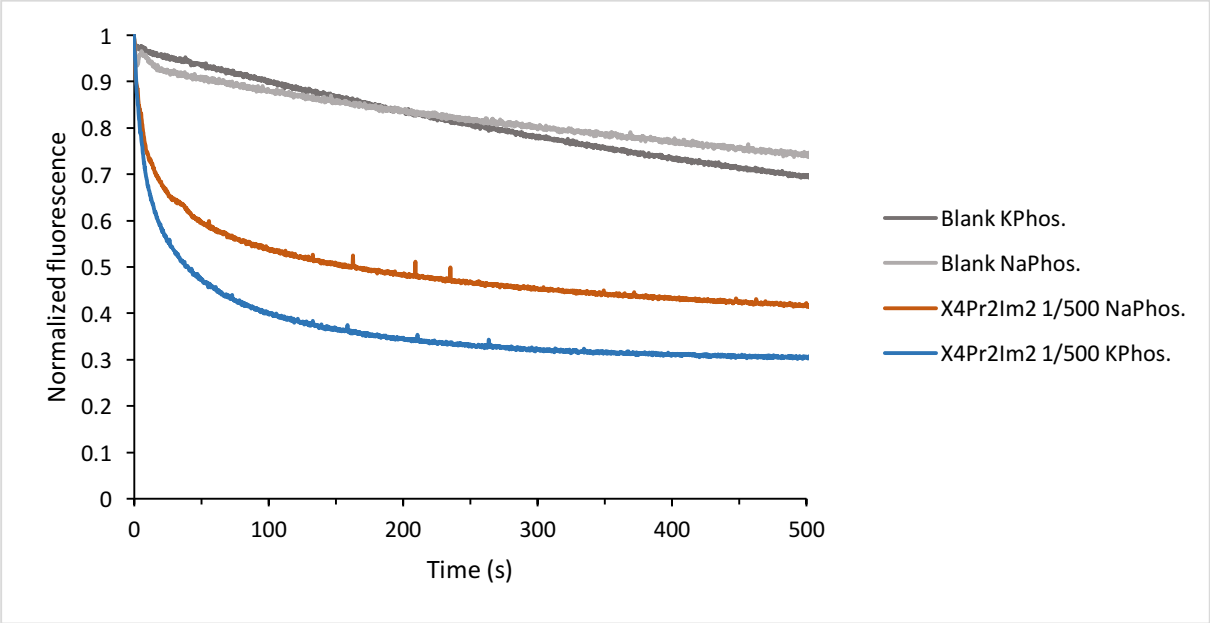

Figure 39: Comparison between sodium and potassium phosphate buffers using ***$X_4Pr_2Im_2$****. Transport measurements of Cu(I) by following the decrease of fluorescence of BCS (excitation at 278 nm, emission at 393 nm) encapsulated inside LUVs with* ***$X_4Pr_2Im_2$*** *(1/500 transporter to lipids ratio) in 100 mM sodium/potassium phosphate buffer (pH 7). Addition of 200 µL of a 0.5 mM $CuCl_2$ and 0.5 mM sodium ascorbate in 100 mM sodium/ potassium phosphate buffer (pH 7) to 2.8 mL LUVs (0.4 mM lipids) created a Cu^+ gradient. Results were normalized and averaged and blank measurements are shown for comparison.*

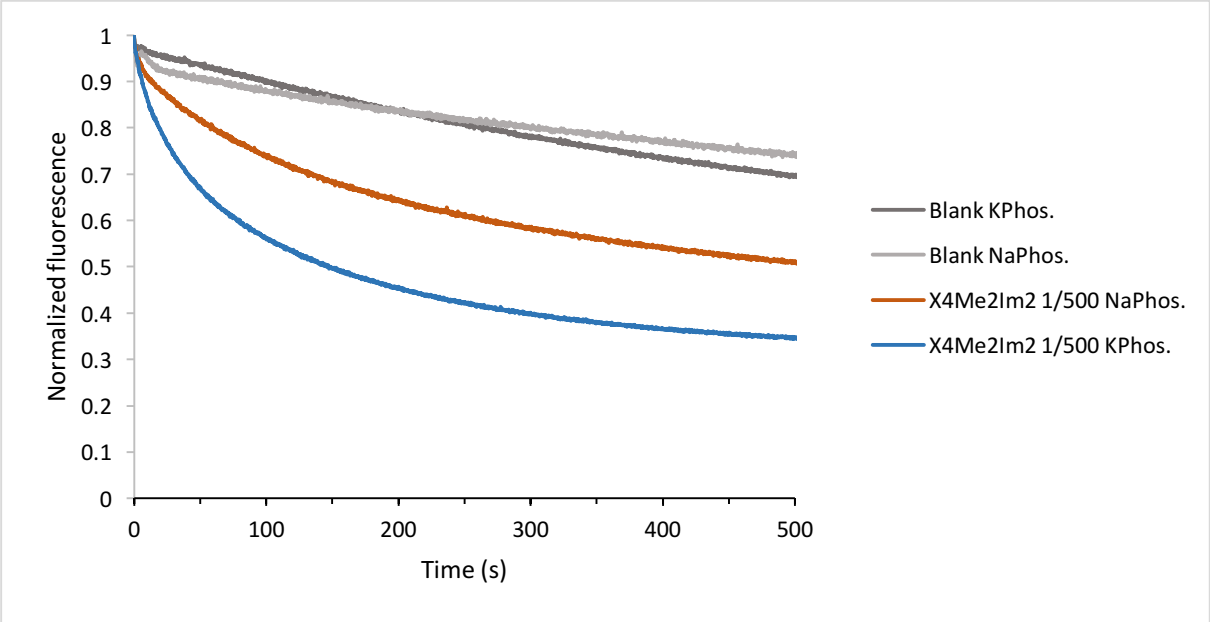

Figure 40: Comparison between sodium and potassium phosphate buffers using ***$X_4Me_2Im_2$****.Transport measurements of Cu(I) by following the decrease of fluorescence of BCS (excitation at 278 nm, emission at 393 nm) encapsulated inside LUVs with $X_4Pr_2Im_2$ (1/500 transporter to lipids ratio) in 100 mM sodium/potassium phosphate buffer (pH 7). Addition of 200 µL of a 0.5 mM $CuCl_2$ and 0.5 mM sodium ascorbate in 100 mM sodium/ potassium phosphate buffer (pH 7) to 2.8 mL LUVs (0.4 mM lipids) created a Cu^+ gradient. Results were normalized and averaged and blank measurements are shown for comparison.*

With both calixarenes, the transport was significantly faster in the potassium than in the sodium phosphate buffer (Figure 39, Figure 40). For **$X_4Pr_2Im_2$**, the half-life was reduced from 140 s in sodium to 90 s in potassium phosphate buffer. For **$X_4Me_2Im_2$**, the half-life was decreased even more, from 400 s in sodium to 200 s in potassium phosphate buffer.

These observations are consistent with the cation complexation results obtained by ^{1}H NMR spectroscopy as the affinity of **$X_4Pr_2Im_2$** and **$X_4Me_2Im_2$** for potassium was lower than for sodium. Thus, in potassium phosphate buffer **$X_4Pr_2Im_2$** and **$X_4Me_2Im_2$** could be more available to copper(I) than in sodium phosphate buffer.

Note that the starting fluorescence amount throughout Cu^+ transport experiments was not always identical and Cu^+ gradient is therefore not consistent, thus the qualitative measurements must be taken with care.

2.3.5. Transport of H^+ with $X_4Pr_2Im_2$

As the calixarenes are able to complex protons and as the experiments were conducted in an aqueous solution, it was likely that copper(I) could not only be exchanged with Na^+ or K^+ but also with H^+. In that case, the copper(I) transport could also be detected by following the pH of the interior of the liposomes. The capacity of **$X_4Pr_2Im_2$** to transport protons was verified using a fluorescent pH probe. However, the results of these experiment were not conclusive and are thus not shown.

3. Conclusions and perspectives

For the first time transmembrane transport of copper(I) with artificial carriers was observed. In order to achieve this, a transmembrane copper transport assay was developed and used to explore the capacities of calix[4]arenes functionalized with two imidazole groups to transport copper(I) into liposomes.

Two calixarenes **$X_4Pr_2Im_2$** and **$X_4Me_2Im_2$** were synthetized and their affinity for Cu^+ was studied by ^1H NMR spectroscopy. $X_4Pr_2Im_2$ bound Cu^+ with a higher affinity and selectivity than **$X_4Me_2Im_2$** and was significantly better resolved in ^1H NMR studies.
The optical properties of the BCS dye were studied upon interaction with copper(I). BCS showed a significant decrease of its fluorescence upon complexation with copper(I). The dye was encapsulated inside liposomes and copper(I) solutions were added outside of liposomes. It was shown from the decrease in fluorescence intensity of encapsulated BCS that **$X_4Pr_2Im_2$** and **$X_4Me_2Im_2$**, when integrated in membrane, are able to transport copper(I). **$X_4Pr_2Im_2$** transported copper(I) faster than **$X_4Me_2Im_2$**. Transport occurred at different rate in different conditions depending on the cations available to compensate the charge imbalance. Copper(I) transport was faster when exchange with potassium cations than with sodium cations.

However, the assay to explore copper(I) transport could be improved in different ways and further experiments could be done:

The separation of the BCS dye from the LUVs remains a challenge and thus the size exclusion column chromatography has to be improved. As some amount of BCS remains in the column, the external amount of BCS is not consistent. Extensive washing of the columns improved the situation as it removed part of the dye but still some BCS remained. An alternative solution would be to simply replace the column after each or few experiments but this is not the most economical solution.

In order to obtain quantitative transport measurements, more control experiments could be performed. It might be possible that some copper(II) is still present in the copper solutions and could prevent correct transport measurement as BCS also binds copper(II). The remaining copper(II) could be discarded by adding EDTA to the copper solutions as it is known to strongly and selectively bind copper(II).[35]

In order to confirm that Cu^+ transport with **$X_4Pr_2Im_2$** and **$X_4Me_2Im_2$** is occurring through a carrier and not a channel mechanism, experiments using DPPC instead of POPC could be conducted. DPPC has a higher phase transition temperature than POPC. At room temperature the liposomes membrane made with DPPC are in a gel phase, in which the transporters acting as mobile carrier cannot move. At higher temperature (45°C), a liquid phase of the membrane is obtained, allowing carriers to function. Thus, by varying the temperature of the experiments the mechanism of transport could be determined.

Other calixarenes and/or different molecules could be tested in order to characterize copper transport and verify if it is specific to the Im-Cu-Im motif or not. New calixarenes and/or different molecules functionalized with other groups known to interact with copper such as cysteine and methionine could be designed to bind copper with a higher affinity and selectivity in hope that they will also be able to transport copper(I) and potentially faster than previously observed.

This research is performed in the context of diseases related to deficiencies in copper transport. Another potential application for small copper transporters could be copper homeostasis disruption that could lead to a reduced proliferation of cancer cells as recent study have showed.[8]

4. Experimental section

4.1. Syntheses and characterisation

4.1.1. General experimental details

The solvents used for the reactions were distilled. Anhydrous DMF was obtained from Acros organics. Anhydrous THF was distilled over Na. The reactions were placed under inert atmosphere with argon. The reactions were followed by thin layer chromatography and/or NMR spectroscopy.
Nuclear magnetic resonance spectroscopy: ^{1}H, ^{13}C and correlation measurements were recorded with a Bruker Avance TM 300 instrument (^{1}H 300 MHz) and/or Bruker Varian Unity 600 VNMR system (^{1}H 600 MHz) and/or Jeol JNM-ECZ400R Spectrometer (^{1}H, ^{13}C, COSY, HSQC 400MHz)
The multiplicities of the signals were abbreviated as follows: s singlet, d doublet, t triplet. The chemical shifts are in ppm and the coupling constants J are in Hz.
The solvents used are chloroform-d_1 ($CDCl_3$), dichloromethane-d_2 (DCM), dimethyl sulfoxide-d_6 (DMSO), acetonitrile-d_3 (CD_3CN). The ^{1}H residual signals of the solvent were used as reference ($CDCl_3$ 7.26 ppm, DMSO 2.5 ppm, CD_3CN 1.94 ppm). The ^{13}C signals of the solvent were used as reference ($CDCl_3$ 77.16)

Thin layer chromatography: TLC was performed on silica gel 60 F_{254} coated aluminium sheets supplied by Merck. Compounds were revealed under UV light or with $KMnO_4$.

Column chromatography: The flash chromatography was performed on silica gel 60 provided by Merck.

4.1.2. Synthesis of calix[4]arene bis-methyl ($X_4Me_2H_2$)

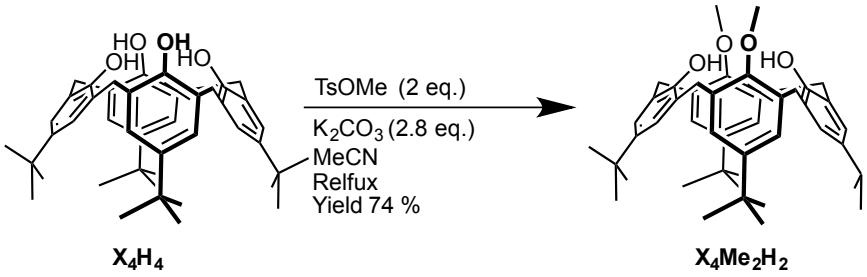

*Figure X 1 : Synthesis of **$X_4Me_2H_2$**.*

In a 100 mL round bottom flask, K_2CO_3 (306.9 mg, 2.22 mmol, 2.8 equiv.) and TsOMe (25 mL, 1.61 mmol, 2 equiv.) were added to a solution of calixarene **X_4H_4** (515.1 mg, 0.79 mmol, 1 equiv.) in MeCN (10 mL). The mixture was stirred and heated under reflux overnight for 14h under inert atmosphere. The solvent was evaporated under reduced pressure. The residue was dissolved in DCM then washed with HCl 1M (10mL) and with water (2x10 mL). The organic layer was evaporated under reduced pressure. The crude product was purified by flash chromatography (cyclohexane/DCM 7:3 v/v) affording calixarene **$X_4Me_2H_2$** (395.7 mg, 0.58 mmol) as a light yellow solid. Yield 74 %.

^{1}H NMR (300MHz, $CDCl_3$, 298K): δ (ppm) = 0.94 (s, 18H, *t*Bu), 1.30 (s, 18H, *t*Bu), 3.33 (d, ^2J = 12Hz, 4H, $ArCH_{2(eq)}$), 3.95 (s, 6H, OCH_3) 4.28 (d, ^2J = 12Hz, 4H, $ArCH_{2(ax)}$) 6.77 (s, 4H, ArH) 7.07 (s, 4H, ArH).

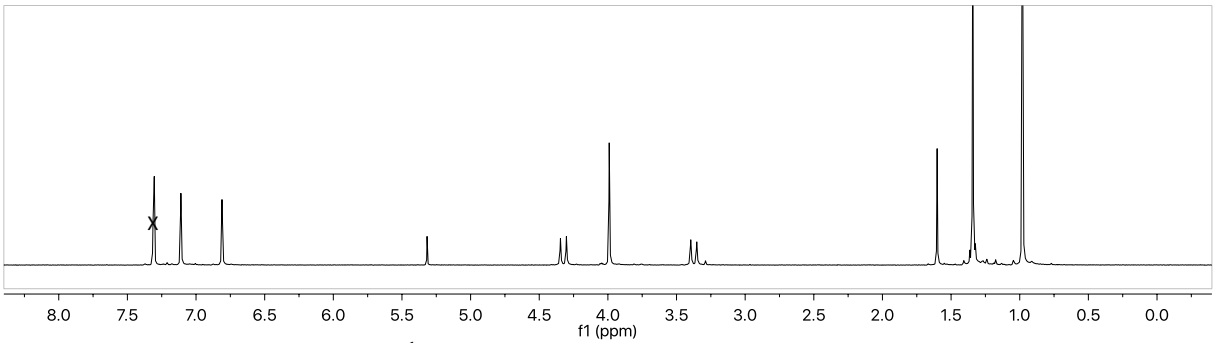

*Figure X 2 : ^{1}H NMR spectrum of **$X_4Me_2H_2$** (300MHz, $CDCl_3$, 298K).*

4.1.3. Synthesis of calix[4]arene bis-methyl bis-imidazole ($X_4Me_2Im_2$)

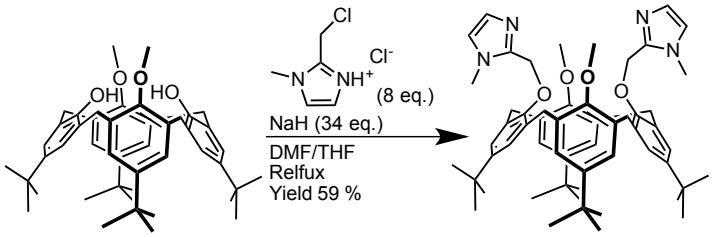

$X_4Me_2H_2$ **$X_4Me_2Im_2$**

*Figure X 3 : Synthesis of **$X_4Me_2Im_2$**.*

In a 50 mL round bottom flask, a solution of calixarene **$X_4Me_2H_2$** (395 mg, 0.58 mmol, 1 equiv.) in anhydrous THF (12 mL) was stirred for 30 minutes under inert atmosphere. 2-(chloromethyl)-1-methyl-1H-imidazole (620 mg, 4.75 mmol, 8 equiv.) dissolved in anhydrous DMF (3.2 mL) and NaH (60% dispersion in mineral oil, 800 mg, 20 mmol, 34 equiv.) were added. The mixture was stirred and heated under reflux for 24h under inert atmosphere. The reaction was quenched with EtOH (10 drops). The solvent was evaporated under reduced pressure. The residue was dissolved in DCM and the solution was then washed with water (2x10mL). The organic layer was evaporated under reduced pressure. The crude product was purified by flash chromatography (DCM/MeOH 95:5 v/v) affording calixarene **$X_4Me_2Im_2$** (299.5 mg, 0.34 mmol) as white solid. Yield 59 %.

^{1}H NMR (300MHz, $CDCl_3$, 298K) The spectrum shows broad signals (Figure X 4).

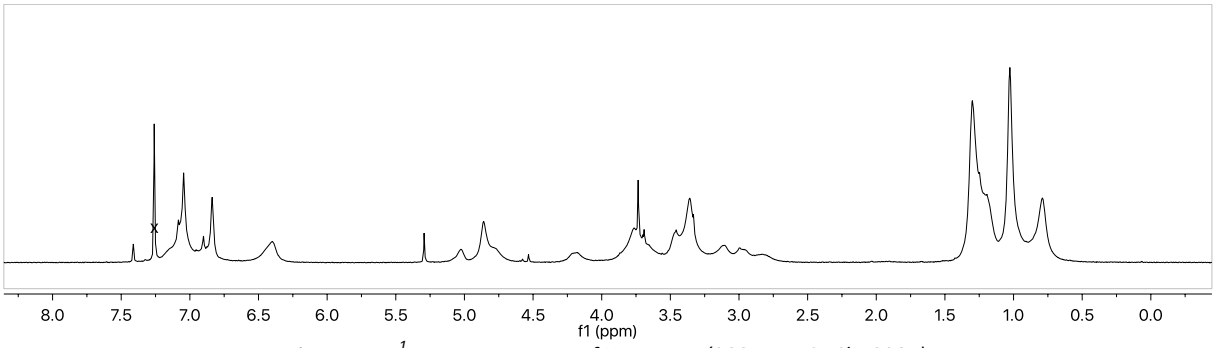

*Figure X 4 : ^{1}H NMR spectrum of **$X_4Me_2Im_2$** (300MHz, $CDCl_3$, 298K).*

4.1.4. Synthesis of calix[4]arene bis-propyl bis-imidazole ($X_4Pr_2Im_2$)

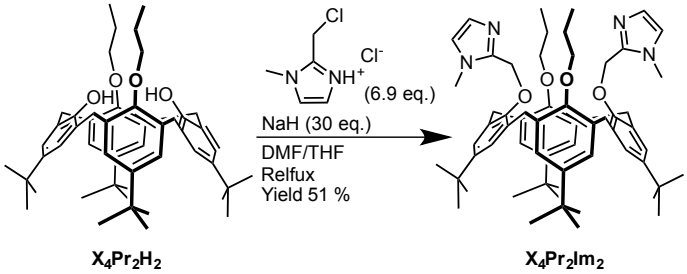

*Figure X 5 : Synthesis of **$X_4Pr_2Im_2$**.*

In a 100 mL round bottom flask, calixarene **$X_4Pr_2H_2$** (82 mg, 0.11 mmol, 1 equiv.) was stirred in anhydrous THF (3.2 mL) for 30 minutes under inert atmosphere. 2-(chloromethyl)-1-methyl-1H-imidazole (101 mg, 0.773 mmol, 6.9 equiv.) dissolved in anhydrous DMF (0.8 mL) and NaH (60% dispersion in mineral oil, 134.5 mg, 3.36 mmol, 30 equiv.) were added. The mixture was stirred and heated until reflux for 24h under inert atmosphere. The reaction was quenched with EtOH (10 drops). The solvent was evaporated under reduced pressure. The residue was dissolved in DCM and then washed with water (2x10 mL). The organic layer was evaporated under reduced pressure. The crude product was purified by flash chromatography (DCM/MeOH 95:5 v/v). The purified product was triturated with MeOH to remove impurities, and washed with H_2O to remove the sodium affording calixarene **$X_4Pr_2Im_2$** (52.7 mg, 0.057 mmol) as white solid. Yield 51 %.

^{1}H NMR (400MHz, $CDCl_3$, 298K): δ (ppm) = 0.78 (s, 6H, CH_3) 0.86 (s, 18H, *t*Bu) 1.28 (s, 18H, *t*Bu), 1.85 (q, ^{2}J = 8Hz, 4H, CH_2) 3.01 (d, ^{2}J = 12Hz, 4H, $ArCH_{2(eq)}$) 3.45 (s, 6H, NCH_3) 3.80 (t, ^{2}J = 8Hz, 6H, OCH_2) 4.34 (d, ^{2}J = 12Hz, 4H, $ArCH_{2(ax)}$) 6.49 (s, 2H, ArH) 6.86 (s, 2H, ArH) 7.02 (s, 2H, ArH) 7.05 (s, 2H, ArH)

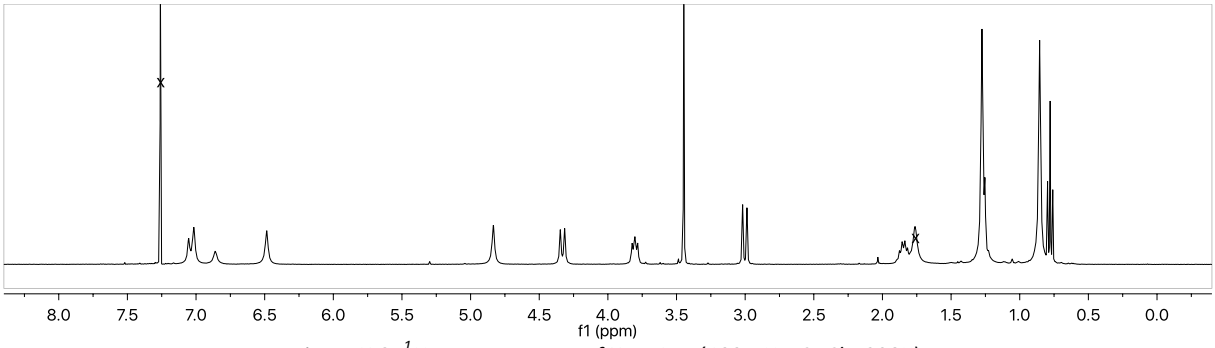

*Figure X 6 : ^{1}H NMR spectrum of **$X_4Pr_2Im_2$** (400MHz, $CDCl_3$, 298K).*

4.1.5. Further characterisation of calix[4]arene bis-propyl bis-imidazole ($X_4Pr_2Im_2$)

Melting point: 253 °C

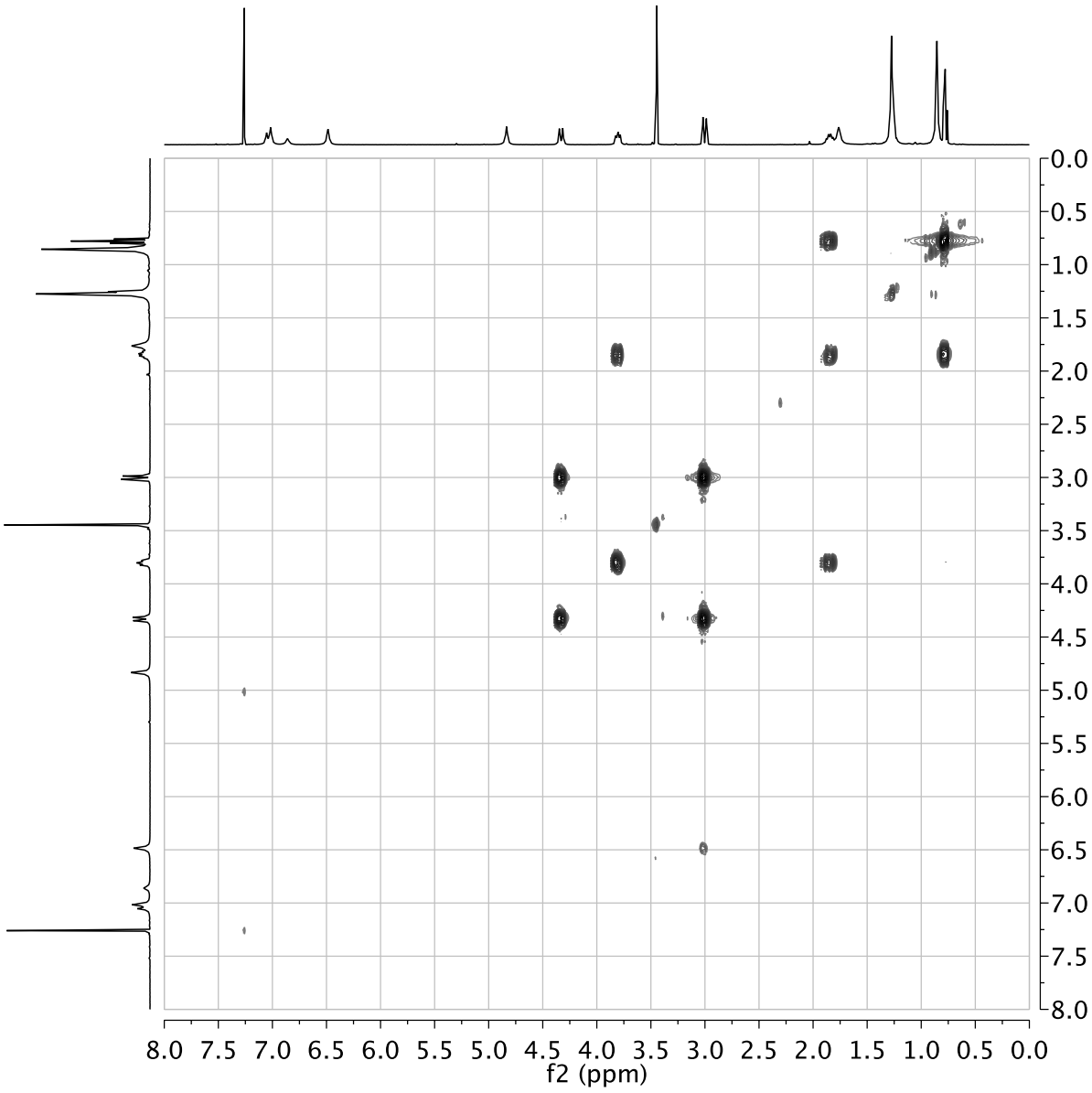

*Figure X 7 : Correlation spectroscopy (COSY) of **$X_4Pr_2Im_2$** (400MHz, $CDCl_3$, 298K).*

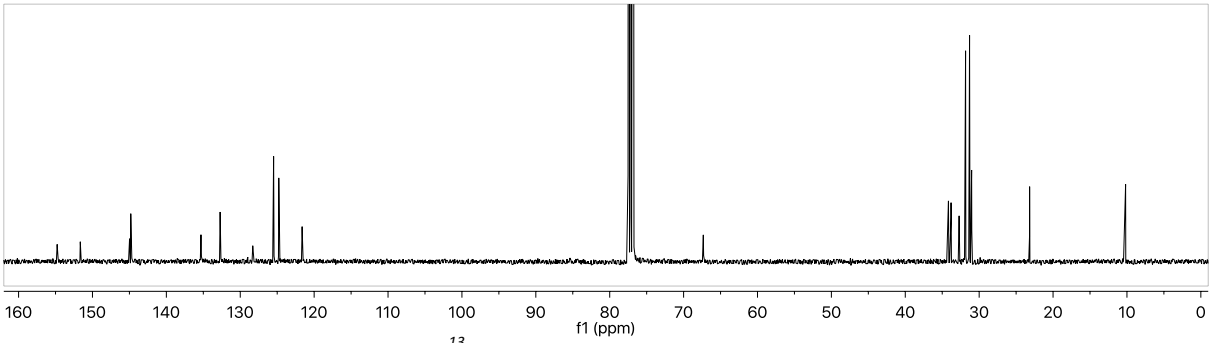

*Figure X 8 : ^{13}C NMR of **$X_4Pr_2Im_2$** (400MHz, $CDCl_3$, 298K).*

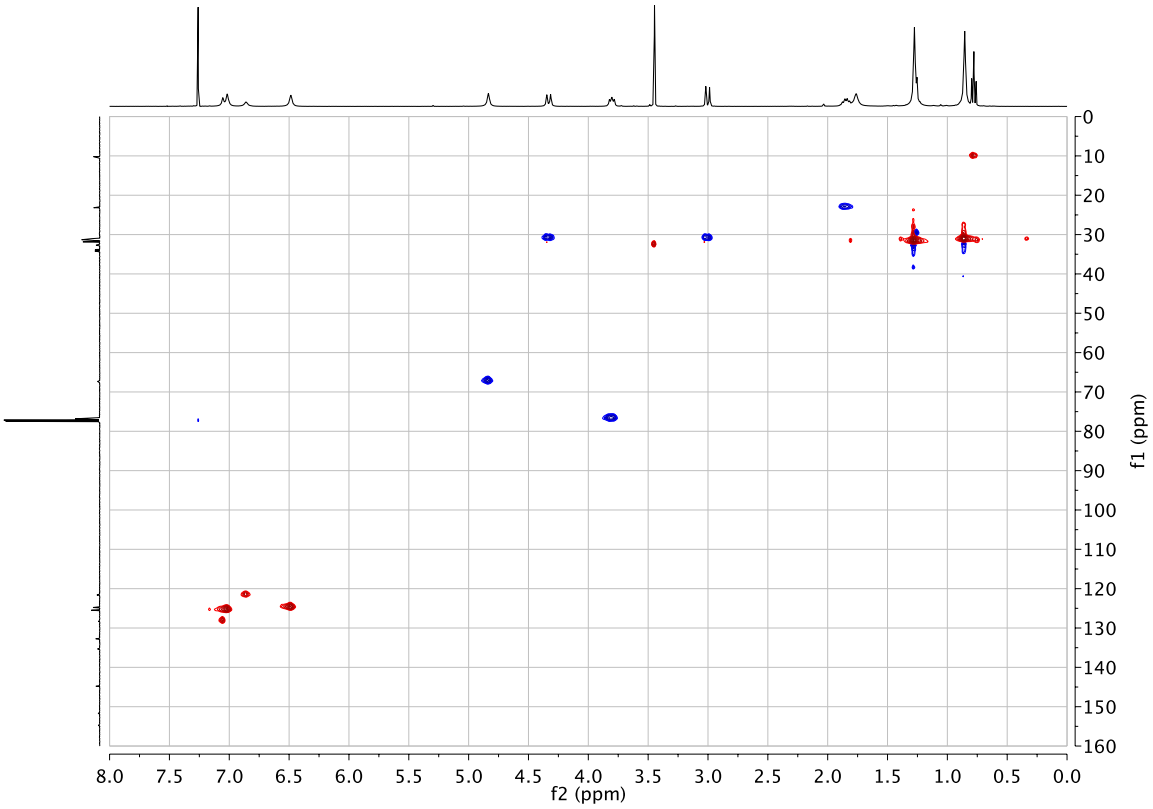

*Figure X 9 : Heteronuclear single quantum coherence spectroscopy (HSQC) of **$X_4Pr_2Im_2$** (400MHz, $CDCl_3$, 298K).*

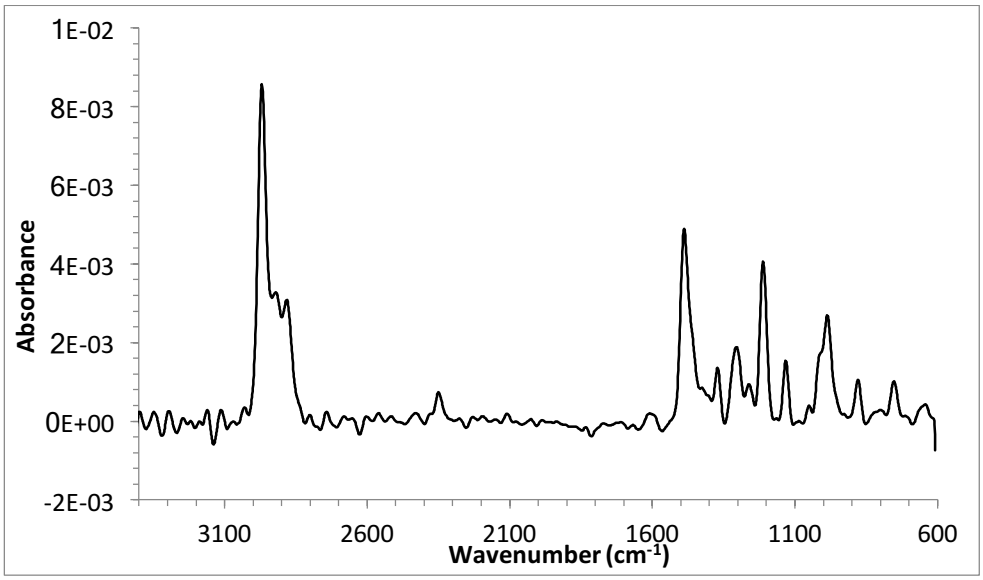

Figure X 10 : Infrared spectrum of **$X_4Pr_2Im_2$** recorded with a Bruker Alpha FT-IR.

Compound Label	*m/z*	RT	Algorithm	Mass
Cpd 1: C60 H80 N4 O4	921.628	0.184	Find By Formula	920.6207

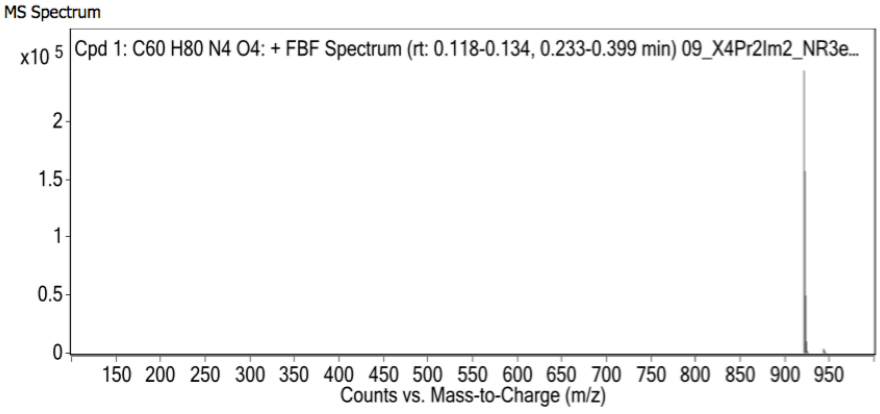

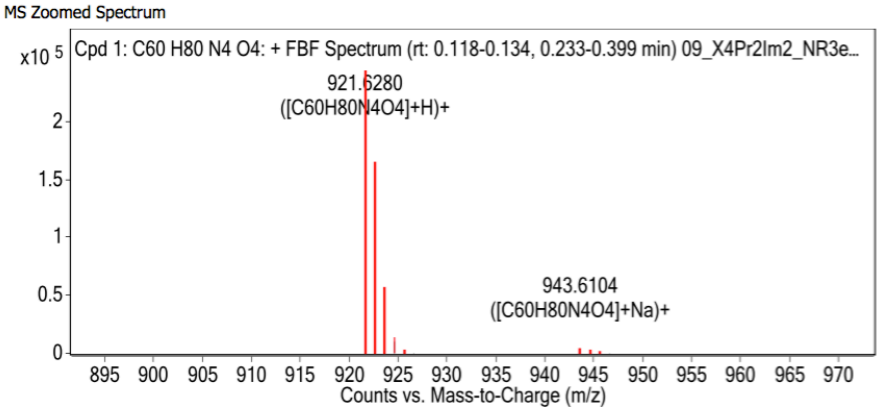

Figure X 11 : High resolution mass spectrometry of ***$X_4Pr_2Im_2$*** *recorded with QTOF 6520 spectrometers provided by the ULB faculty of pharmacy. The signals of* ***$X_4Pr_2Im_2 \supset H^+$*** *and* ***$X_4Pr_2Im_2 \supset Na^+$*** *can be observed.*

4.2. ^{1}H NMR Complexation studies

4.2.1. $X_4Me_2Im_2$ and $X_4Pr_2Im_2$ protonation and cations complexation

^{1}H NMR measurements were performed on a Varian Unity 600 VNMR system (^{1}H, 600 MHz). Parameters for the measurements were a 90° Pulse 7.1 µs, acquisition time 3 s, relaxation delay 15 s, 8 scans.

Binding abilities and complexation constants of calixarenes with cations were evaluated by titrations with various salt solutions. The complexation of four cations was tested: H^+ (TFA), Na^+ (Na-tetrakis(3,5-bis(trifluoromethyl)phenyl) borate), K^+ (KPF_6) and Cu^+ (Tetrakis(acetronitrile)copper(I) tetrafluoroborate) at 298 K. All salts were dissolved in CD_3CN. Solutions of calixarene (**$X_4Me_2Im_2$** or **$X_4Pr_2Im_2$**) were prepared in a mixture of deutered solvents (CD_3CN/CD_3Cl 4:1) and then titrated with the salt solutions by 0.2 equivalent increments until the NMR spectrum showed no significant changes anymore. The results of the titrations are shown in Figure 26 ($X_4Pr_2Im_2$ by K^+) and in Figure X 15 to Figure X 17.

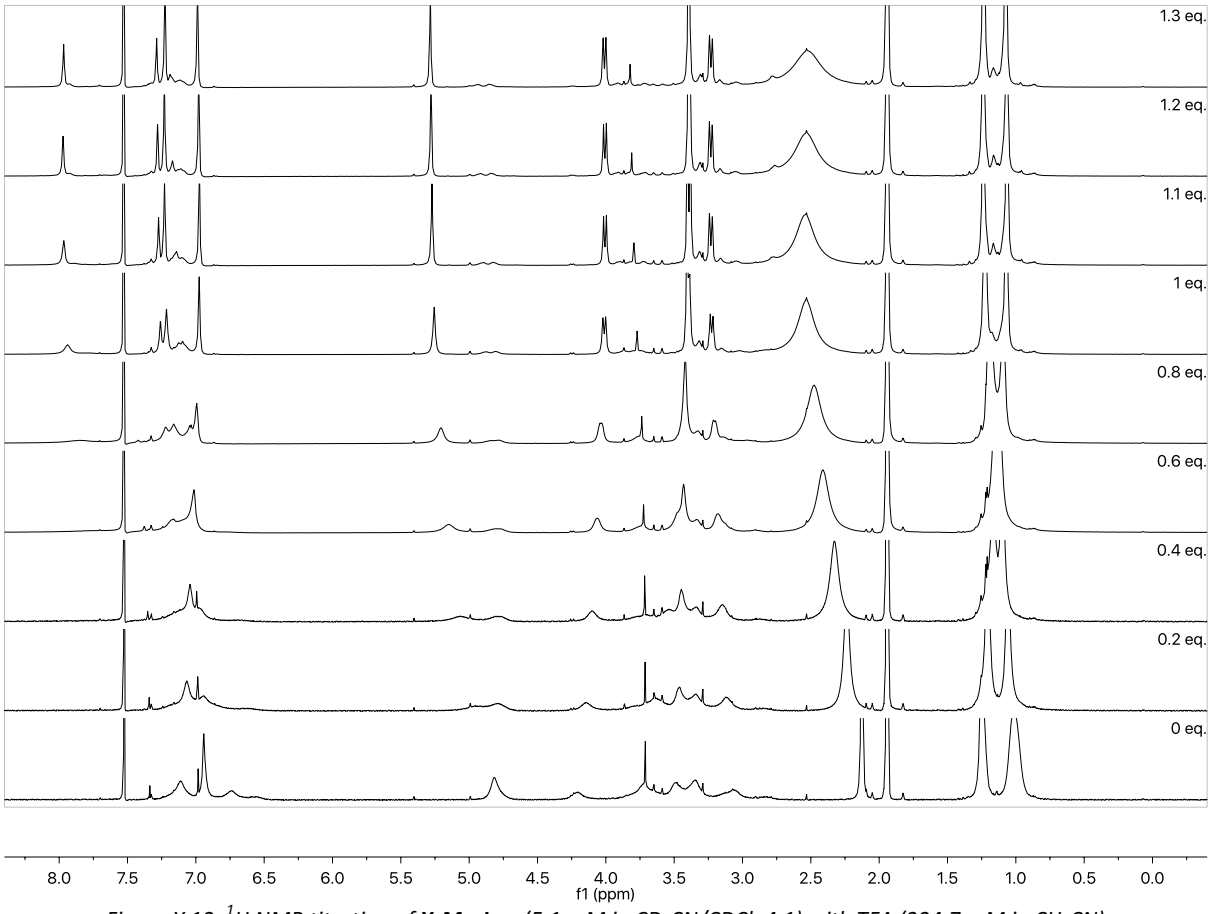

*Figure X 12: ^{1}H NMR titration of **$X_4Me_2Im_2$** (5.1 mM in $CD_3CN/CDCl_3$ 4:1) with TFA (224.7 mM in CH_3CN).*

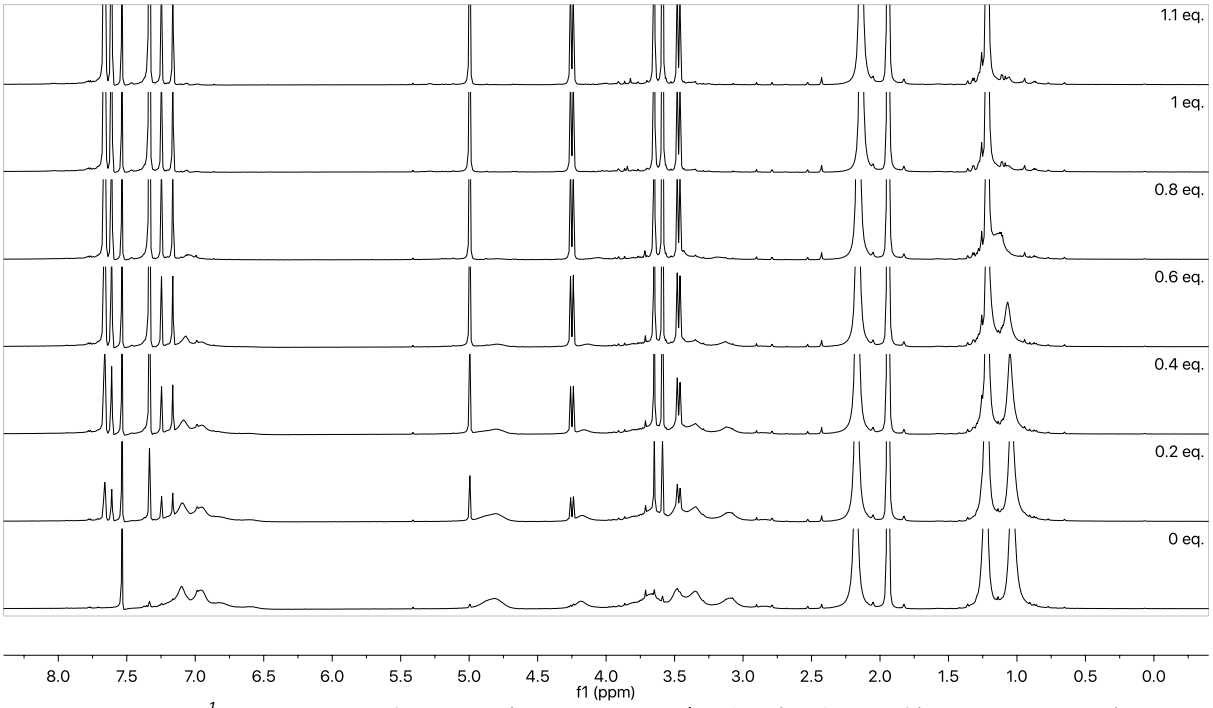

*Figure X 13: ^{1}H NMR titration of **$X_4Me_2Im_2$** (4.4 mM in $CD_3CN/CDCl_3$ 4:1) with NaBarf (122.1 mM in CH_3CN).*

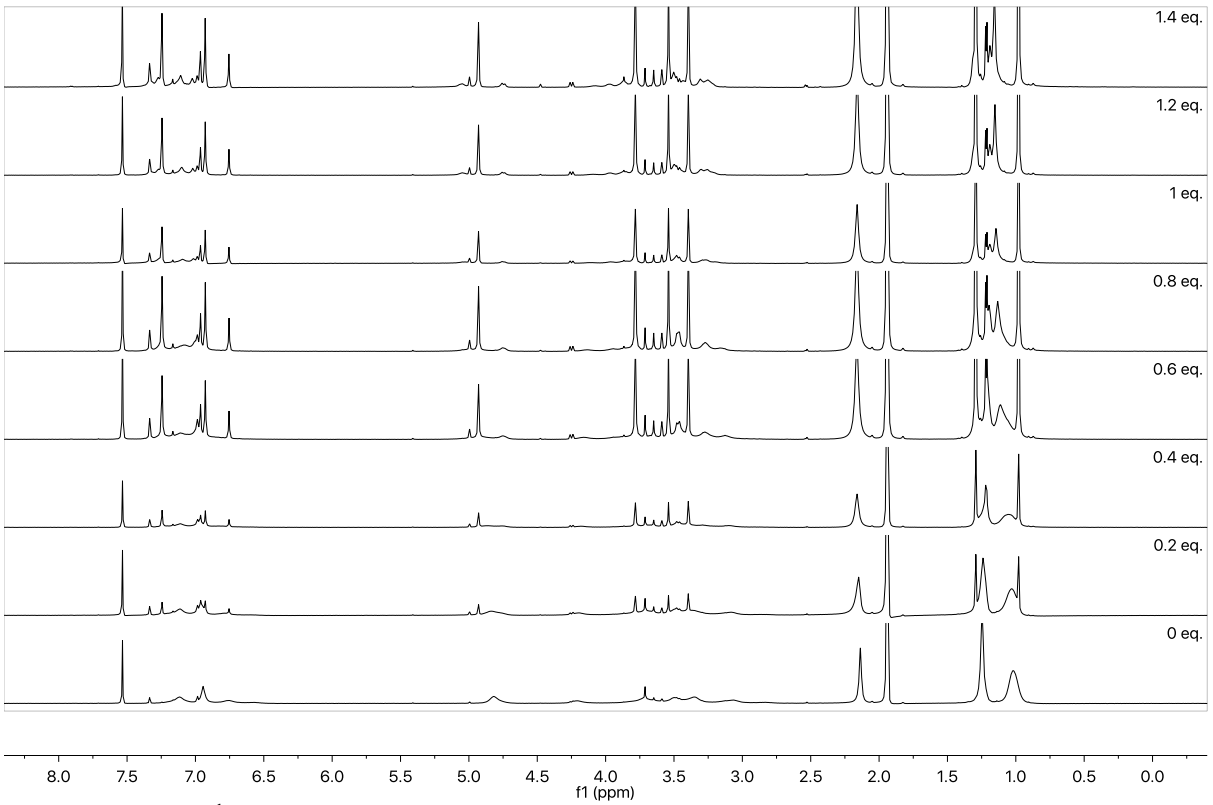

*Figure X 14: ^{1}H NMR titration of **$X_4Me_2Im_2$** (5.2 mM in $CD_3CN/CDCl_3$ 4:1) with $K^+PF_6^-$ (245.3 mM in CH_3CN).*

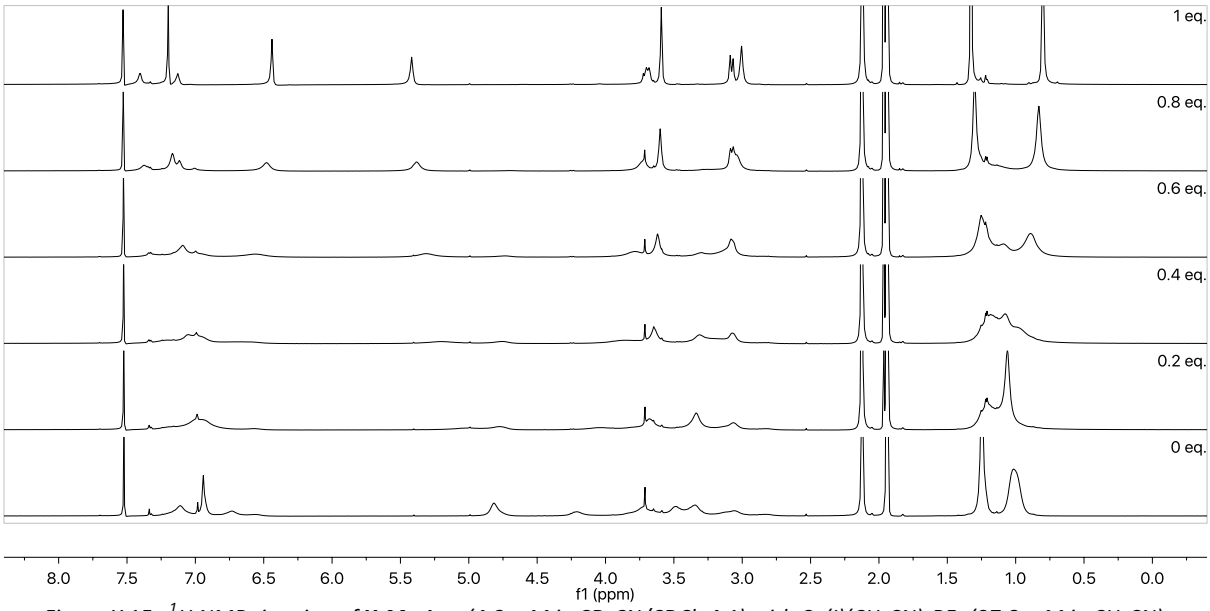

*Figure X 15 : ^{1}H NMR titration of **$X_4Me_2Im_2$** (4.8 mM in $CD_3CN/CDCl_3$ 4:1) with Cu(I)$(CH_3CN)_4BF_4$ (37.8 mM in CH_3CN).*

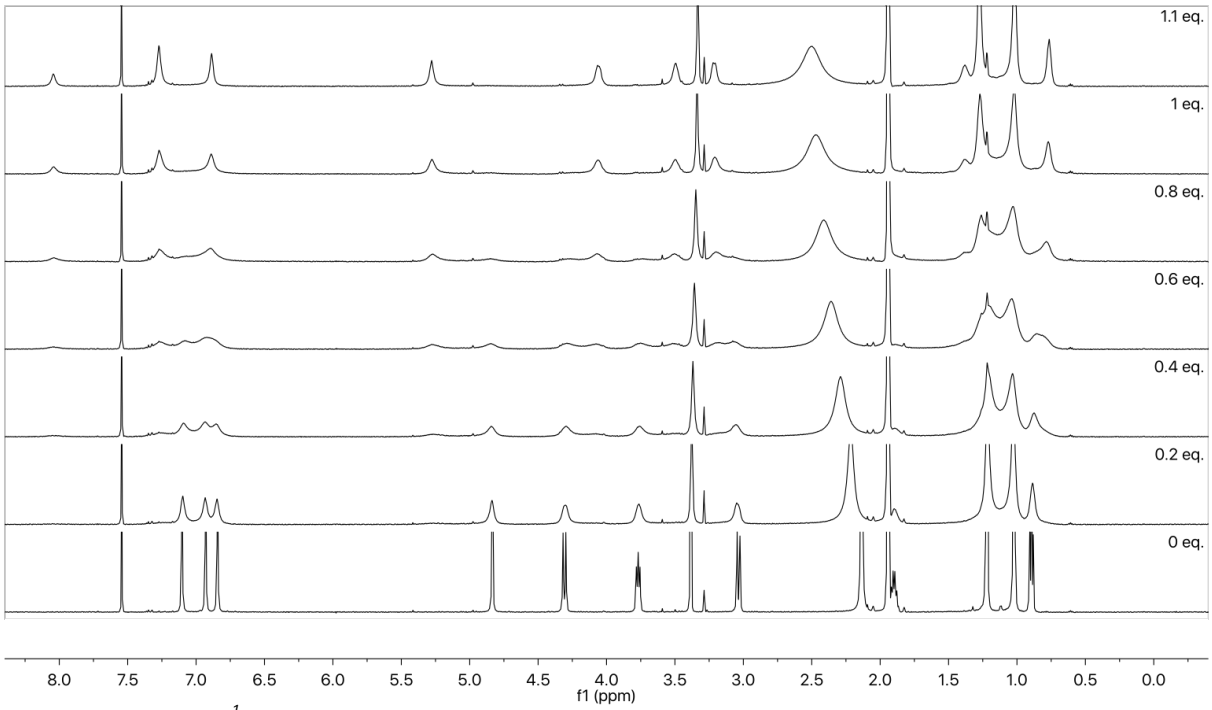

*Figure X 16: ^{1}H NMR titration of **$X_4Pr_2Im_2$** (4.5 mM in $CD_3CN/CDCl_3$ 4:1) with TFA (224.7 mM in CH_3CN).*

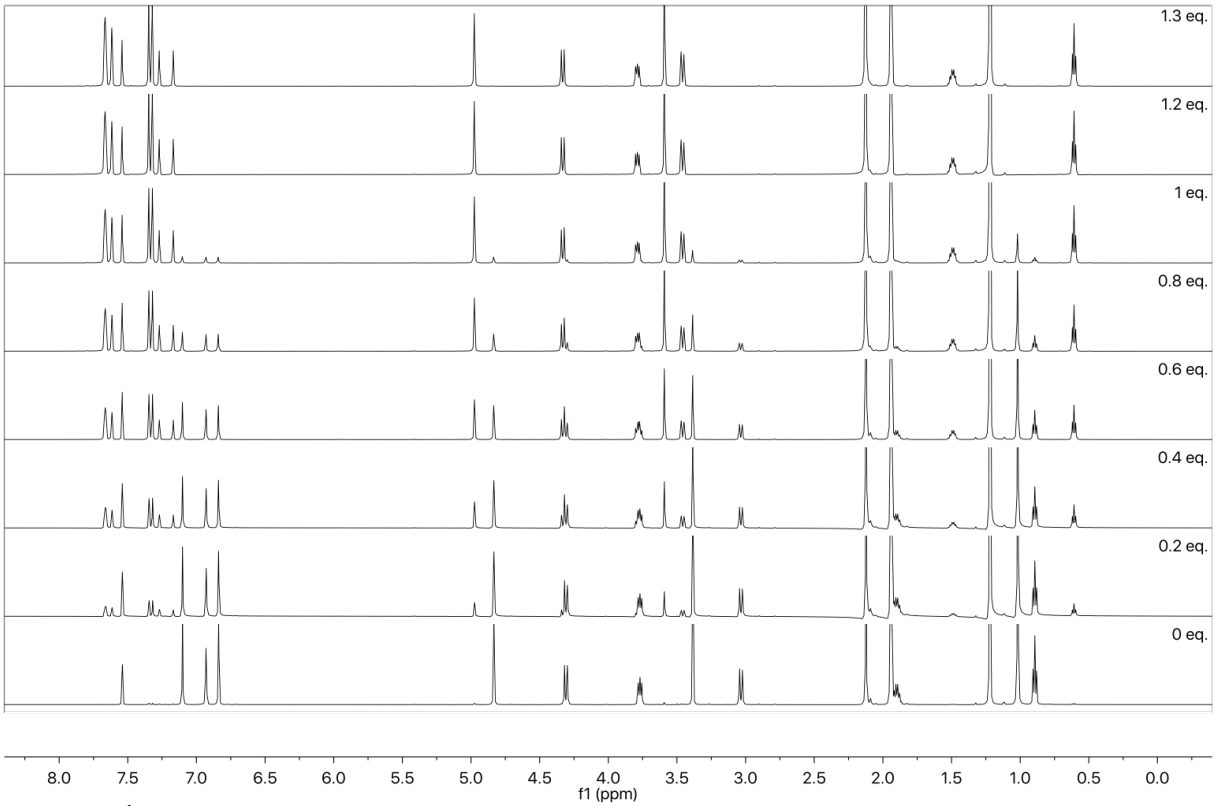

*Figure X 17: ^{1}H NMR titration of **$X_4Pr_2Im_2$** (4.9 mM in $CD_3CN/CDCl_3$ 4:1) with NaBarf (122.1 mM in CH_3CN).*

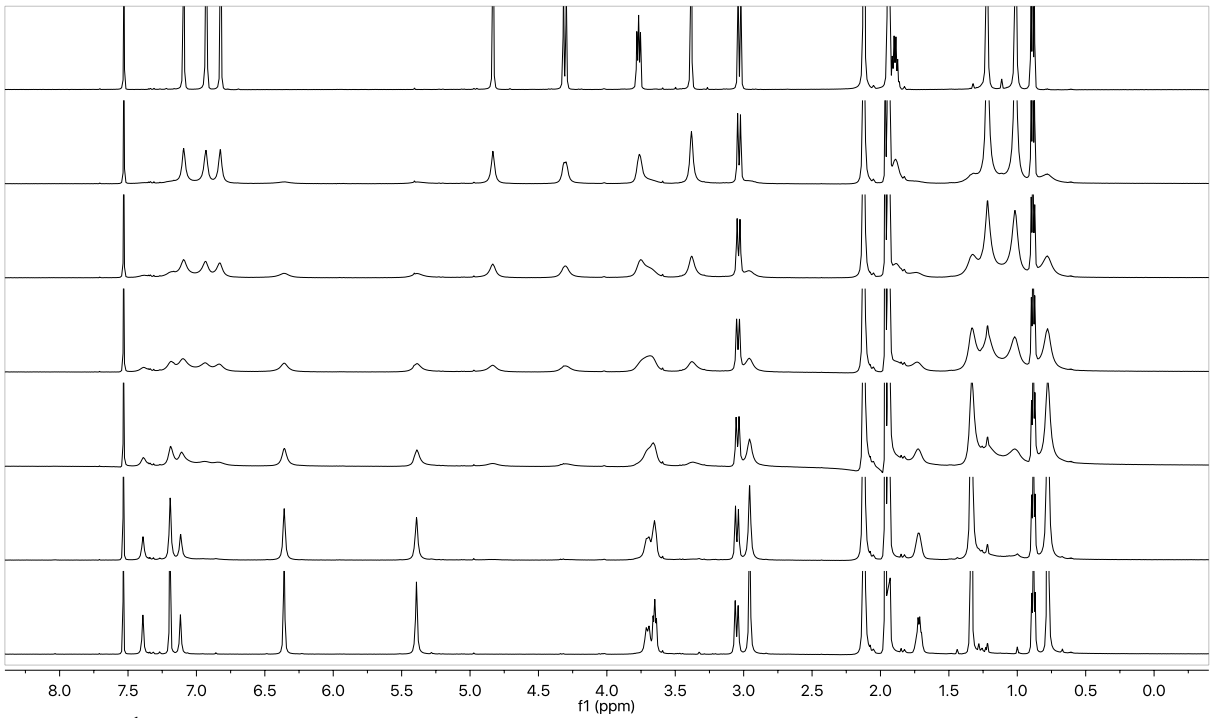

*Figure X 18 : ^{1}H NMR titration of **$X_4Pr_2Im_2$** (4.5 mM in $CD_3CN/CDCl_3$ 4:1) with $Cu(I)(CH_3CN)_4BF_4$ (37.8 mM in CH_3CN) at 298 K, 600 MHz.*

4.2.2. $X_4Me_2Im_2$ and $X_4Pr_2Im_2$ complexation: competition between Cu^+ and H^+, Na^+, and K^+

The NMR tubes containing solutions of the complexes with H^+, Na^+, and K^+ were then titrated with the Cu^+ solution by 0.5 equivalent increments until the amounts of Cu^+ and previous cations were equal. The relative integral of the peaks corresponding to the different species was measured and compared in order to calculate the relative affinity of $\mathbf{X_4Pr_2Im_2}$ and $\mathbf{X_4Me_2Im_2}$ for Cu^+ relative to other cations using Equation 1 to 5. The ^1H spectra of these experiments are given below. (The spectrum are stacked starting from the bottom).

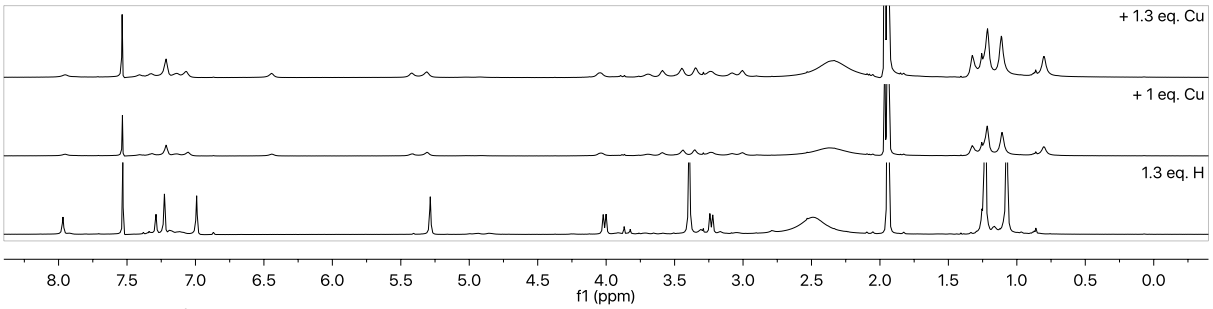

Figure X 19: ^1H NMR titration of $\mathbf{X_4Me_2Im_2}\supset H^+$ (1.3 eq. of TFA added) with $Cu(I)(CH_3CN)_4BF_4$ (37.8 mM in CH_3CN).

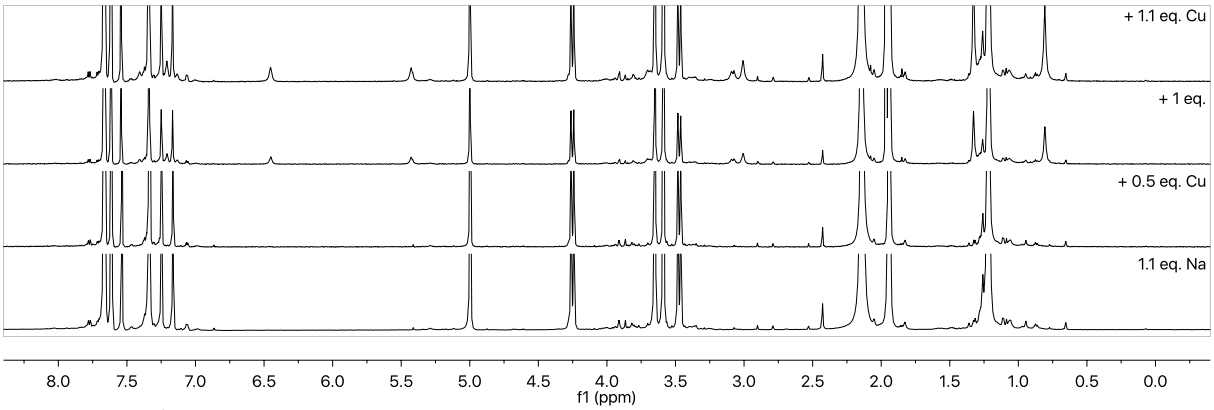

Figure X 20: ^1H NMR titration of $\mathbf{X_4Me_2Im_2}\supset Na^+$ (1.1 eq. of NaBarf added) with $Cu(I)(CH_3CN)_4BF_4$ (37.8 mM in CH_3CN).

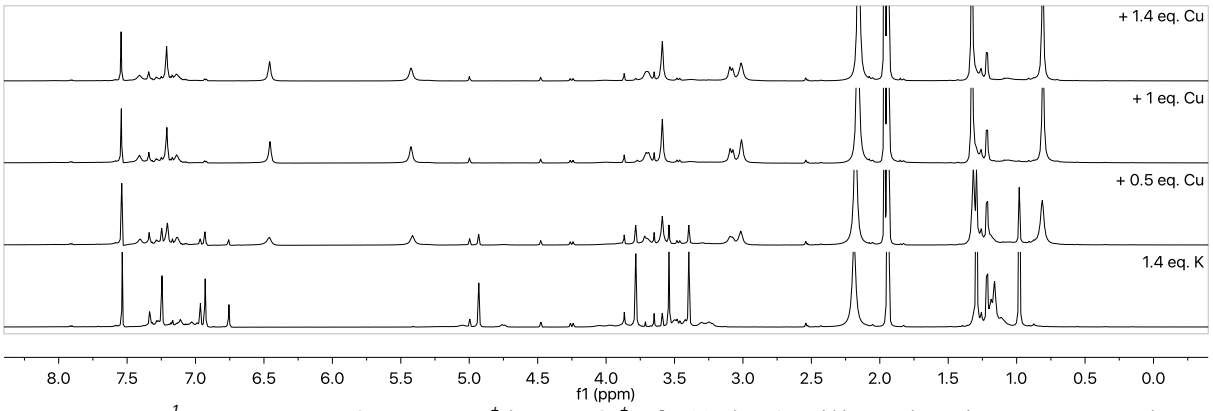

Figure X 21: ^1H NMR titration of $\mathbf{X_4Me_2Im_2}\supset K^+$ (1.4 eq. of $K^+PF_6^-$ added) with $Cu(I)(CH_3CN)_4BF_4$ (37.8 mM in CH_3CN).

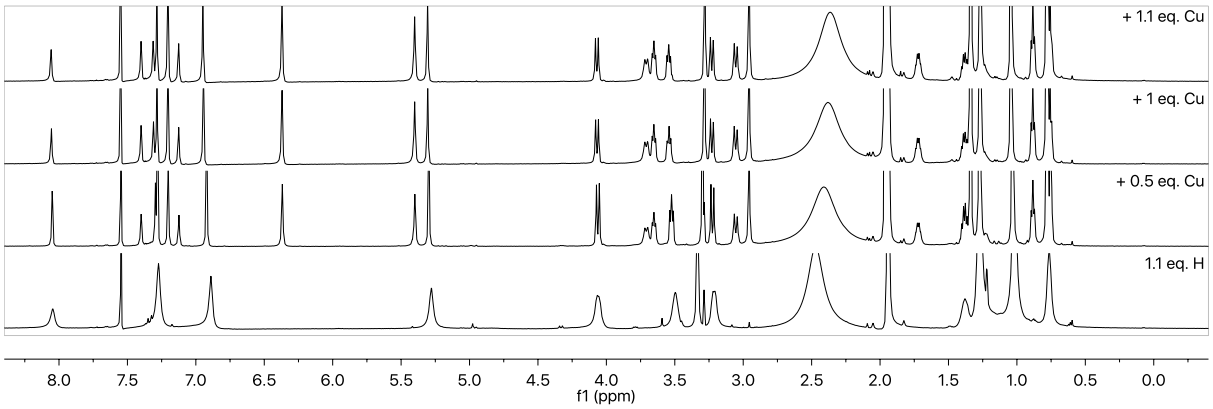

*Figure X 22: ^{1}H NMR titration of **$X_4Pr_2Im_2$⊃H^+** (1.1 eq. of TFA added) with Cu(I)$(CH_3CN)_4BF_4$ (37.8 mM in CH_3CN).*

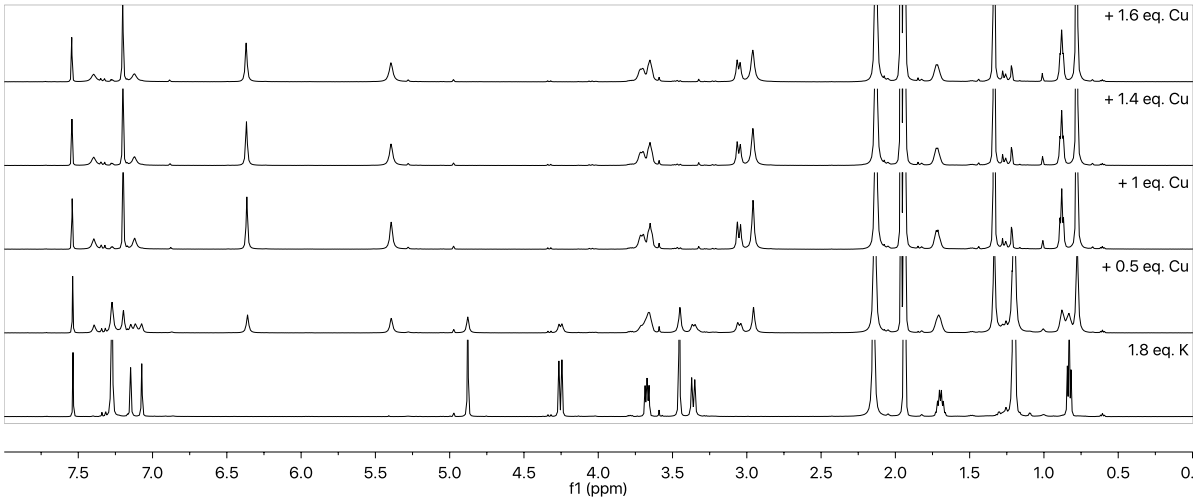

*Figure X 23: ^{1}H NMR titration of **$X_4Pr_2Im_2$⊃K^+** (1.8 eq. of $K^+PF_6^-$ added) with Cu(I)$(CH_3CN)_4BF_4$ (37.8 mM in CH_3CN).*

4.3. Optical characterisation of BCS

Absorption spectroscopy and fluorescence spectroscopy were used to study the optical properties of BCS upon addition of copper(I). The absorption was measured from 800 nm to 200 nm with a Shimadzu UV-Vis-NIR UV-3600 spectrometer. The fluorescence measurements were performed with a Horiba FluoroMax 4 spectrometer. For the fluorescence spectroscopy the excitation was done at the two absorption maxima: 278 nm and 479 nm. The emission was measured from 300 nm to 500 nm and from 500 nm to 800 nm respectively with both slits opening set up at 1 nm.
A solution of BCS (2.5 mL, 10 μM BCS) in salt buffer (100 mM potassium phosphate at pH 7) was placed in a four-faced quartz cuvette. The BCS solution was titrated with a solution of copper(I) ($CuCl_2$ 0.5 mM + sodium ascorbate 0.5 mM in potassium phosphate at pH 7) until the fluorescence signal showed no significant decrease anymore. After each addition, an absorption and both emission spectra were measured.

4.4. Transport studies

4.4.1. Solutions and materials

Stock solution of lipids and calixarene were prepared using deacidified $CHCl_3$ and stored in a freezer. $CHCl_3$ was deacidified by passing through activated basic alumina. The lipids used in order to prepare the liposomes are 2-oleoyl-1-palmitoyl-sn-glycero-3-phosphocholine (POPC), from Sigma Aldrich (purity ≥ 99%) and cholesterol from Acros Organics (purity of 95%). The aqueous solutions were prepared with milipore water. Different salt solutions were prepared: potassium phosphate, sodium phosphate, NMDGH-Cl and NMDGH-sulphate at a concentration of 100 mM, at a controlled pH. N-Methyl Glucamine (NMDG) is a carbohydrate which can be combined with an acid in water to form a salt. NMDGH-X solutions were prepared by mixing an aqueous solution of NMDG with hydrochloric acid or sulphuric acid and the pH was adjusted to 7 (± 0.05). The phosphate buffers were prepared by mixing the two solutions of the mono- and the di-protonated phosphate salt. The copper(I) solutions were obtained by mixing $CuCl_2$ (or $CuSO_4$) with sodium ascorbate (or ascorbic acid). Different copper(I) concentrations (0.5 mM or 1.8 mM) and different copper to ascorbate ratio (1:1 or 2:1 respectively) were used and are specified in the figure caption. The copper solutions were prepared freshly as they were unstable over time. The solutions of the dye (BCS or HPTS) were prepared in each of the different salt solutions at a 10 mM concentration.
Fluorescence measurements were performed with a Horiba FluoroMax 4 spectrometer using a 4-faced quartz cuvette (10 mm x 10 mm) of 5mL volume. For the copper(I) transport assay monitored with BCS, the excitation was set up at 278 nm and emission was recorded at 393 nm with an opening for both slits of 3 nm and an integration time of 0.2 seconds.

4.4.2. Preparation of liposomes

The calixarene and lipids solutions were taken out of the freezer and left sealed for an hour at room temperature. The solutions were mixed in different ratio in a 5 mL round bottom flask. The POPC/Cholesterol molar ratio remained constant and was 7:3 respectively. The ratio of calixarene to lipid was variable and ranged from 1/200 to 1/5000. For each condition two

batches were made: one prepared with the transporter of choice, the other without transporter. Total amount of lipids per batch was variable and depends on the amount of liposomes solution required for the experiment. The solvent was evaporated under gentle air flow and then at high vacuum for at least an hour. 500 µL of the dye solution and a magnetic stir bar were added in the flask. The flask was then sonicated for 30 seconds and placed under magnetic agitation for at least an hour. The solution was frozen with liquid nitrogen and heated back to room temperature with warmed water ten times over. The solution was transferred from the flask to the syringe of an extrusion kit, the flask was rinsed with about 0.5 mL of the same salt solution as the dye in order to reach a volume of 1 mL in the syringe. The liposome solution was filtered with the extrusion kit equipped with a filter of 200 nm pores 29 times over. The solution was eluted through a size exclusion column (SEC) and then diluted to obtain concentration of 0.4 mM in lipids. The SEC were reused for multiple experiments and abundantly rinsed with distilled water and then with a salt solution. Despite all washing, dye molecules were still present in the column giving out variable amount of exterior dye and thus different starting level of fluorescence.

4.4.3. Transport measurement

Part of the liposomes solution (2.8 mL) was transferred in a cuvette and placed inside the fluospectrometer and continually stirred with a magnetic stirrer. 30 seconds after the start of the measurement, copper solutions were added. Other additions were also made with individual components and are specified in each experiment. Depending on the experiment the the duration of the measurements varies. The experiments were usually stopped once the signal did not change significantly anymore. A micellar lipid solution (Triton) is usually used in transport experiments to lyse the liposomes at the end of the experiment in order to observe the final level of fluorescence. This was not feasible as triton absorb light at 278 nm. Attempts to break liposomes were made and this method showed some potential but was not confirmed to be reliable.

The data showed in section 2.3 were treated as follows: for each run the initial plateau and the initial vertical drop due to the quenching of the exterior dye (1-4 seconds after the addition) were removed. Then the signal was normalised by dividing the fluorescence values (F) by the first value (F_0) following the quenching of the exterior dye. The average of each normalised run (F/F_0) was then calculated and plotted over time.
Transport curve were fitted to a simple exponential in order to calculate their half-life values.

4.4.4. Transport measurement results with BCS

A first copper(I) transport assay followed with BCS was performed. The absorbance was measured to verify that light was able to reach most of the cuvette volume. The initial concentration (in lipids) of the liposomes solution was 1 mM but was diluted later on to reduce the absorption. Two batches of liposomes were prepared: one with a 1/200 $X_4Pr_2Im_2$ to lipids ratio, the other without any transporter.

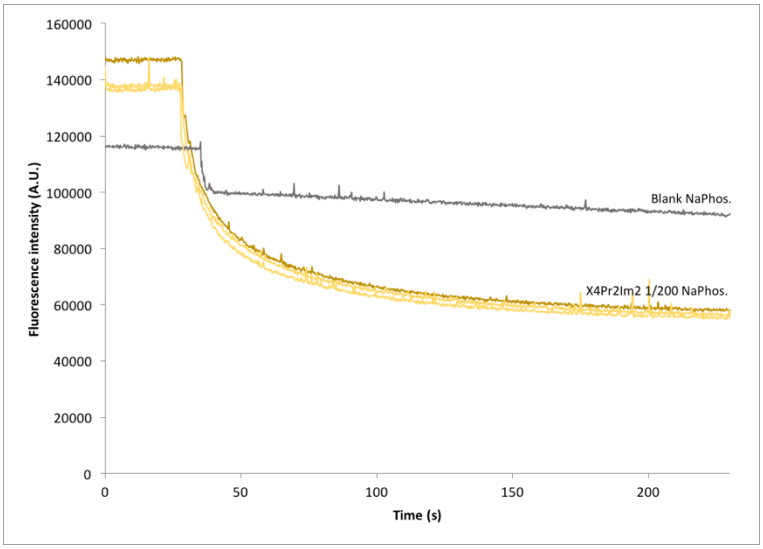

Figure X 24: Transport measurements of Cu(I) by following the decrease of fluorescence of BCS (excitation at 278 nm, emission at 393 nm) encapsulated inside LUVs with ***$X_4Pr_2Im_2$*** *(1/200 transporter to lipids ratio) in 100 mM sodium phosphate buffer (pH 7). Addition of 200 μL of a 1.8 mM $CuCl_2$ and 0.9 mM sodium ascorbate in 100 mM sodium phosphate buffer (pH 7) to 2.8 mL LUVs (0.33 mM lipids) created a Cu^+ gradient.* A blank measurement is shown for comparison.

On another experiment, the effect of different species on the fluorescence was verified. Various additions were made to the liposome solution prepared with **$X_4Pr_2Im_2$**: Na ascorbate, $CuSO_4$, $CuCl_2$ separately and also a mix of $CuSO_4$ and Na ascorbate, and a mix of $CuCl_2$ and Na ascorbate. The concentrations of all added species were 0.5 mM.

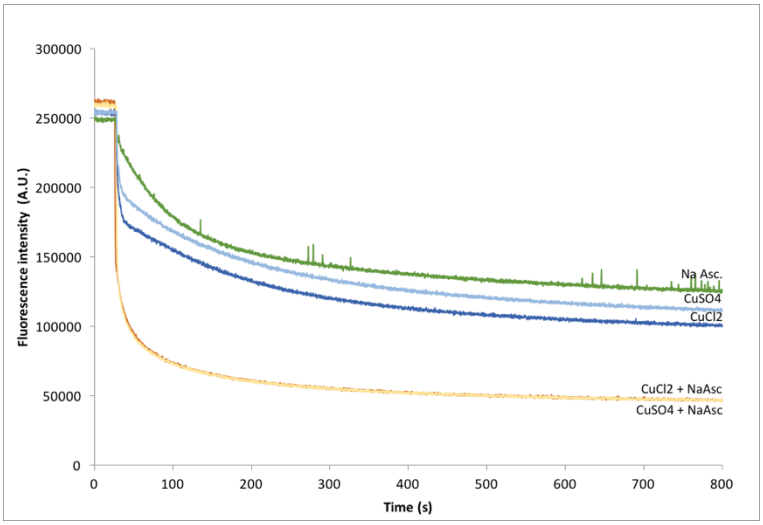

Figure X 25 : Comparison of effect on the fluorescence signal of BCS when adding different species (excitation at 278 nm, emission at 393 nm) encapsulated inside LUVs with ***$X_4Pr_2Im_2$*** *(1/200 transporter to lipid ratios) in 100 mM sodium phosphate buffer (pH 7). Addition of 200 μL of a 0.5 mM sodium ascorbate, 0.5 mM $CuSO_4$, 0.5 mM $CuCl_2$, 0.5 mM $CuCl_2$ + 0.5 mM sodium ascorbate, or 0.5 mM $CuSO_4$ + 0.5 mM sodium ascorbate in 100 mM sodium phosphate buffer (pH 7) separately to 2.8 mL LUVs (0.4 mM lipids).*

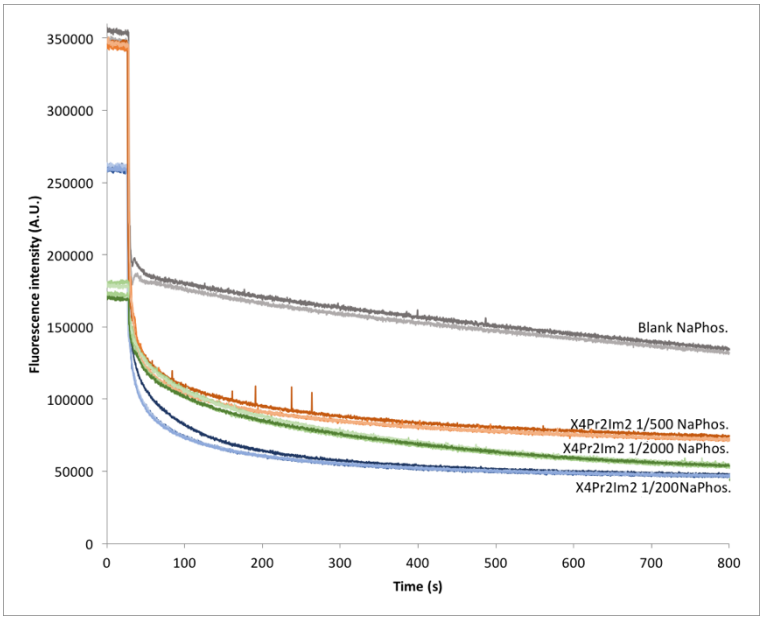

Figure X 26 : Comparison between different transporter concentrations. Transport measurements of Cu(I) by following the decrease of fluorescence of BCS (excitation at 278 nm, emission at 393 nm) encapsulated inside LUVs with ***$X_4Pr_2Im_2$*** *(1/200, 1/500, 1/2000 transporter to lipid ratios) in 100 mM sodium phosphate buffer (pH 7). Addition of 200 µL of a 0.5 mM $CuCl_2$ and 0.5 mM sodium ascorbate in 100 mM sodium phosphate buffer (pH 7) to 2.8 mL LUVs (0.4 mM lipids) created a Cu^+ gradient.* Blank measurements are shown for comparison.

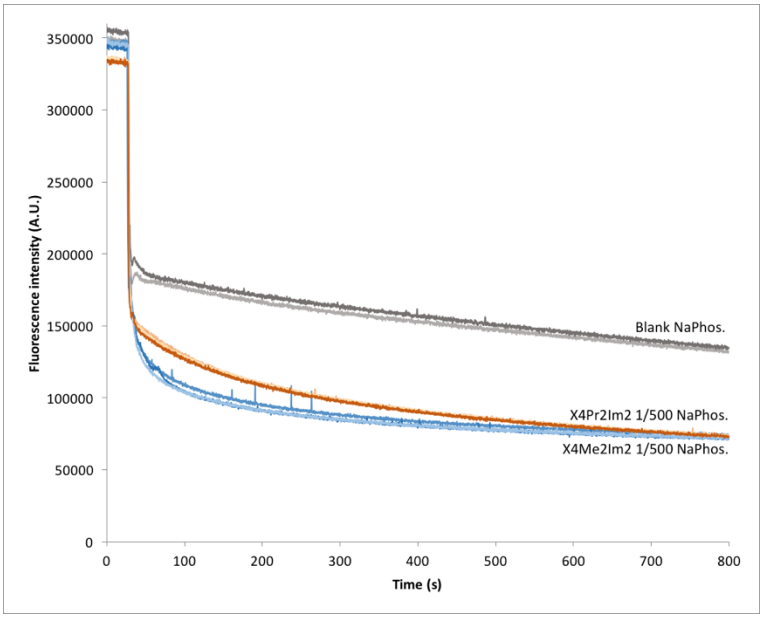

Figure X 27 : Comparison between ***$X_4Pr_2Im_2$*** *and* ***$X_4Me_2Im_2$****. Transport measurements of Cu(I) by following the decrease of fluorescence of BCS (excitation at 278 nm, emission at 393 nm) encapsulated inside LUVs with* ***$X_4Pr_2Im_2$*** *and* ***$X_4Me_2Im_2$*** *(1/500 transporter to lipids ratio) in 100 mM sodium phosphate buffer (pH 7). Addition of 200 µL of a 0.5 mM $CuCl_2$ and 0.5 mM sodium ascorbate in 100 mM sodium phosphate buffer (pH 7) to 2.8 mL LUVs (0.4 mM lipids) created a Cu^+ gradient. Blank measurements are shown for comparison.*

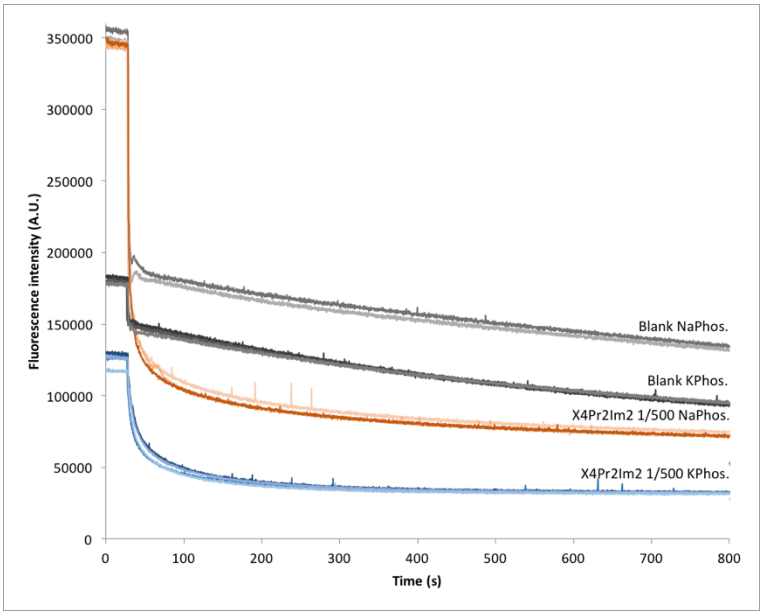

Figure X 28 Comparison between sodium and potassium phosphate buffers using ***$X_4Pr_2Im_2$****. Transport measurements of Cu(I) by following the decrease of fluorescence of BCS (excitation at 278 nm, emission at 393 nm) encapsulated inside LUVs with* ***$X_4Pr_2Im_2$*** *(1/500 transporter to lipids ratio) in 100 mM sodium/potassium phosphate buffer (pH 7). Addition of 200 μL of a 0.5 mM $CuCl_2$ and 0.5 mM sodium ascorbate in 100 mM sodium/ potassium phosphate buffer (pH 7) to 2.8 mL LUVs (0.4 mM lipids) created a Cu^+ gradient. Blank measurements are shown for comparison.*

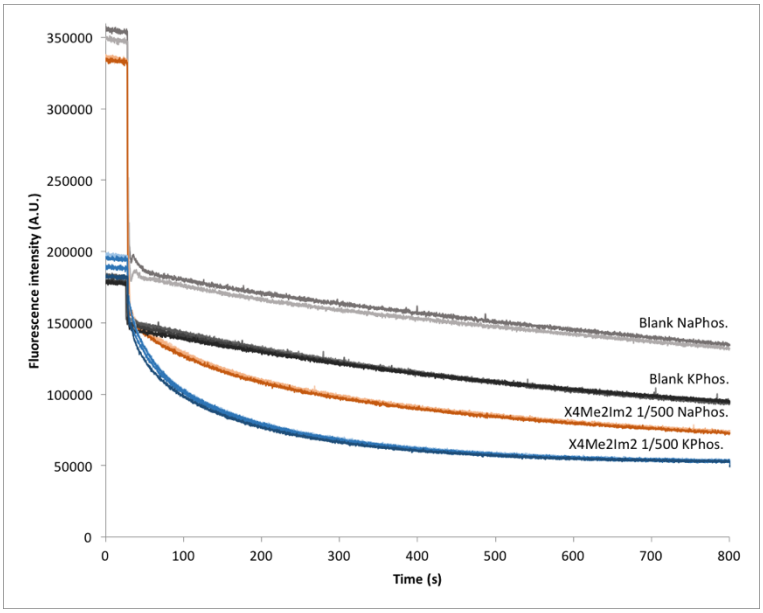

Figure X 29 : Comparison between sodium and potassium phosphate buffers using ***$X_4Me_2Im_2$****.Transport measurements of Cu(I) by following the decrease of fluorescence of BCS (excitation at 278 nm, emission at 393 nm) encapsulated inside LUVs with* ***$X_4Pr_2Im_2$*** *(1/500 transporter to lipids ratio) in 100 mM sodium/potassium phosphate buffer (pH 7). Addition of 200 μL of a 0.5 mM $CuCl_2$ and 0.5 mM sodium ascorbate in 100 mM sodium/ potassium phosphate buffer (pH 7) to 2.8 mL LUVs (0.4 mM lipids) created a Cu^+ gradient. Blank measurements are shown for comparison.*

The results obtained in NMDGH-X solutions are not shown as those conditions lead to an unstable system and thus the results were inconclusive.

4.4.5. Transport measurements with HPTS

The transport assay followed with the variation of fluorescence of HPTS were performed according to these parameters: the excitation was set up at 403 nm and at 454 nm, the emission was recorded at 510 nm with both slits opening of 1 nm. At neutral pH the molecule shows a strong excitation band at 403 nm when the pH rises the intensity of the excitation band at 403 nm decrease and another excitation band appears at 454 nm. A ratio (454 nm:403 nm) of the intensities of these excitation bands is a direct measurement of the pH in the environment of the dye. An increase of the signal is an increase in pH inside the liposomes and imply transport of proton from the inside to the outside of the LUVs.

In these experiments, a pH gradient was introduced and sometimes also a copper(I) gradient. The exchange of copper(I) or sodium with proton, through antiport, was studied in different conditions allowing not only copper to exchange with proton but also sodium. Conditions where no other transportable cations unless copper(I) and proton were tested. To achieve that, another salt solution was required, NMDG. NMDGH-Cl and NMDGH-sulphate were prepared and tested separately. The main distinction between the two conditions rely on the fact that sulphate was not likely to be transported with a proton, through symport, but chloride was.
Towards the end of the measurement, the liposomes were lysed in order to observe the total amount of potential signal changes of the probe. This was performed by adding a detergent (triton) that will integrate in the bilayer and thus collapse the liposomes. At the start and at the end of each experiments an excitation spectrum was recorded.

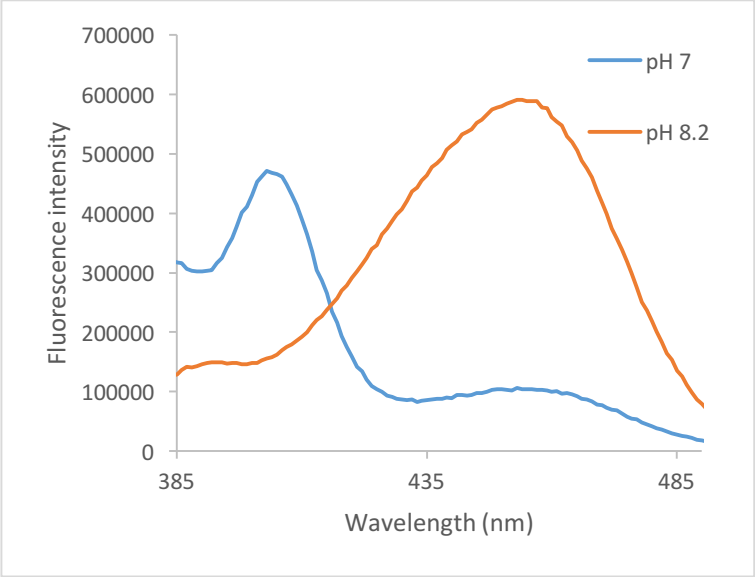

Figure X 30 : Comparison of the excitation spectra of HPTS (excitation between 385 nm and 490 nm, emission at 510 nm) encapsulated inside LUVs in a 100mM potassium phosphate buffer at pH 7.The spectra are shown before and after addition of 70 µL of an aqueous solution of NaOH 0.25 M and 50 µL of and triton (5%) to 3 mL LUVs (0.2 mM lipids).

The data showed in section 4.4.6 were treated as follows: each run were normalised from 0 to 1. The initial fluorescence values (F_0) was subtracted to the fluorescence value (F). The result was then divided by the difference between the final fluorescence value (F_F) and F_0. The average of each normalised run ($F-F_0/F_F-F_0$)) was then calculated and plotted over time.

4.4.6. Transport measurement results with HPTS

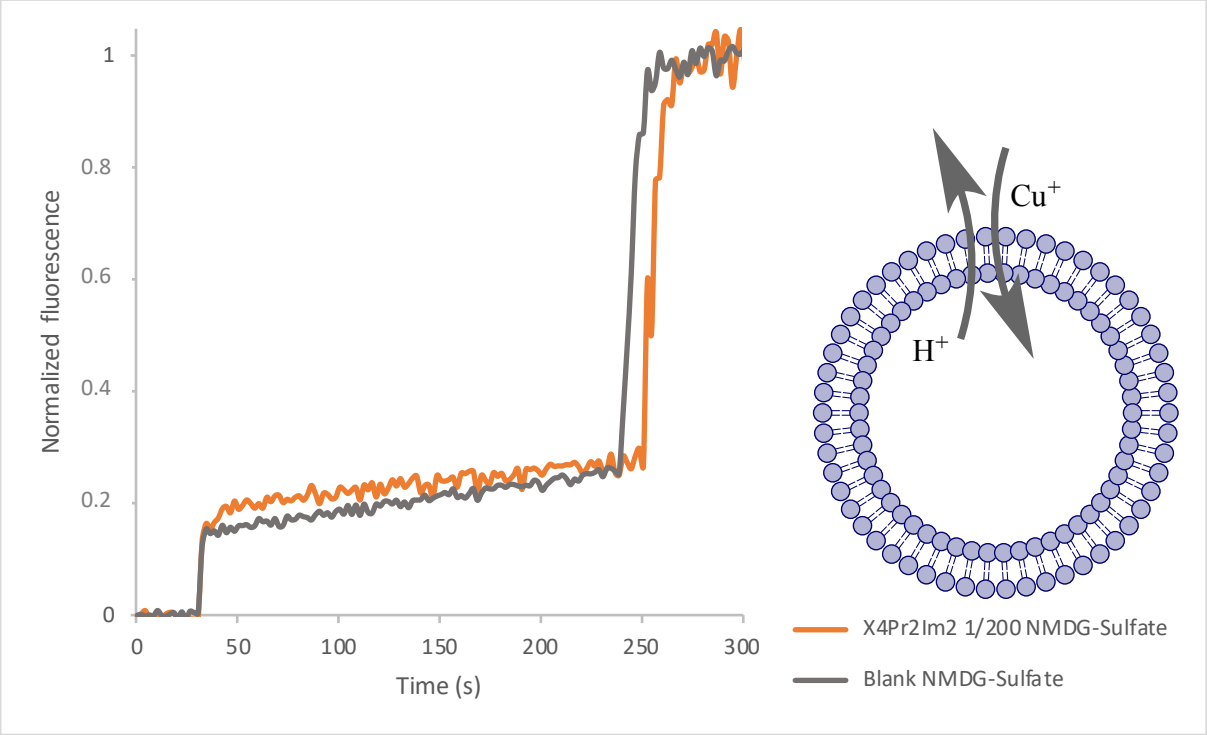

Figure X 31 : Transport measurements of Cu(I) by following the increase of the fluorescence ratio of HPTS (excitation at 403 nm and 454 nm, emission at 510 nm) encapsulated inside LUVs with ***$X_4Pr_2Im_2$*** *(1/200 transporter to lipids ratio) in a 100mM NMDG-sulphate buffer at pH 7. Addition of 200 µL of a copper(I) solution ($CuCl_2$ 1.8 mM + Na Ascorbate 0.9 mM) in a 100mM NMDG-sulphate buffer at pH 7 and 15 µL of an aqueous solution of 15 µL of NMDG after 30 seconds and 50 µL of and triton (5%) after 4 minutes to 3 mL LUVs (0.2 mM). Results were normalized and averaged and a blank measurement is shown for comparison.*

4.4.7. DLS measurements

The dynamic light scattering measurements were performed with a Malvern zetasizer at the faculty of pharmacy at the ULB in order to verify the size distribution of the LUVs.

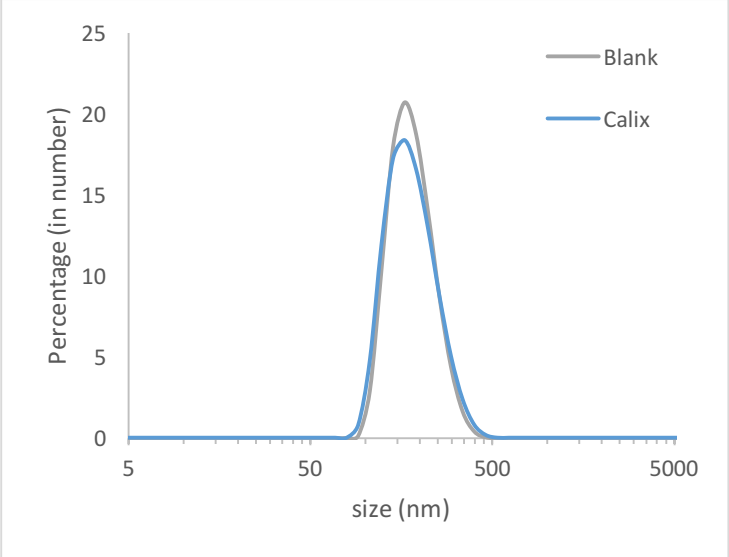

Figure X 32 : Dynamic light scattering measurements of LUVs solution (0.4 mM lipids) in 100 mM Na Phosphate buffer. Comparison of the size distribution between LUVs with ***$X_4Pr_2Im_2$*** *and without. Results are averaged and show the number distribution versus the size in nm on a logarithmic scale.*

5. Bibliography

[1] Stillwell, W. Membrane Transport. In *An Introduction to Biological Membranes*; Elsevier, **2016**; pp 423–451.
[2] Appling, D. R.; Anthony-Cahill, S. J.; Mathews, C. K. *Biochemistry: Concepts and Connections with Mastering Chemistry, Global Edition;* **2015**
[3] Festa, R. A.; Thiele, D. J. Copper: An Essential Metal in Biology. *Current Biology* **2011**, *21*, R877–R883.
[4] Crisponi, G.; Nurchi, V. M.; Fanni, D.; Gerosa, C.; Nemolato, S.; Faa, G. Copper-Related Diseases: From Chemistry to Molecular Pathology. *Coordination Chemistry Reviews* **2010**, *254* (7–8), 876–889.
[5] Kodama, H.; Fujisawa, C.; Bhadhprasit, W. Inherited Copper Transport Disorders: Biochemical Mechanisms, Diagnosis, and Treatment. *Current Drug Metabolism,* **2012,** *13,* 237-250.
[6] Rubino, J. T.; Chenkin, M. P.; Keller, M.; Riggs-Gelasco, P.; Franz, K. J. A Comparison of Methionine, Histidine and Cysteine in Copper(i)-Binding Peptides Reveals Differences Relevant to Copper Uptake by Organisms in Diverse Environments. *Metallomics* **2011**, *3* (1), 61–73.
[7] Pushie, M. J.; Shaw, K.; Franz, K. J.; Shearer, J.; Haas, K. L. Model Peptide Studies Reveal a Mixed Histidine-Methionine Cu(I) Binding Site at the N-Terminus of Human Copper Transporter 1. *Inorganic Chemistry* **2015**, *54* (17), 8544–8551.
[8] Wang, J.; Luo, C.; Shan, C.; You, Q.; Lu, J.; Elf, S.; Zhou, Y.; Wen, Y.; Vinkenborg, J. L.; Fan, J.; et al. Inhibition of Human Copper Trafficking by a Small Molecule Significantly Attenuates Cancer Cell Proliferation. *Nature Chemistry* **2015**, *7* (12), 968–979.
[9] Alfonso, I.; Quesada, R. Biological Activity of Synthetic Ionophores: Ion Transporters as Prospective Drugs? *Chemical Science* **2013**, *4* (8), 3009.
[10] Mamedov, V. A.; Kalinin, A. A. Quinoxaline Macrocycles. In *Advances in Heterocyclic Chemistry*; Elsevier, 2014; Vol. 112, pp 51–115.
[11] Mollenhauer, H. H.; James Morré, D.; Rowe, L. D. Alteration of Intracellular Traffic by Monensin; Mechanism, Specificity and Relationship to Toxicity. *Biochimica et Biophysica Acta (BBA) - Reviews on Biomembranes* **1990**, *1031* (2), 225–246.
[12] Valkenier, H.; Davis, A. P. Making a Match for Valinomycin: Steroidal Scaffolds in the Design of Electroneutral, Electrogenic Anion Carriers. *Accounts of Chemical Research* **2013**, *46* (12), 2898–2909.
[13] Gutsche, C. D. *Calixarenes: An Introduction*; Monographs in Supramolecular Chemistry; The Royal Society of Chemistry, 2008.
[14] Zinke, A.; Ziegler, E. Zur Kenntnis des Härtungsprozesses von Phenol-Formaldehyd-Harzen, X. Mitteilung. *Berichte der deutschen chemischen Gesellschaft (A and B Series)* **1944**, *77* (3–4), 264–272.
[15] Ikeda, A.; Shinkai, S. Novel Cavity Design Using Calix[n]Arene Skeletons: Toward Molecular Recognition and Metal Binding. 22.
[16] Scheerder, J.; Vreekamp, R. H.; Engbersen, J. F. J.; Verboom, W.; van Duynhoven, J. P. M.; Reinhoudt, D. N. The Pinched Cone Conformation of Calix[4]Arenes: Noncovalent Rigidification of the Calix[4]Arene Skeleton. *The Journal of Organic Chemistry* **1996**, *61* (10), 3476–3481.
[17] Agrawal, Y. K.; Pancholi, J. P.; Vyas, J. M. Design and Synthesis of Calixarene. **2009**, *68*, 25.
[18] Wieser, C.; Dieleman, C. B.; Matt, D. Calixarene and Resorcinarene Ligands in Transition Metal Chemistry. 69.
[19] Maurin, A.; Varatharajan, S.; Colasson, B.; Reinaud, O. A Water-Soluble Calix[4]Arene-Based Ligand for the Selective Linear Coordination and Stabilization of Copper(I) Ion in Aerobic Conditions. *Organic Letters* **2014**, *16* (20), 5426–5429.
[20] Clainche, L. L.; Giorgi, M.; Reinaud, O. Synthesis and Characterization of a Novel Calix[4]Arene-Based Two-Coordinate Copper(I) Complex That Is Unusually Resistant to Dioxygen. *European Journal of Inorganic Chemistry* **2000**, *2000* (9), 1931–1933.
[21] de Mendoza, J.; Cuevas, F.; Prados, P.; Meadows, E. S.; Gokel, G. W. A Synthetic Cation-Transporting Calix[4]Arene Derivative Active in Phospholipid Bilayers. *Angewandte Chemie International Edition* **1998**, *37* (11), 1534–1537.
[22] Sidorov, V.; Kotch, F. W.; Abdrakhmanova, G.; Mizani, R.; Fettinger, J. C.; Davis, J. T. Ion Channel Formation from a Calix[4]Arene Amide That Binds HCl. *Journal of the American Chemical Society* **2002**, *124* (10), 2267–2278.
[23] Okunola, O. A.; Seganish, J. L.; Salimian, K. J.; Zavalij, P. Y.; Davis, J. T. Membrane-Active Calixarenes: Toward 'Gating' Transmembrane Anion Transport. *Tetrahedron* **2007**, *63* (44), 10743–10750.
[24] Grauwels, G.; Valkenier, H.; Bartik, K.; Jabin, I.; Calix[6]arene-based receptors as carriers for the transmembrane transport of chloride and organic ion-pairs. *Wiley-VCH* Manuscript in preparation.

[25] Gale, P. A.; Davis, J. T.; Quesada, R. Anion Transport and Supramolecular Medicinal Chemistry. *Chemical Society Reviews* **2017**, *46* (9), 2497–2519.
[26] Chen, D.; Darabedian, N.; Li, Z.; Kai, T.; Jiang, D.; Zhou, F. An Improved Bathocuproine Assay for Accurate Valence Identification and Quantification of Copper Bound by Biomolecules. *Analytical Biochemistry* **2016**, *497*, 27–35.
[27] Collins, E. M.; McKervey, M. A.; Harris, S. J. Molecular Receptors with the Calix[4]Arene Substructure. Synthesis of Derivatives with Mixed Ligating Functional Groups. *J. Chem. Soc., Perkin Trans. 1* **1989**, No. 2, 372–374.
[28] Campbell, M. K.; Farrell, S. O. *Biochemistry*; Cengage Learning, **2011**.
[29] Valkenier, H.; Judd, L. W.; Li, H.; Hussain, S.; Sheppard, D. N.; Davis, A. P. Preorganized Bis-Thioureas as Powerful Anion Carriers: Chloride Transport by Single Molecules in Large Unilamellar Vesicles. *Journal of the American Chemical Society* **2014**, *136* (35), 12507–12512.
[30] Haynes, William M., ed. CRC *Handbook of Chemistry and Physics* **2011.**
[31] Xu, J.; Jordan, R. B. Kinetics and Mechanism of the Reaction of Aqueous Copper(II) with Ascorbic Acid. *Inorg. Chem.* **1990**, *29* (16), 2933–2936.
[32] Rapisarda, V. A.; Volentini, S. I.; Farías, R. N.; Massa, E. M. Quenching of Bathocuproine Disulfonate Fluorescence by Cu(I) as a Basis for Copper Quantification. *Analytical Biochemistry* **2002**, *307* (1), 105–109.
[33] Stern, O.; Volmer, M. über die Abklingzeit der Fluoreszenz, *Zeitschrift für* Physik, Vol. 20, **1919**, pp. 183-188.
[34] Ogawa, S.; Ichiki, R.; Abo, M.; Yoshimura, E. Revision of Analytical Conditions for Determining Ligand Molecules Specific to Soft Metal Ions Using Dequenching of Copper(I)−Bathocuproine Disulfonate as a Detection System. *Analytical Chemistry* **2009**, *81* (21), 9199–9200.
[35] Xiao, Z.; Wedd, A. G. The Challenges of Determining Metal–Protein Affinities. *Natural Product Reports* **2010**, *27* (5), 768.